CHEMICAL AND OPTICAL STUDIES OF THE HYDROGEN-EXCHANGED OPTICAL WAVEGUIDES IN LITHIUM NIOBATE.

This thesis is submitted to University of Glasgow for the degree of Master of Science

by

ABDEL MAJEED ALI FOAD
B.Sc.(Physics)

Department of Chemistry
University of Glasgow
Glasgow G12 8QQ

October, 1988

ProQuest LLC.
789 East Eisenhower Parkway
P.O. Box 1346
Ann Arbor, MI 48106 – 1346

To my family in Baghdad.

ACKNOWLEDGEMENTS.

I would like to thank Professor J. Lamb for allowing me to use the many facilities of the Electronic and Electrical Engineering Department.

I sincerely thank my supervisors (and friends) Dr. J.M. Winfield (Chemistry Dept.) and Professor R.M.De La Rue (E.& E.E.Dept.) for their encouragement, help and guidance during the past two years.

I would like to thank my friend Dr. A. Loni for his help in teaching me the basics of the techniques and for many useful discussions.

My thanks to Professor G. Webb, Dr. R.D. Peacock and Dr. K. Campbell for the useful discussion.

The technical assistance of Mrs. F. Lawrie and Mr. G. McCulloch in the infrared studies and Mr. M. Beglen and Mr. J. McCaig in the atomic absorption studies is very much appreciated.

I would like to acknowledge:
Mr. R. Spence for his general technical advice.
Members of the Glassblowing workshop and Mechanical workshop for their help in the construction and repair of my equipment.
Mr. K. Piechowick (E.& E.E.Dept) for cutting and polishing my lithium niobate samples.
Mr. A. Stark (E. & E.E. Dept.) for his help in the SEM studies.
My thanks to Messrs. L. McGhee, D. Wilson, J. McIver for their

assistance, W. Smith and R. Henderson for their friendship. Special thanks go to my family in Baghdad for their love, encouragement and patience during the past two years.

My thanks to Mrs. Liz Hughes for skilfully typing this text.

Finally, I would like to thank the Ministry of Higher Education and Scientific Research, Iraq for providing this scholarship and for the generous financial support during the difficult time of war.

TABLE OF CONTENTS

CHAPTER TWO:EXPERIMENTAL TECHNIQUES USED FOR THE CHARACTERIZATION OF [^{1}H] AND [^{2}H] HYDROGEN-EXCHANGED OPTICAL WAVEGUIDES.

SUMMARY

Integrated optics is a key technology for many optical applications like communications, signal processing, optical sensors and instrumentation. The hydrogen-exchange "proton-exchange" is a new technique for fabricating large refractive index difference optical waveguides. The aim of this thesis is to investigate the stability of these waveguides, especially using [^{2}H]-hydrogen incorporated from benzoic acid by [^{2}H] hydrogen-exchange, with respect to the surrounding environment at room and elevated temperatures. The possibility of fabricating waveguides with superior performance and larger change in refractive index using phosphorus containing acids was investigated. This possibility is of particular interest in non-linear optics applications. The crystal change in stoichiometry and crystal structure of the widely used ferroelectric lithium niobate were described. The available techniques for fabricating optical waveguides on lithium niobate were described with emphasis on the hydrogen-exchange technique. The methods of preparation of the [^{1}H] and [^{2}H]-hydrogen labelled benzoic and phosphoric acids were described.

Infrared spectroscopy has been used to determine the extent of the exchange reactions and to monitor the incorporation of [^{1}H] and [^{2}H] hydrogen into lithium niobate crystals under various conditions. Atomic absorption spectroscopy has been utilized to detect and determine the lithium out-diffused from the crystal into the acid. The prism-coupling technique has been used to measure the mode angles

and hence to determine the refractive indices/depth profiles of the waveguides. The stability of the [^{2}H] hydrogen-exchanged waveguides has been investigated by the exposure of x- and z-cut $LiNbO_3$ waveguides to [^{1}H] water vapour at room temperature.

The z-cut [^{2}H] hydrogen-exchanged waveguides showed reversible behaviour when exposed to [^{2}H]-hydrogen labelled water vapour successively, unlike the x-cut waveguide which exhibited non-reversible behaviour. Isotopic-exchange reactions were also examined at elevated temperatures and incorporation of [^{1}H] and [^{2}H] hydrogen was observed when slow flow rates were used. The stability of the effective refractive indices of the [^{2}H] hydrogen-exchanged waveguides was monitored during the period of exposure to water vapour in ambient air.

Lithium detected in the acids after the exchange reactions was smaller in the [^{2}H]-hydrogen labelled acids than in the [^{1}H]-hydrogen acids and a relationship was established between the quantity of benzoic acid used in the reaction and the extent of the reaction. The extent of the reaction deduced via spectroscopic and optical measurements has been established for z-cut waveguides fabricated in ortho and pyrophosphoric acids.

X-cut lithium niobate waveguides have been successfully fabricated, for the first time using pyrophosphoric acid at 200^{o}C for times ranging from 4 to 30 min.

Isotopic-exchange reactions at room and elevated temperatures were investigated on waveguides prepared

using [^{2}H]-hydrogen labelled orthophosphoric acid. Lithium was detected in the phosphoric acid samples and a relationship between the quantity of acid used and the extent of reactions was established.

CHAPTER ONE.

INTRODUCTION.

1.1 INTEGRATED OPTICS TECHNOLOGY.

Integrated optics technology came into being in the early 1970's; it grew as a natural extension of the technology of micro-electronics to form compact optical circuits. A wide range of applications was found in fields such as communications, signal processing, instrumentation, sensors and many others. Early optical communication systems had been based on relatively large cored multimode fibres with losses around 20 dB km^{-1}.[1] The current "state of art" technology involves the fabrication of a single mode fibre[2] with losses of 0.2 dB km^{-1} at a wavelength of 1.55 μm in the infrared region. Integrated optic circuits basically consist of components such as lasers, optical modulators, switches, couplers, detectors, polarizers and waveguiding structure which is the most fundamental. An integrated optical waveguide is a structure in which a thin layer of dielectric material possessing a high refractive index is sandwiched between two media of a lower refractive index. The optical signal, the propagating mode is confined and propagated via total internal reflection. The light propagation characteristics depend on the opto-geometrical properties of the waveguide. Generally, there are two basic waveguide structures. Stripe waveguides, can be produced photolithographically to a discrete width (typically 2 - 15 μm). Slab or planar waveguides, are those in which the waveguiding layer is in the form of a

plane supported by a substrate and covered by air. This later type, fabricated using lithium niobate, is the subject of this study.

A planar waveguide can support a single mode or several propagating modes. It can be represented theoretically as an eigensolution of the wave equation depending upon the characteristics of the waveguide,[3] for example, the depth of the waveguiding layer and difference between the refractive indices of the guiding layer and the substrate. The most widely used material commercially, in the realization of integrated optical devices is lithium niobate.

Lithium niobate, $LiNbO_3$, is a man-made high temperature ferroelectric material. It was first described by Zachariasen in 1928[4] and successfully grown as single crystals by Ballman using the Czochralski technique.[5] Lithium niobate possesses a useful combination of physical properties which include a large piezoelectric coupling coefficient, a large electro-optic effect, low acoustic losses, large optical non-linearity, photorefractive effect (local changes in the refractive index during illumination by a high power laser), pyroelectric effect (generation of current during heating the crystal) and the bulk photovoltic behaviour (generation of current along the optical axis during illumination of the crystal by laser).[6] This mixture of properties makes lithium niobate suitable for a broad range of applications including,

surface acoustic wave devices,[7] acoustic delay lines and fillers, Q-switching of YAG:Nd lasers, optical amplitude and phase modulators,[8] second-harmonic generators,[9] phase conjugators, parametric oscillators and many others.

1.1.1 Stoichiometry and crystal growth of lithium niobate.

The initial investigation of the Li_2O-Nb_2O_5 phase diagram was undertaken by Reisman and Holtzberg[10] with further elaboration by Lerner et al[11] and Svaasand et al.[12,13] The overall phase diagram presented by Svaasand is reproduced in figures 1.1a and 1.1b. Lithium niobate is one of four compounds in the system Li_2O-Nb_2O_5 and it has a relatively large solid solution range from 44 to 50 mole % on the Li deficient side. It should be pointed out that stoichiometric lithium niobate melts incongruently, the congruent composition occurs at a lithium deficient composition of 48.45 mole % Li_2O.[14,15] The congruent melting point denoted by "a" in Figure 1.1b has important consequences for the crystal growth conditions. Svaasand et al[13] demonstrated that a significant amount of the $LiNb_3O_8$ phase was precipitated from the $LiNbO_3$ phase on annealing congruent crystals for 17 h at temperatures between 600 and 900°C. Precipitation of $LiNb_3O_8$ increases the optical scattering in the crystal.[16] The observed rate of phase precipitation was temperature dependent, being greatest at around 800°C. Lerner et al[11] found that $LiNbO_3$ boules, pulled by the Czochralski

Figure 1.1a Phase Diagram for the Li_2O-Nb_2O_5 System (Svaasand et al[13]).

Figure 1.1b Extended phase diagram for the Li_2O-Nb_2O_5 system (Svaasand et al[12]).

(a)

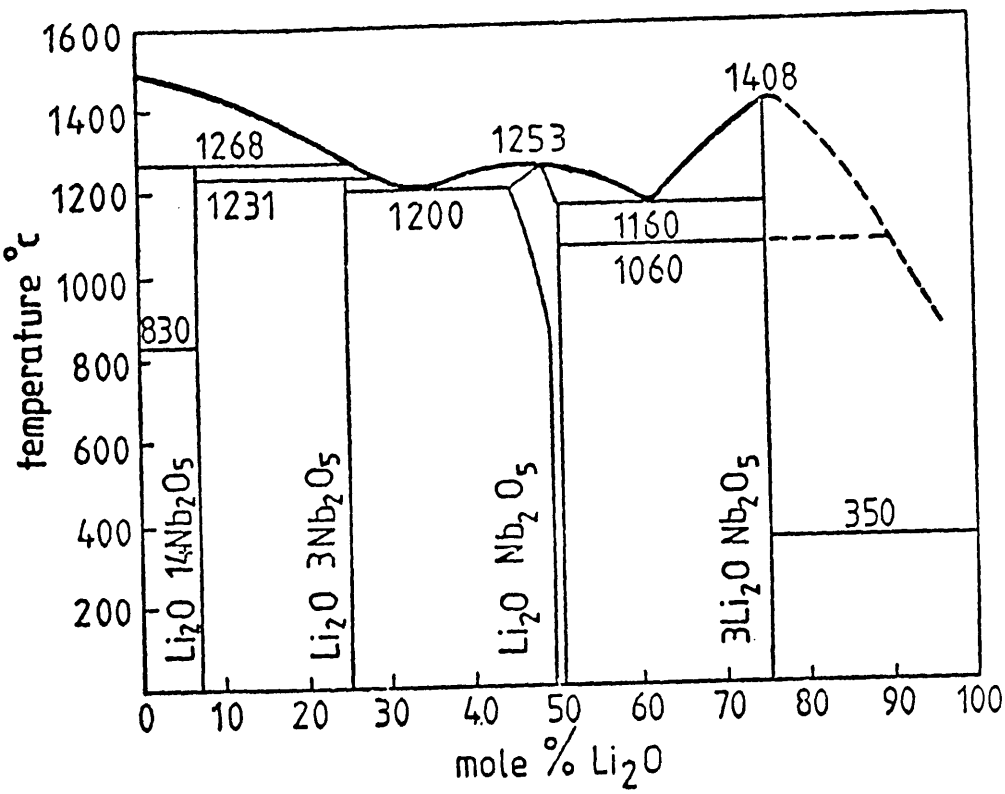

(b)

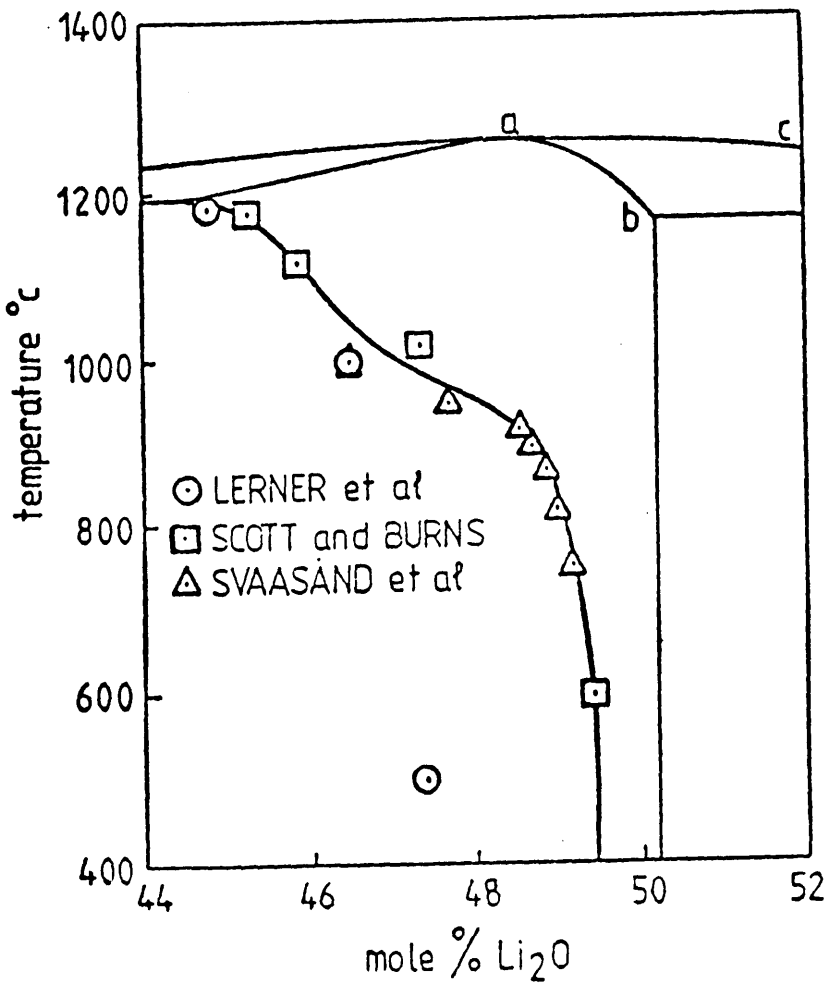

technique from stoichiometric melts changed in composition along their long axis as a result of the change in the liquid composition during the course of growth from 50 to 55% Li_2O or higher. The extraordinary refractive index of such a crystal would vary by 0.14 or more over its length. Bergman et al [17] reported both the ordinary and the extraordinary refractive indices, n_o and n_e respectively, at 0.6328 μm as a function of melt stoichiometry over a composition range of 44.4 to 54.5 mole % Li_2O. The growth of lithium niobate single crystals by the Czochralski technique has been the most successful method for producing large, homogeneous and defect free crystals. It is superior to techniques such as crystal growth from flux,[18] hydrothermal growth [19] or the growth by the vapour method.[20] The starting materials for growth of $LiNbO_3$ are highly pure lithium carbonate Li_2CO_3 and niobium pentoxide Nb_2O_5, the charge is mixed in the correct proportions for the production of a congruent crystal in a platinum crucible then fired at a temperature about 50 - 100°C below the melting point (m.p. = 1250°C)[21] for 12 h to ensure that the reaction of the constituents occurs. The reaction is represented by the equation:

$$Li_2CO_3 + Nb_2O_5 \longrightarrow 2LiNbO_3 + CO_2 \qquad (1.1)$$

Pulling of $LiNbO_3$ by Czochralski technique was reported in detail by Nassau.[22] A schematic diagram of the apparatus used for the crystal growth is shown in figure 1.2. Good quality congruent $LiNbO_3$ crystals

Figure 1.2 Schematic of a Czochralski pulling apparatus for crystal growth of $LiNbO_3$ (O'Bryan et al[14]).

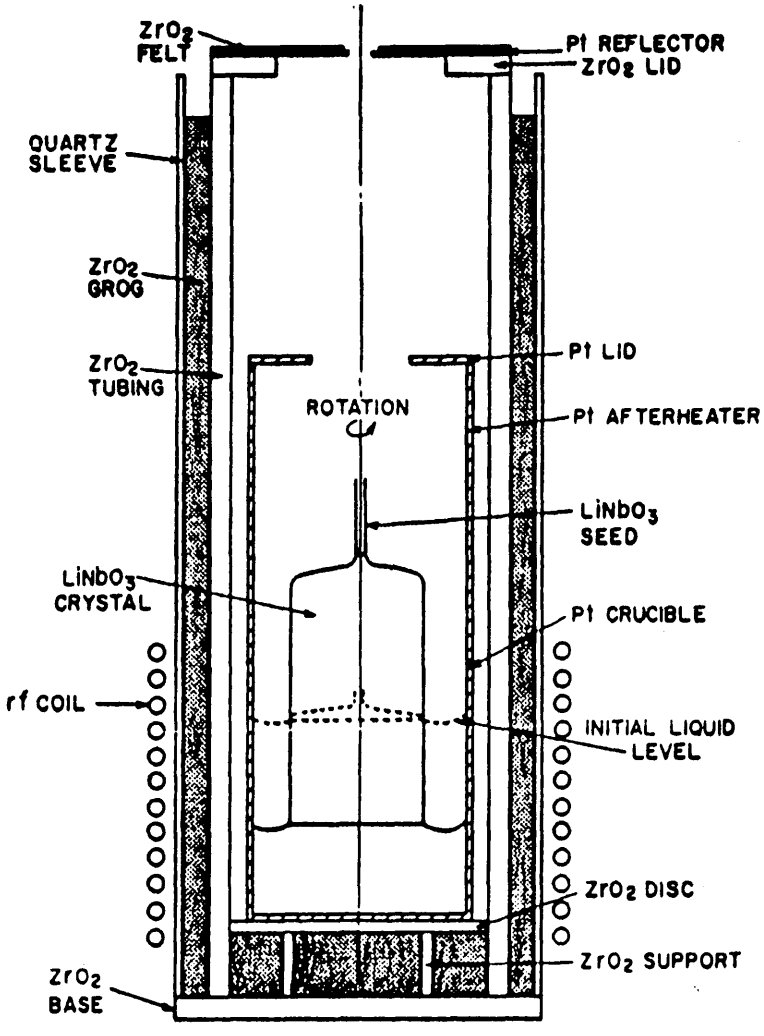

have been grown by using slow pulling and rotation rates (0.15 - 2.5 cm h^{-1}; 15 rpm)respectively, slow heating rates, the use of large crucible charges and very slow cooling from the freezing point. Lithium niobate crystals are usually grown on either the Z or Y-direction.[23]

Single domain $LiNbO_3$ crystals have been produced by poling the boule either during or after growth.[22] The conventional process involves heating the boule to the Curie temperature (Tc = 1140°C for congruent composition crystals[14]) at which point the structure becomes paraelectric. The application of a small electric field then displaces the Li^+ ions towards the cathode and this ordered structure is locked in place by cooling below Curie temperature before removal of the electric field. Recently, Haycock et al[24] reported a new technique for poling $LiNbO_3$ at temperatures well below the Curie point. This method involves ionization of the crystals by the passage of energetic electrons while under the influence of an electric field along the C-axis. For 1mm thick crystal, poling was obtained by heating the crystal to 600°C while applying a field of 10 Vcm^{-1} and using a beam energy of 1.8 MeV.

1.1.2 The Crystal Structure of Lithium Niobate.

The crystal structure of lithium niobate at temperatures below its ferroelectric Curie temperature has been unambiguously established by x-ray and neutron

diffraction studies of single domain crystals by Abrahams et al.[25,26] It consists of planar sheets of oxygen atoms in a distorted hexagonal close-packed structure. The resulting octahedral interstices formed are one-third filled by lithium atoms, one-third filled by niobium atoms and one-third vacant. In the +C direction the atoms in the interstices are in the following order...., Nb, vacancy, Li, Nb, vacancy, Li...., figure 1.3 shows a unit cell of lithium niobate along the C-axis (Polar axis). The negatively charged oxygen ions form the corners of the octahedron, the smaller, positively charged lithium and niobium ions occupy the space within the octahedron, in the order mentioned above. The choice of the coordination system in which the physical tensor properties of lithium niobate was the Cartesian X, Y, Z system. It is related to the hexagonal axes in a way that the Z-axis is chosen to be parallel to the C-axis. The X-axis is chosen to coincide with any of the equivalent a_H axes, the Y-axis is consequently chosen so that the system is right handed. Thus, Y-axis must lie in a plane of mirror symmetry. The Ferroelectric behaviour of lithium niobate can be comprehended as follows. At temperatures above the Curie point, the lithium ions lie within the plane of the oxygen ions triangles, the niobium ions are midway between the planes. Hence, the crystal has no charge (paraelectric). At temperatures below the Curie point, both the niobium and lithium ions are displaced in the same direction resulting in a positive

Figure 1.3 A three-dimensional view of a [illegible] crystal. The top view of a unit cell illustrates the ions seen along the direction of the polar axis. Negatively-charged oxygen ions from the corners of an octahedron. The smaller, positively-charged lithium and niobium ions occupy the space within the octahedron in an ordered fashion (bottom view) (Landise [147]).

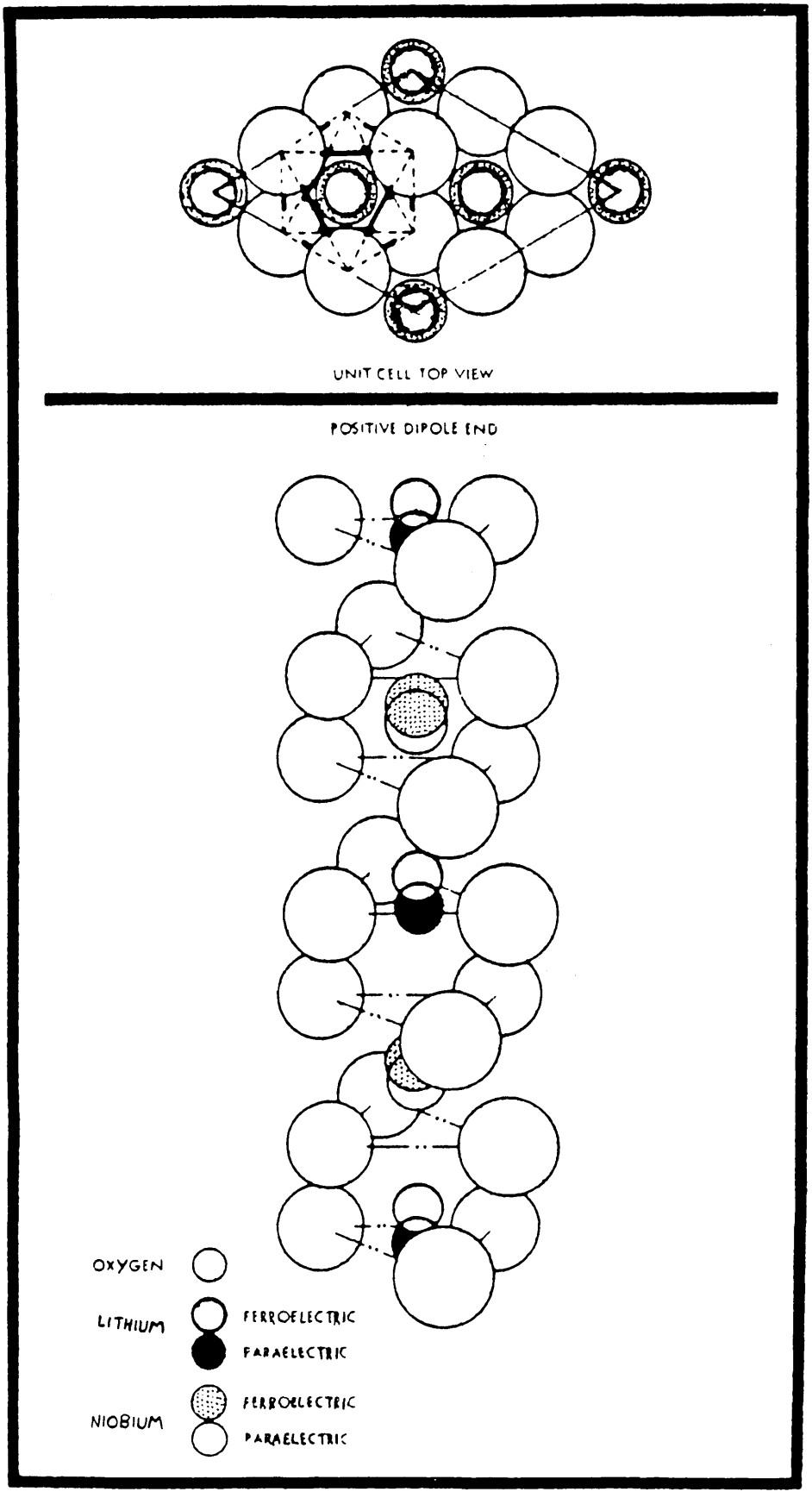

C-axis end (ferroelectric), see figure 1.3 . Lithium niobate is therefore, non centro-symmetric and has six formula units per hexagonal and two per equivalent rhombohedral unit cell. The parameters of the unit cell of lithium niobate and some physical properties are presented in Table 1.1.

The congruent composition of 48.45 mol % Li_2O and 51.55 mol % Nb_2O_5[14] necessarily corresponds to a defect structure. The detailed x-ray analysis on congruent lithium niobate reported by Abrahams et al[15] showed an occupancy of Li- sites of 94.1% Li, 5.9% Nb atoms and Nb-sites occupancy of 95.3% Nb. Each missing Li^+ ion in the structure was hence replaced by an Nb^{+5} ion, leaving corresponding vacancies at the original Nb sites as represented by the formula $[Li_{1-5x}\ Nb_{5x}]Nb_{1-4x}\ O_3$ with x = 0.0118 at the congruent composition. This implies that a Nb atom in approximately every three unit cell occupies an Li site.[15,27]

Since $LiNbO_3$ crystal structure is anisotropic, the atoms arrangement in the lattice viewed perpendicular to the major axes of the crystal (X,Y,Z) is reproduced in figure 1.4a,b,c.[28]

Table 1.1 : Physical Properties of Congruent (48.45 mol % Li_2O) and Stoichiometric Lithium Niobate.

Property	Congruent $LiNbO_3$	Stoichiometric $LiNbO_3$
Lattice parameters		
Hexagonal C_H	13.86496 Å	13.85614 Å
a_H	5.15052 Å	5.14739 Å
equivalent rhombohedral a_R	5.494 Å	
α	55° 52	
Volume of unit cell	318.513 $Å^3$	317.941 $Å^3$
space group (>Tc)	R3C	R3C
Point group	3m (C_6V)	3m(C_6V)
M.W.	148.551	147.846
Density	4.646 gm cm^{-3}	4.6327 gm cm^{-3}
T_c	1140°C	1213°C
n_e	2.2026±0.0003	
n_o	2.2869±0.0001	

Figure 1.4 Arrangement of lattice sites in the crystal structure of $LiNbO_3$ perpendicular to the major crystal axes X,Y,Z (X-, Y- and Z- cut respectively) (Götz[28]).

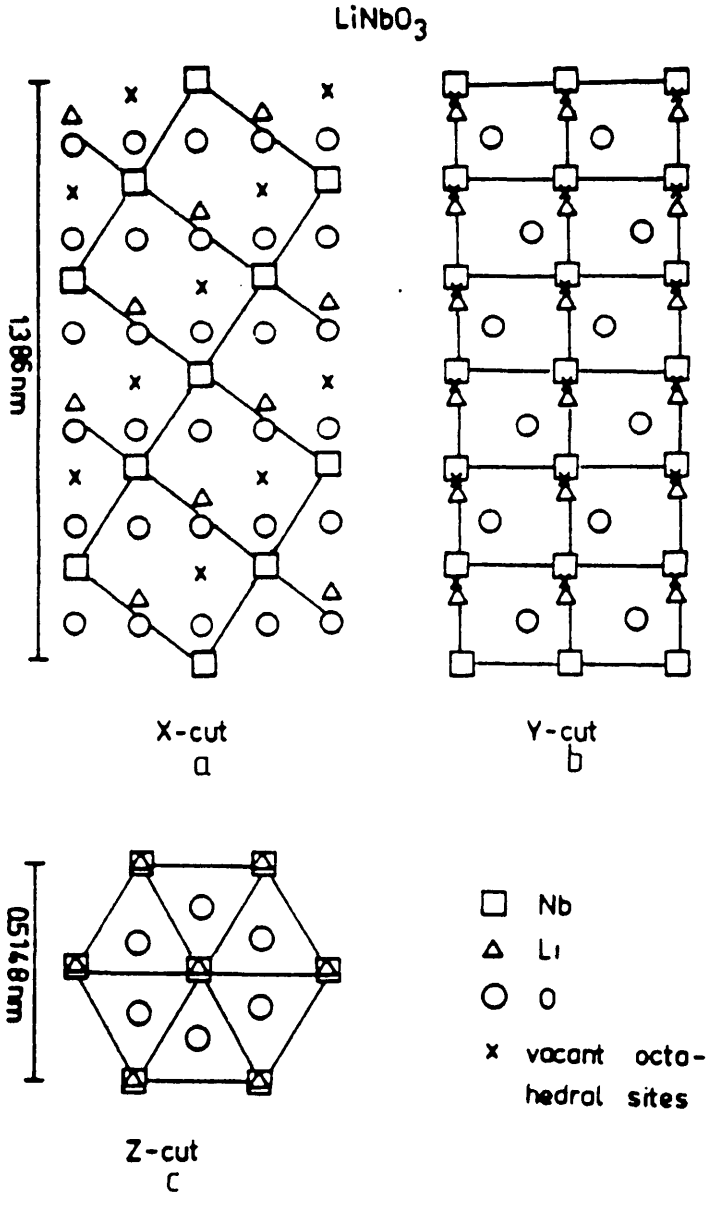

1.2 TECHNIQUES USED FOR PRODUCING OPTICAL WAVEGUIDES IN LITHIUM NIOBATE.

Planar and stripe dielectric waveguides have been formed in lithium niobate using various processes.

Waveguide fabrication aims to create a local variation of refractive index with graded or step profile by using techniques such as vacuum thin-film deposition, thermal diffusion, hydrogen exchange and ion implantation. Several diffusion processes for producing optical waveguides in lithium niobate have been reported and are briefly described in turn.

1.2.1 Lithium oxide out-diffusion.

The production of optical waveguides in lithium niobate by out-diffusion of lithium oxide from the crystal surface was first demonstrated by Kaminow.[29] It involves thermal treatment at 1000 - 1100°C for several hours in vacuum or oxidising atmosphere. This technique increases the extraordinary refractive index by $\Delta n_e = 10^{-3}$ to 10^{-2} (the index at which the electric field vector of the optical beam is parallel to the optical polar axis), whereas the ordinary refractive index (the electric field vector of the optical beam is perpendicular to the optical polar axis) is not effected. Woods et al[30] found that the rate of lithium out-diffusion was greater if the crystal was nearer to the stoichiometric composition and the activation energy was independent of the stoichiometry.

The out-diffusion process can create waveguides of thicknesses in the order of 10 μm with high insertion losses due to scattering. This problem strictly limits the operation of integrated electrooptic devices which, in most applications, require stripe waveguides owing to the formation of the unwanted surface guiding layer on the extraordinary wave.

1.2.2 Titanium in-diffusion.

Several species of metal atoms, such as Mg, Ni, Zn, Fe, Co, Cr, V and Ti have been used as diffusants into $LiNbO_3$ producing modifications in the refractive index.[31] Thin films (10 - 100 nm) of metal are first deposited on the crystal surface by vacuum evaporation or sputtering. The diffusion process occurs at high temperatures (850 - 1150°C) in an inert gas or a reactive atmosphere. The study of titanium in-diffusion into lithium niobate has received most attention because titanium produces good light confinement, with an increase in both the ordinary and extraordinary refractive indices ($\Delta n_o \leqslant 0.02$, $\Delta n_e \leqslant 0.04$). In addition, it produces low optical loss planar and stripe waveguides (<1 $dBcm^{-1}$).[32,33] Diffusion of a Ti thin layer has been carried out at temperatures ranging from 900 to 1150°C in argon, nitrogen, oxygen or ambient atmosphere, for diffusion times ranging from 0.5 to 30 h. Electron microprobe and x-ray micro-analysis showed Gaussian Ti concentration depth profiles.[34]

Considerable attention has been devoted to the observation of the intermediate stages of the diffusion process and to understand the mechanism of the waveguiding layer formation. Various analytical techniques have been used, such as scanning electron microscopy (SEM), Rutherford back-scattering (RBS) secondary ion mass spectroscopy (SIMS), Auger electron spectroscopy (AES) and glancing angle x-ray diffraction (XRD).[35,36,37]

During the Ti-diffusion process, lithium oxide out-diffusion occurs which significantly affects the performance of stripe and monomode waveguides. Several methods for suppressing the out-diffusion of lithium oxide have been successfully used. The suppression occurs when the titanium diffuses in the samples in a Li_2O rich and/or "wet" (H_2O/gas) atmospheres.[38,39] Another problem in the Ti-diffused waveguides is the photorefractive effect or "optical damage", but this can be prevented by diffusing Ti in a wet atmosphere.[40]

1.2.3 Ion-implantation.

Ion-implantation involves implantation of helium ions deep into the crystal and the creation of a maximum lattice disorder. This is associated with a reduction in the refractive index and allows light to be guided between this disordered region and the $LiNbO_3$/air interface.[41] High energy (1MeV) helium implantation can produce waveguides of depth up to 2.3 μm[42] and can define buried wave-

guides at various depths. Generally, the depth of the waveguides can be estimated by the ion energy and the refractive index reduction depends on the ion dose.[43] Ion induced damage can be removed by post-annealing of the waveguides, typically at temperatures from 100 to 220°C, and the annealing process also reduces optical losses.[44]

1.2.4 [^{1}H] Hydrogen-exchange ; "Proton-exchange"

The [^{1}H] hydrogen-exchange technique was described originally by Jackel et al as a means of making the new compound $HNbO_3$ [45,46] from reactions between $LiNbO_3$ powder and aqueous acids. Subsequently, it was presented as a new technique for fabricating optical waveguides.[47] The reaction involves an exchange between lithium present in the crystal and hydrogen from a protonic source. The reaction can be described by the equation

$$LiNbO_3 + H^+ \longrightarrow Li_{1-x} H_x NbO_3 + Li^+ \qquad (1.2)$$

where H^+ represents a protonic source. Only partial exchange is of interest in producing optical waveguides (with $x \leq 0.75$)[48] since total hydrogen exchange produces structural changes from hexagonal to cubic ReO_3 and the accompanying volume change causes the crystal to break up and destroy the waveguiding layer. Hydrogen-exchange in benzoic acid produces a high change in the extraordinary refractive index $\Delta n_e = 0.128$ and decreases the ordinary index $\Delta n_o = -0.04$ at wavelength $\lambda = 0.6328\ \mu m$ [49,50]. In

other words, it increases the birefringence $(n_o - n_e)$ of $LiNbO_3$. This implies that x- and y- cut crystals can support the transverse electric (TE) modes only whereas z-cut crystals support the transverse magnetic (TM) modes only.

The structure and properties of hydrogen-exchange waveguides have been systematically investigated using several techniques. The waveguides have been optically characterized by the prism coupling technique. Strains, defects and crystal structure modification have been studied using the x-ray diffraction method while Rutherford backscattering spectroscopy (RBS) has been used to study the kinetics of waveguide formation and the exchange process. Concentrations and profiles of H and Li have been estimated via nuclear reactions.[51,52,53,54].

Channel waveguides have been analysed using transmission electron microscopy (TEM) and secondary-ion mass spectroscopy (SIMS).[53] Modelling of the refractive index profile together with the diffusion coefficients and activation energies have been presented for both x- and z- cut $LiNbO_3$ waveguides.[55,56,57]

The high refractive index change produced by this method implies a large confinement of the optical energy in the waveguide. This enables the fabrication of narrow and shallow stripe guides since it has been shown that lithographic masking procedures can be used for the definition of stripe guides.

A wide range of integrated optical devices has been demonstrated using the hydrogen-exchange technique.[58] These include various types of planar lens and grating structures[59,60], electro-optic devices [61,62], acousto-optic devices[63], ring resonators [64], non-linear optical devices[65] and polarizing components.[66]

Several problems have been identified in the waveguides fabricated by hydrogen-exchange. These include refractive index instability [67,68], severe damage of the waveguiding layer in y- cut $LiNbO_3$ [69], reduction in the electro-optic effect,[70] and relatively high optical losses caused mainly by in-plane scattering.[71] Extensive studies have been undertaken to improve the optical quality of hydrogen-exchanged waveguides. Successful demonstration of waveguides and devices with substantial or complete improvement of these problems have been reported in the literature. Two techniques have been employed. The first is buffering the benzoic acid by lithium benzoate in a mole fraction ranging between 0.1% to 3.5%.[72,73] The second is annealing (heating) of the waveguides in a temperature range of 250 - 400°C.[51,74] A combination of both processes is valuable in improving the quality of [^{1}H] hydrogen-exchanged waveguides.[57] A detailed study of both techniques using a variety of mole fractions (up to 2.42%) and annealing times and temperatures was carried out by A. Loni.[57] Isotopic [^{2}H] hydrogen-exchange has been investigated by several workers. Rice et al[76] used deuterium-exchanged wave-

guides to produce a concentration profile using the nuclear reaction

$$^{3}He + ^{2}H \longrightarrow ^{4}He + ^{1}P \qquad (1.3)$$

They concluded a non-linear relationship between the refractive index profile and the deuterium concentration. Gonzalez et al[77] calculated the diffusion coefficient of deuterium diffused into $LiNbO_3$ crystal from [^{2}H]-hydrogen labelled water vapour at elevated temperatures. Loni et al used the [^{1}H]- [^{2}H]-hydrogen isotopic-exchange technique to monitor the properties of [^{1}H] hydrogen-exchanged waveguides.[78]

The [^{1}H] hydrogen-exchanged waveguides have been shown to react reversibly if exposed to [^{2}H]-hydrogen labelled water vapour then exposed to H_2O water vapour in air.

1.2.5 Titanium diffusion associated with hydrogen-exchange (TIHE).

The TIHE waveguides have been fabricated by using Ti-diffusion first, followed by hydrogen-exchange. They have been reported to possess interesting properties.[79] This method proved that the hydrogen-exchange technique reduces the ordinary refractive index n_o of the waveguide since the titanium diffusion process increases both the ordinary and extraordinary refractive indices whereas TIHE

guides either support less or no ordinary modes depending on the exchange conditions. On y- cut $LiNbO_3$, it has been found that Ti acts as a protection and hydrogen-exchange was possible without destructive damaging of the guide. TIHE waveguides have interesting non-linear optical properties. They permit the extension of the maximum phase matched pump wavelength from 1.1 μm in Ti-diffused waveguides to 1.24 μm enabling the production of harmonic radiation at ambient temperature.[80,81]

1.3 THE CHEMICAL REACTION BETWEEN LITHIUM NIOBATE AND ACIDS.

The hydrogen-exchange reaction or "proton-exchange" involving lithium niobate is the replacement of lithium by hydrogen. It takes place when the lithium niobate is placed in a protonic source, an acid or hydrate melt. Exchange can be complete, with all the lithium replaced, or partial, depending on the reaction conditions and the protonic source used. Jackel et al[82] have used a variety of acids and hydrate melts which are listed in Table 1.2. For less than about 76% of the lithium substituted with hydrogen in single crystal lithium niobate, however, a surface layer of rhombohedral $Li_{1-x}H_xNbO_3$ can be formed.[48] The phase diagram of the stoichiometric system $LiNbO_3$-$HNbO_3$ and the structural behaviour of $Li_{1-x}H_xNbO_3$ powder have been studied in detail by Rice et al.[84] The hexagonal lattice parameter C_H has been found to expand and a_H has reduced

Table 1.2 Some Protonic Sources for Hydrogen-exchange (reproduced from literature [82]).

Protonic source	Temperature range (°C)	Results
HNO_3	$T \leq 100$	total exchange
$Mg(NO_3)_2.6H_2O$	$89<T<170$ (loses water at high T)	partial exchange ($x \leq 0.5$)
Benzoic acid	$120<T<250$	partial exchange (x 0.75; etch y-cut)
Benzoic acid + 1% lithium benzoate	$120<T<250$	partial exchange (no etching)
β-naphthoic acid	$185<T\leq300$*	partial exchange etch y-cut

*Must be used in an evacuated container or in inert gas, to prevent decomposition.

progressively as x in the formula $Li_{1-x}H_xNbO_3$ increases. Complicated structural behaviour has been identified for $0.56 \leq x < 0.75$ where four rhombohedral phases have been identified in the β-$Li_{1-x}H_xNbO_3$ phase. By comparing infrared spectra of lithium niobate powder and congruent single crystal exchanged under the same conditions, using benzoic acid buffered with small portion of lithium benzoate, Rice inferred that the surface x was in the range $0 < x \leq 0.12$ (α-$Li_{1-x}H_xNbO_3$ phase), although other workers previously estimated $x = 0.72$,[71] $0.58 < x < 0.72$[58] and $x \simeq 0.8$[48] for guides fabricated in neat benzoic acid. For greater extents of exchange ($0.76 \leq x \leq 1$) a drastic structural change of rhombohedral lithium niobate to cubic $HNbO_3$ occurs. This change in structure is accompanied by a change in volume which, in the case of a single crystal, exerts a large strain on the interface between the waveguiding layer and the bulk. This eventually leads to a plastic relaxation by breaking up the surface of the crystal and destruction of the waveguiding layer.[68] The preparation of hydrogen niobate was first reported by Jackel et al[45] by a topotactic reaction of $LiNbO_3$ powder in $Mg(NO_3)_2.6H_2O$ at 195°C. Later, Rice et al[46] and Fourquet et al[85] characterized its structure by x-ray and neutron diffraction thermogravimetric analysis and NMR spectroscopy. Strong acids such as HNO_3, HF and H_2SO_4 have been reported to cause severe etching of single crystal lithium niobate, the process was used by Nassau[86] to polish or etch $LiNbO_3$ crystals at temperature ranging from room temperature to 100°C.

Hydrogen-exchange reactions at high temperatures and over a long period have been found to etch y-cut, x-cut and y-cut $LiNbO_3$ when benzoic and phosphoric acid were used respectively. However, only partial exchange using these acids is necessary for waveguide fabrication.

1.4 SOME CHEMISTRY OF BENZOIC AND PHOSPHORIC ACIDS.

Benzoic acid ($C_6H_5CO_2H$) is a simple carboxylic acid which is a colourless crystalline solid at room temperature. The crystal structure of benzoic acid has been determined by Feld et al using x-ray and single crystal neutron diffraction methods,[87,88] it consists of centrosymmetric dimers in which two molecules are linked by a pair of hydrogen bonds between their carboxyl groups, see figure 1.5 . Furic [89] has examined the structure of molten benzoic acid by Raman spectroscopy. He proposed that the dimer possesses a symmetry lower than that in the solid at room temperature and that it is not a planar structure.

Benzoic acid has been chosen as a protonic source for the hydrogen-exchange reactions since it possesses a large liquid range, m.p = 122°C; b.p = 249°C, and hence the exchange reactions have been carried out at temperature range between 150 to 250°C.[57] In addition, benzoic acid is non-toxic, inexpensive and easy to handle.

Figure 1.5 The centrosymmetric dimer of Benzoic acid. The monomer units are linked by a pair of hydrogen bonds with O-H....O always close to 2.64 $\overset{o}{A}$. The four atoms ($C-CO_2$) constituting a carboxyl group are coplanar. The intervening centre of symmetry here is marked by an asterisk (Feld et al[87])

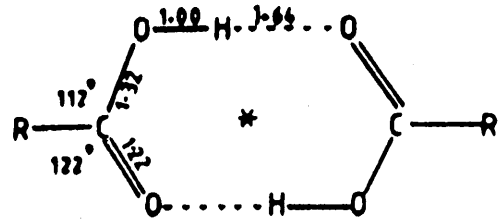

Recently, Bollmann[91] has suggested a mechanism for the hydrogen-exchanged reactions between benzoic acid and lithium niobate single crystal. He assumed that molten benzoic acid decomposes slowly into anhydride benzoic acid and water according to the equation

$$2C_6H_5COOH \longrightarrow (C_6H_5CO)_2O + H_2O \qquad (1.4)$$

The water reacts with O^{2-} ions at the surface of the $LiNbO_3$ crystal according to the equation

$$H_2O + \overset{2-}{O} \longrightarrow 2OH^- \qquad (1.5)$$

Hydrogen-exchange of lithium niobate in orthophosphoric acid was first proposed by Yokomoto et al.[83,92] The results published indicated that phosphoric acid produces a higher change in the refractive index ($\Delta n_e = 0.145$) than in the case of benzoic acid ($\Delta n_e = 0.128$) which implies a higher confinement of the optical energy and higher power densities in the waveguide. This is particularly important for non-linear integrated optics applications.[93,94,95,96] Orthophosphoric acid (monophosphoric acid) H_3PO_4 is the simplest oxyacid of phosphorus. It has a strong ionizing hydrogen atom and dissociates according to the scheme

$$H_3PO_4 \rightleftharpoons H^+ + H_2PO_4^- \rightleftharpoons 2H^+ + HPO_4^{2-} \rightleftharpoons 3H^+ + PO_4^{3-} \qquad (1.6)$$

with dissociation constants $K_1 = 7.1 \times 10^{-3}$, $K_2 = 6.3 \times 10^{-8}$ and $K_3 = 4.4 \times 10^{-13}$. Anhydrous crystalline H_3PO_4, m.p = 42.3°C, when pure melts to a syrupy liquid which can

readily be supercooled to produce a glass.[97] The structure of orthophosphoric acid consists of a hydrogen bonded layer structure in which each $OP(OH)_3$ molecule is linked to 6 others by H bonds. A diagram of the crystal structure is presented in figure 1.6 . In a dilute aqueous solution H_3PO_4 behaves similarly to a strong acid but all the acid species described in equation 1.6 are present.[98] Molten orthophosphoric acid dissociates extensively to produce pyrophosphoric acid ($H_4P_2O_7$), $H_4PO_4^+$ and $H_2PO_4^-$ ions.[99] The reactions are described by the equations

$$2H_3PO_4 \rightleftharpoons H_2O + H_4P_2O_7 \qquad (1.7)$$

$$2H_3PO_4 \rightleftharpoons P(OH)_4^+ + H_2PO_4^- \qquad (1.8)$$

Pyrophosphoric acid (diphosphoric acid) $H_4P_2O_7$ is the second member of the linear polyphosphoric acid series. It exists in two anhydrous crystalline forms with melting points 54.3 and 71.5°C. It is very hygroscopic. In dilute aqueous solution, $H_4P_2O_7$ is a stronger acid than H_3PO_4 ; the four dissociation constants at 25°C are ; $K_1 = 10^{-1}$, $K_2 = 1.5\times10^{-2}$, $K_3 = 2.7\times10^{-7}$ and $K_4 = 2.4\times10^{-10}$ Condensed polyphosphoric acids can be made readily by evaporating orthophosphoric acid or by adding phosphorus pentoxide to phosphoric acid. During the process of preparing condensed phosphoric acids by evaporation of water from orthophosphoric acid, the liquid became brown when a platinum crucible was used. The intensity of the colouration depended on the heating time and on the temperature. However, by continued heating the

Figure 1.6 The structure of orthophosphoric acid (H_3PO_4), it has a continuous two-dimensional sheet-like structure formed by hydrogen bonds. (Corbridge[97]).

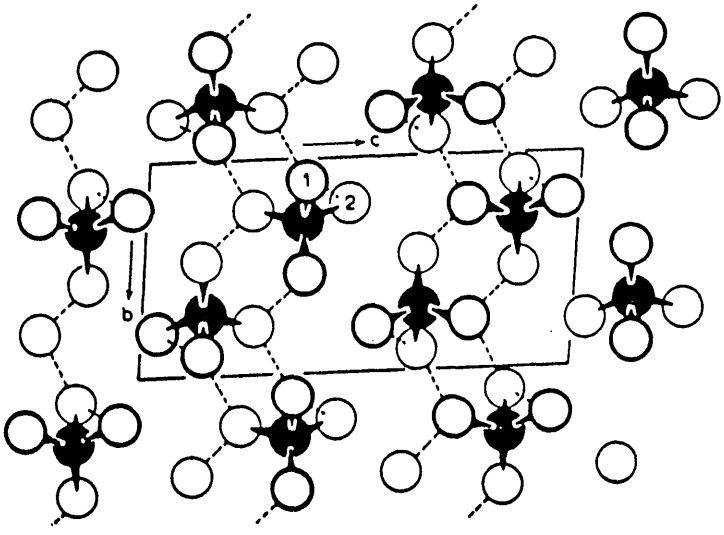

colouration, a deep reddish amber, could be quite intense.[100]

The condensation reactions produce long chain polyphosphoric acids of general composition ($H_{n+2}P_nO_{3n+1}$).[101] The drawbacks of fabricating waveguides in phosphoric acid have appeared during the measurements of the electro-optic coefficients which showed a reduction to $^1/_{30}$ of the constants in the bulk crystals compared to $^1/_{20}$ in the case of benzoic acid samples.[102] Fabrication is limited to z-cut $LiNbO_3$ crystals since phosphoric acid damages x- and y-cut $LiNbO_3$.

1.5 THE AIM OF THE PRESENT WORK.

Work has been carried out at the University of Glasgow by A. Loni[78] on the properties of [^{2}H]-labelled hydrogen-exchanged waveguides and the [^{1}H - ^{2}H]-hydrogen isotopic-exchange on [^{1}H] hydrogen-exchanged waveguides.

The aim of the present work is to study and characterize [^{2}H]-labelled hydrogen-exchanged waveguides fabricated using [^{2}H]-hydrogen labelled benzoic and phosphoric acids on x- and z-cut $LiNbO_3$. The stability of these waveguides, to the ambient atmosphere, was investigated using the [^{1}H - ^{2}H]hydrogen isotopic-exchange, infrared spectroscopy, and the prism coupling technique. Atomic absorption spectroscopy was used to determine quantitatively, the lithium out diffused from the crystal and present in the acid. Yamamoto et al[83] reported

the fabrication of superior waveguides by hydrogen-exchange using phosphoric acid. The optical and infrared properties of waveguides fabricated using pyrophosphoric and orthophosphoric, prepared were assessed on z-cut $LiNbO_3$. Monomoded waveguides were fabricated for the first time on x-cut $LiNbO_3$.

1.6 THE TECHNIQUES USED IN THIS STUDY.

1.6.1 Infrared Spectroscopy.

Infrared spectra originate from transitions between vibrational levels of a molecule in the electronic ground state which are induced by infrared radiation (10^2-10^4 cm^{-1} or 1-10^2 μm). The hydroxyl stretching region (2000-4000 cm^{-1}) has been observed to characterize the hydrogen-exchanged waveguides in lithium niobate. In the case of [^{2}H]-labelled hydrogen-exchanged waveguides, the vibrational frequencies were observed to occur at lower frequencies than those of [^{1}H]hydrogen-exchanged waveguides. The large isotopic mass effect of deuterium upon the vibrating oscillator containing such atom reduces the frequency of oscillation.[103] This change in frequency can be predicted theoretically in the case of a diatomic O - D stretching frequency with respect to a O - H oscillator by the ratio

$$\frac{F_D}{F_H} = \sqrt{\frac{(m + 2)}{(2m + 2)}}$$

where m is the mass of oxygen atoms.[104]

Hydroxyl OH bands are present in the OH stretching region in bulk single crystal $LiNbO_3$ at $\nu_{max} = 3480\ cm^{-1}$. They have been reported as defects in the crystal structure.[105,106] It has been proposed that the OH groups were incorporated into bulk $LiNbO_3$ from moisture in the atmosphere, either during crystal growth or during poling of the crystal. This band consisted of two peaks and had been found to be polarized perpendicular to the C-axis to within $\pm 5^{\circ}$. Later, Kovacs et al [107] found a dependency of the number and shape of the bands on the stoichiometry of the crystal, these bands are reproduced in figure 1.7. For the hydrogen-exchanged waveguides in x-cut $LiNbO_3$, infrared spectra showed two absorption bands, a sharp well-defined band at $\nu_{max} = 3505\ cm^{-1}$ and a broad band at $\nu_{max} = 3250\ cm^{-1}$ overlaps the sharp absorption band. In z-cut hydrogen-exchanged waveguides, a sharp band at $\nu_{max} = 3505\ cm^{-1}$ and a trace of the broad band at $\nu_{max} = 3250\ cm^{-1}$ could only be observed.

Spectra of $[^2H]$-labelled hydrogen-exchanged waveguides show a sharp narrow band at $\nu_{max} = 2588\ cm^{-1}$ overlapping a broad band at $\nu_{max} = 2410\ cm^{-1}$ for x-cut and a sharp band at $\nu_{max} = 2588\ cm^{-1}$ overlap a trace of the broad band at $\nu_{max} = 2410\ cm^{-1}$ for z-cut $LiNbO_3$. Infrared bands of x- and z-cut $[^1H]$- and $[^2H]$-labelled hydrogen-exchanged waveguides are shown in figure 1.8a,b,c,d.

The shape of the infrared bands in x- and z-cut $LiNbO_3$ hydrogen-exchanged waveguides can be rationalised

Figure 1.7 Infrared absorption bands of $LiNbO_3$ crystals of various compositions, dashed lines indicating the results of a Gaussian fitting. The spectra were measured at room temperature (Kovács et al[107]).

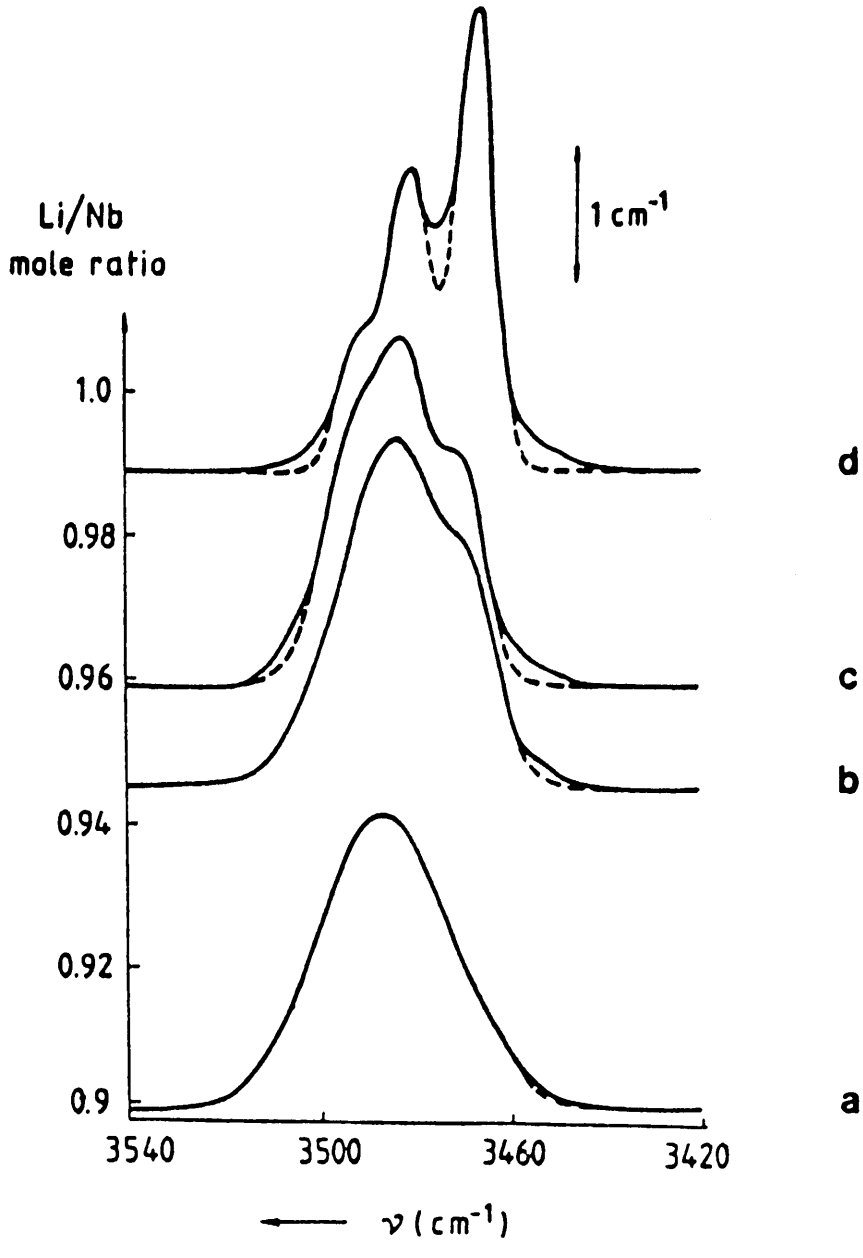

Figure 1.8 Infrared spectra of X- and Z-cut $LiNbO_3$ waveguides. Spectra (a) and [(b)] are X- and [Z-cut] $LiNbO_3$ [^1H] hydrogen-exchanged at 235°C [230°C] for 4h [4h] ; F7, [F6]. Spectra (c) and [(d)] are X- and [Z-cut] $LiNbO_3$, [^2H] hydrogen-exchanged at 235°C [225°C] for 3.5h [4h] in air [Ar atmosphere] ; FD1, [FD3] .

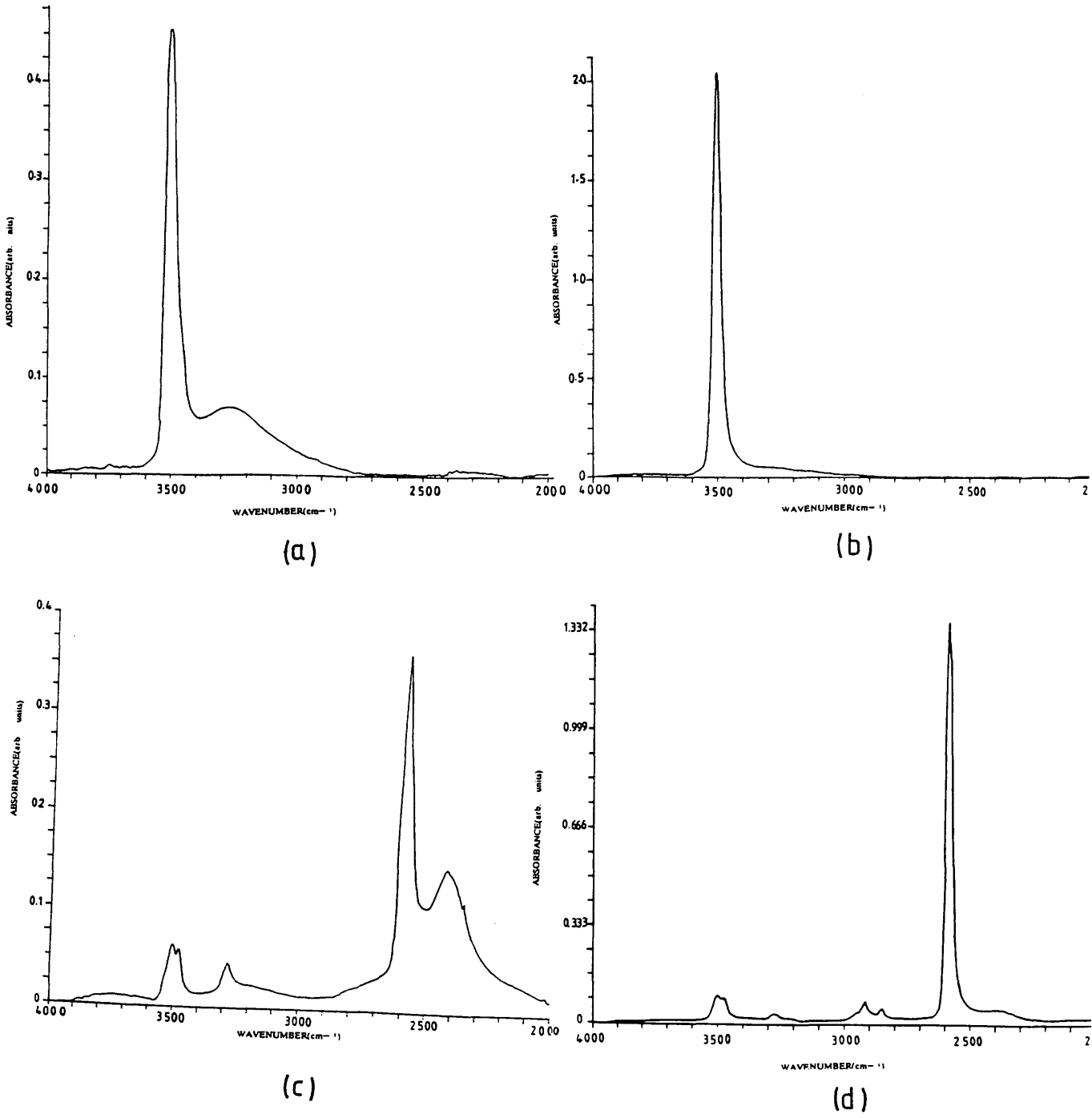

by considering the potential energy curves for the vibrating OH - groups. It is assumed that the hydrogen vibrates against the massive and approximately stationary oxygen atom. A free hydroxyl group has a narrow potential energy curve corresponding to a narrow potential well.[109] Such a potential gives rise to a sharp, well-defined band at ν_{max} = 3505 cm^{-1} in x- and z-cut hydrogen-exchanged waveguides. Hydrogen-bonded OH-hydroxyl groups have broad potential energy curves and give rise to the broad absorption band at ν_{max} = 3250 cm^{-1} in x-cut hydrogen-exchanged waveguides.

Polarized infrared radiation, where the electric vectors of the radiation are parallel and oriented along a unique axis, has been used to gain information on the directionality of the bonds in the hydroxyl stretching region of the [^{1}H]- and [^{2}H]-labelled hydrogen-exchanged waveguides. The relationships between the polarization direction of the radiation and the crystal axes are shown in Figure 1.9a,b,c,d.

1.6.2 Atomic Absorption Spectroscopy.

The atomic absorption spectroscopy technique has been used to detect and determine the lithium out diffused from the $LiNbO_3$ crystal during the hydrogen-exchange reactions and thus present in the reacted acid. The technique involves spraying a nebulised aqueous solution of the analyte sample into a high-temperature flame (1200 - 1500°C), producing an atomic vapour in which most of the atoms are in an unexcited state.[110] The atoms

Figure 1.9 Relationships of the polarized infrared radiation with the crystal geometry of $LiNbO_3$ waveguides.

(a) 0^o polarization, E-vector is along the Y-axis of Z-cut $LiNbO_3$.

(b) 90^o polarization, E-vector is along the X-axis of Z-cut $LiNbO_3$.

(c) 0^o polarization, E-vector is along the Y-axis of X-cut $LiNbO_3$.

(d) 90^o polarization, E-vector is along the Z-axis of X-cut $LiNbO_3$.

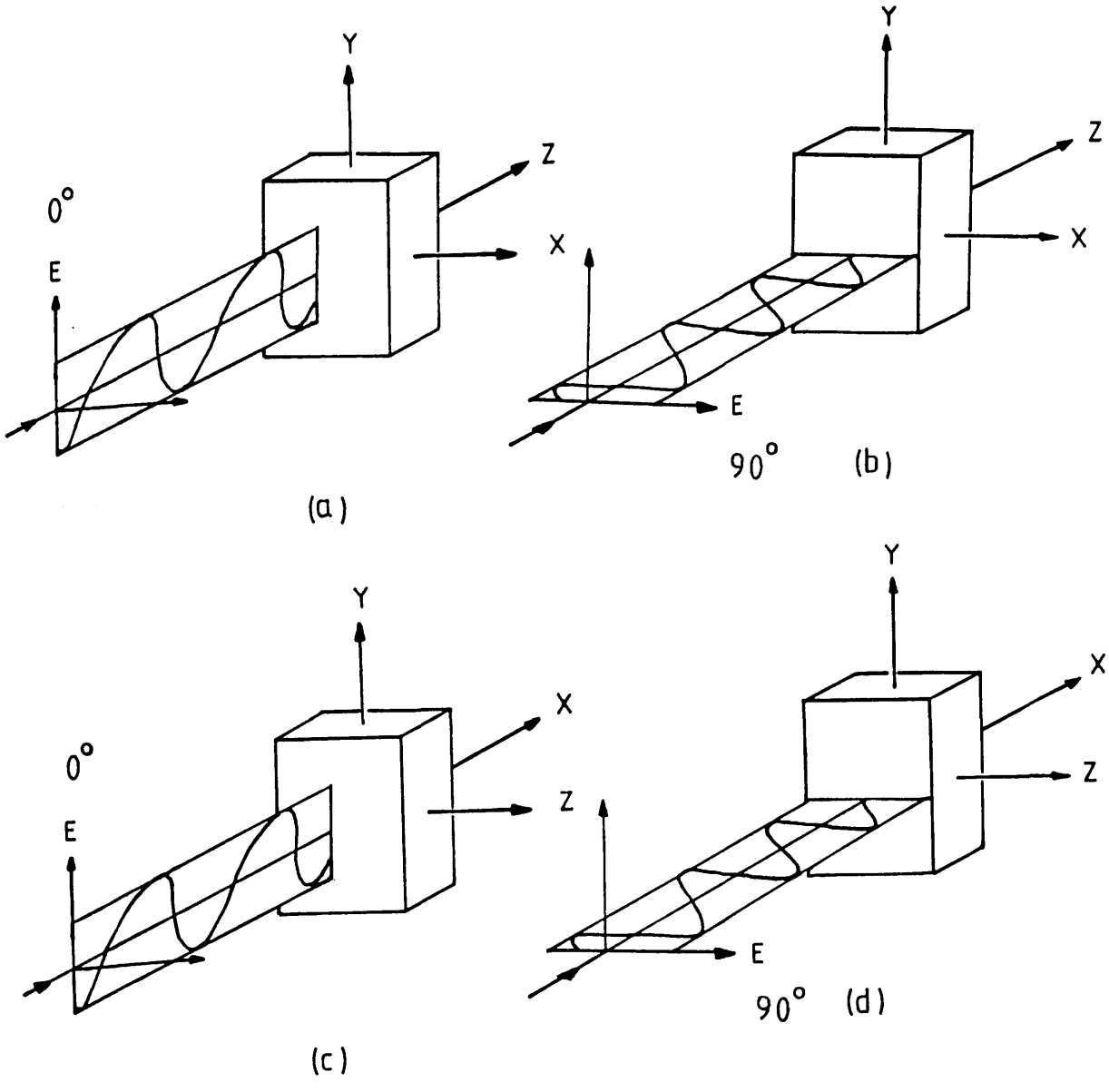

then, excited by absorbing photons of a selected wavelength of light passed through the flame. The transmitted intensity is then detected and compared with a reference intensity and the absorption can be estimated. The absorption is directly proportional to the atomic population in the flame.[111] The sensitivity of the spectrometer (Perkin Elmer 306) was approximately 0.035 μg/ml for 1% absorption.[111,112]

1.6.3 The Prism-Coupling Technique.

The prism coupling technique[3,113] has been employed to characterise the hydrogen-exchanged optical waveguide. The physical principle of the technique depends on clipping a prism, made of a material with refractive index higher than that of the waveguide, to the waveguiding layer and shining a laser beam on the face of the prism. This incoming beam totally reflects at the base of the prism and the light wave in the prism is coupled into the waveguide through the evanescent fields. This is shown in figure 1.10a. The laser beam, therefore propagates in the waveguide by the total internal reflection. The propagating optical modes can be represented geometrically by a zig zag wave, figure 1.10b. By changing the angle of the incident laser beam, different propagating modes can be excited. From the measured angle (between the incident beam and the normal to the prism face), the effective refractive index can be

Figure 1.10a. In the prism coupler, the light wave from a laser, is totally reflected at the prism base. The field distributions in the prism and in the film show that their evanescent fields overlap each other in the gap region (Tien[3]).

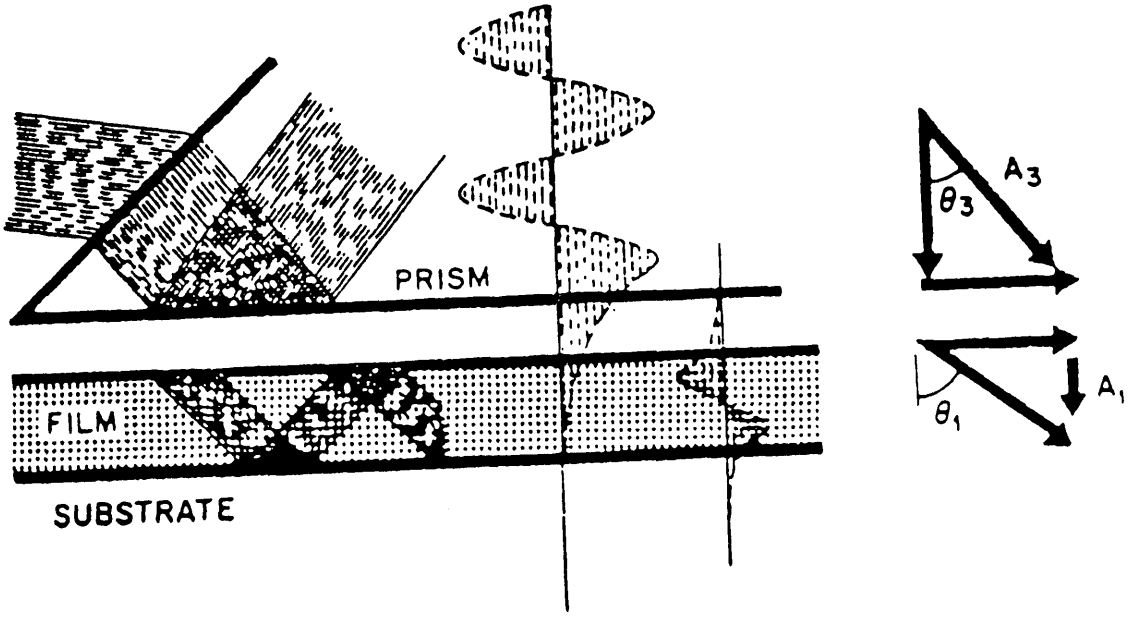

Figure 1.10b The properties of the normal propagating modes of a waveguide. The m = 0 mode has the largest zigzag angle and m = 4 has a zigzag angle close to the critical angle (Tien[3]).

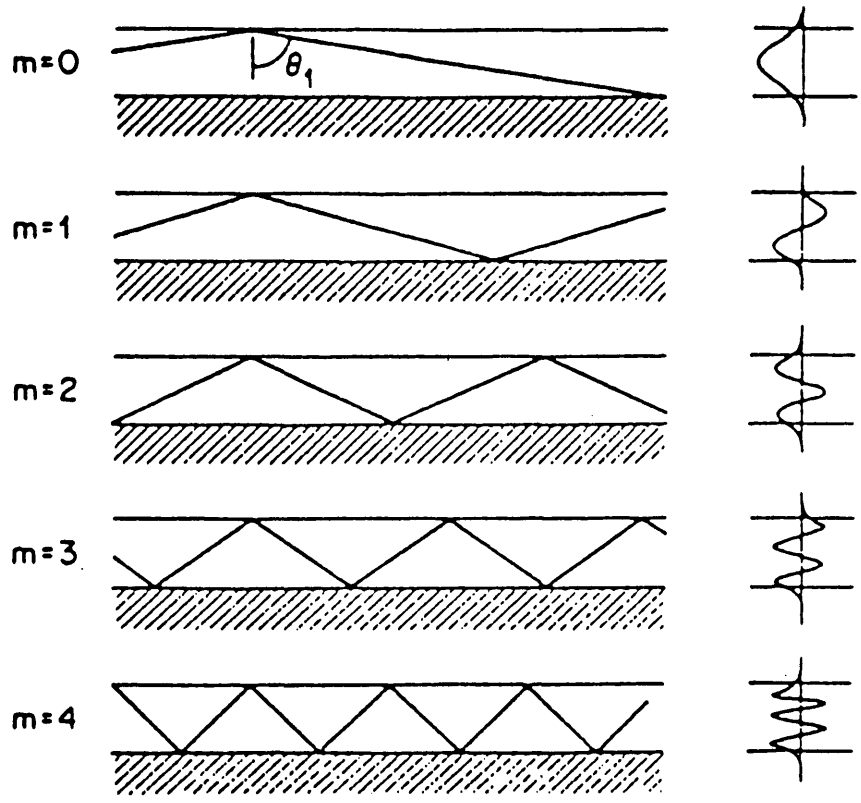

calculated using the equation

$$N_{eff} = n_p \text{ Sin } [A + \text{Sin}^{-1}(\frac{\text{Sin}\theta_i}{n_p})] \qquad (1.9)$$

where n_p is the refractive index of the prism, θ_i is the measured incident angle. Derivation of equation 1.9 is presented in appendix A.

The refractive index profiles of the waveguides have been calculated by two different computer programs. In the first, the step index program, the effective refractive indices were used as the input for a program based on normalised step index equations given by Kogelink and Ramaswamy.[114] The step index assumption has been verified by modelling the diffusion profile of the planar waveguides by a finite difference solution of one dimensional ion exchange equation.[56,115] In the second program, the WKB method[116,117] was used. This method assumes that the index/depth profile of the waveguide n(x) can be represented approximately by a piece-wise linear function. The profile was determined by calculating the depth at which the refractive index in the guiding medium is equal to the effective index of the supported mode, using an area-minimizing technique to estimate both the best-fit turning point, depth of each mode and the waveguide depth. A typical step-like profile of the refractive index of a hydrogen-exchanged waveguide in x-cut $LiNbO_3$ is depicted in figure 1.11. By plotting the waveguide depths (diffusion depths) versus the(reaction

Figure 1.11 A typical refractive index/depth profile of a [^{1}H] hydrogen-exchange waveguide, F3.

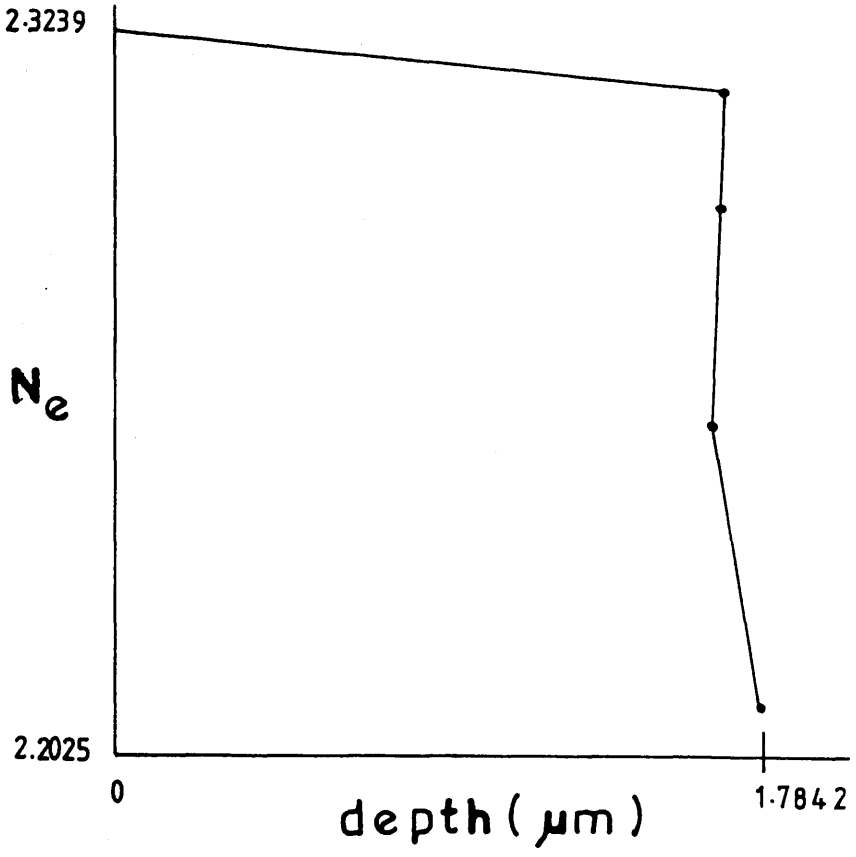

times)$^{\frac{1}{2}}$, the diffusion coefficient can be produced, assuming the diffusion depth varies as:

$$d = 2\ (t.D(T))^{\frac{1}{2}} \qquad (1.10)$$

where d is the waveguide depth (μm), t is the reaction time (h) and D(T) is the diffusion coefficient. The dependence of D on temperature is given by the Arrhenius law:

$$D(T) = D_o\ Exp\ (-Q/RT) \qquad (1.11)$$

where D_o is a constant, R is the universal gas constant and Q is the activation energy.[118]

CHAPTER TWO.

EXPERIMENTAL TECHNIQUES USED FOR THE CHARACTERISATION OF [^{1}H]- AND [^{2}H] HYDROGEN-EXCHANGED LITHIUM NIOBATE OPTICAL WAVEGUIDES.

2.1 PREPARATION OF MATERIALS.

2.1.1 Vacuum line, glove box and chemicals.

A Pyrex glass high vacuum line consisting of a rotary vacuum pump (SPEEDOVAC), a glass mercury diffusion pump (Jencons) and a manifold to transfer materials under vacuum was employed in this work. An indication of the pressure in the line was obtained using an Edwards model 2G vacustat gauge; pressures were usually 10^{-3} mbar or lower. Standard glass joints were greased with Apiezon N high vacuum grease. Manipulations involving moisture sensitive and [^{2}H]-hydrogen labelled compounds were carried out in a nitrogen atmosphere glove box (Lintott) in which the moisture level was in the range 2 - 10 p.p.m. The chemicals used together with their purity and their suppliers are listed in Table 2.1.

2.1.2 Preparation of the substrate.

Single crystal lithium niobate wafers (supplied by Barr and Stroud Ltd, Pilkington electro-optic materials) of congruent composition (48.45% mole Li_2O, 51.55 % mole Nb_2O_5) were cut to a high precision along the crystallographic lattice parameters that were x-ray-defined by the supplier. The samples were cut to a typical dimension of 0.1 x 0.5 x 1.5 cm and mechanically polished on both faces to an optically smooth finish (using Syton W15 submicron powder) for infrared spectroscopy.

Table 2.1 : Chemicals used in the study.

	Purity	Supplier
Benzoyl chloride (gold label)	99+%	Aldrich
Phosphorus pentoxide	>99%	Koch-Light
Phosphorus oxychloride	>99%	Koch-Light
Benzoic acid	AnalaR	B.D.H.
85% Orthophosphoric acid.	AnalaR	B.D.H.
Pyrophosphoric acid.	99%	Fluka
$[^2H]$-Hydrogen labelled water	99.8%	Fluorochem
Lithium nitrate (1000 p.p.m)	Spectrosol	B.D.H.
Absolute alcohol	99.86%	James Burrogh

The samples were degreased and carefully cleaned by soaking in 1,1,1-trichloroethane, methanol and acetone successively, with 5 min ultrasonic agitation in each case. Finally, the samples were washed with isopropyl alcohol and blow dried. This cleaning procedure was adopted to ensure clean surfaces of the sample on which the wave-guide structure would be formed.

The infrared spectrum of the crystals after cleaning showed no sign of additional OH hydroxyl group absorption as a result of this procedure.

2.1.3 Preparation of the acids used for the exchange reaction.

2.1.3.1 Preparation of benzoic acid.

Benzoic acid was prepared according to the equation:-

$$C_6H_5COCl + H_2O \rightarrow C_6H_5CO_2H + HCl \qquad (2.1)$$

The apparatus used for the preparation is shown in figure 2.1, it consisted of an arrangement of PTFE/Pyrex glass stopcocks denoted S1, S2 and S3 (Rotaflo and J. Young). Water (3.6 cm^3) was added dropwise through stopcock S1 to benzoyl chloride (2.8 cm^3). The mixture was stirred thoroughly using a magnetic stirrer and heated to 115-120^oC using an oilbath over a period of 2 h, it was then allowed to cool and a colourless solid was obtained. The hydrogen chloride generated during the reaction was removed through S3. The solid was dried by pumping overnight in vacuo.

Figure 2.1 The apparatus used to prepare ordinary and [^{2}H]-hydrogen labelled benzoic acid. S1, S2 and S3 are PTFE/Pyrex glass stopcocks.

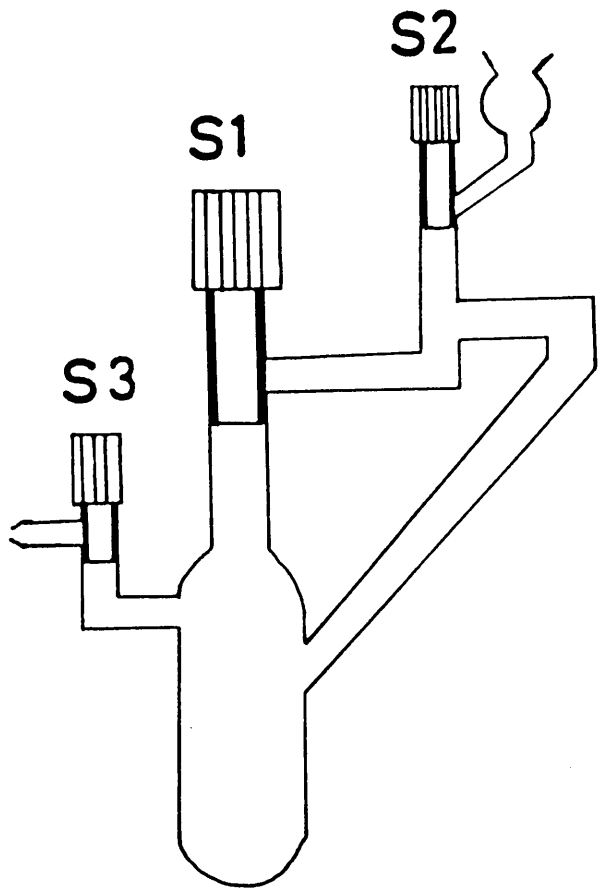

The infrared spectra of the product was identical to that of AnalaR benzoic acid. Its melting point was 122.5°C. The quoted temperature required for benzoic acid is 121 - 123°C.[90]

2.1.3.2 Preparation of [^{2}H]-hydrogen labelled benzoic acid ($C_6H_5CO_2{}^2H$).

[^{2}H]-Hydrogen labelled benzoic acid was prepared according to the equation:-

$$C_6H_5COCl + {}^2H_2O \rightarrow C_6H_5CO_2{}^2H + {}^2HCl \qquad (2.2)$$

Using the apparatus described in section 2.1.3.1, [^{2}H]-hydrogen labelled water (2.6 cm^3) was added through stopcock S1 to benzoyl chloride (18.2 cm^3). During the reaction, stopcock S2 was kept closed whilst S3 was open and connected to a U-shaped tube containing a layer of phosphorus pentoxide and cooled to -78°C using a dichloromethane, dry ice bath to prevent moisture in the air gaining access to the apparatus. Later, additional [^{2}H]-hydrogen labelled water (0.5 cm^3) was added to ensure a high degree of ^{2}H incorporation in the hydroxyl group. The mixture was heated for 2 h, and then allowed to cool. It was degassed and volatile materials, the residue of [^{2}H] labelled water and hydrogen chloride, were removed by pumping. Finally, the product was sealed and transferred into the glove box.

The infrared spectrum of the [^{2}H]-hydrogen labelled

acid was in agreement with literature.[119,120] The melting point of the [^{2}H]-hydrogen labelled acid was 118^{o}C. The fundamental frequencies for ordinary and [^{2}H]-hydrogen labelled benzoic acid are listed in Table 2.2.

2.1.3.3 Preparation of Orthophosphoric acid (H_3PO_4).

[^{1}H]- and [^{2}H]-Hydrogen labelled orthophosphoric acids were prepared by four different methods as described below.

In the first method, orthophosphoric acid was prepared according to the equation:-

$$H_4P_2O_7 + H_2O \rightarrow 2H_3PO_4 \qquad (2.3)$$

Colourless crystalline pyrophosphoric acid (11.68 gm) was refluxed in water (1.2 cm^3) overnight at 105^{o}C in a 50 ml round-bottomed flask to give an off-white crystalline substance which was transferred in the stoppered reaction vessel to the glove box. In the second procedure, orthophosphoric acid was prepared by slow hydrolysis of phosphorus pentoxide according to the equation:-

$$P_4O_{10} + 6H_2O \rightarrow 4H_3PO_4 \qquad (2.4)$$

Phosphorus pentoxide was first purified by sublimation at 270^{o}C under vacuum using the apparatus shown in figure 2.2a. The starting material was placed in a 2 inch diameter Pyrex glass vessel previously flamed out using an oxygen/ methane torch, the temperature was raised using a small

Table 2.2 : Infrared fundamental frequencies of the prepared ordinary and [^{2}H]-hydrogen labelled benzoic acid in the region 3500 - 600 cm^{-1}.

Ordinary benzoic acid (cm^{-1})	[^{2}H]-hydrogen labelled benzoic acid (cm^{-1})	Assignment (104, 119, 120, 121)
	648 (s)	out-of-plane O-D def.
710 (vs)	720 (vs)	out-of-plane ring def.
1027 (m)	1027 (m)	O-D def. — -C-H bend and semistretch
	1042 (s)	
1073 (m)	1073 (m)	
1100 (w)		
1180 (m)		
1290 (vs)	1290 (w)	C-O ring stretch
	1367 (vs)	O-D def.
1420 (s)		O-H def.
1453 (s)	1453 (vs)	C-H def. and
1493 (w)	1493 (m)	semistretch
1584 (s)	1583 (s)	C=C quadrant stretch
1604 (s)	1604 (m)	
1689 (vs)	1690 (vs)	C=O stretch of dimeric unit
1792 (w)		
	1853 (w)	
	1910 (w)	
	2173 (m)	O-D stretch
	2240 (s)	
2833 (w)		
2924 (w)	2924 (w)	C-H stretch
3077 (w)	3074 (w)	

vs = very strong; s = strong; m = medium; w = weak;
vw = very weak.

Figure 2.2.a The apparatus used to purify phosphorus pentoxide.

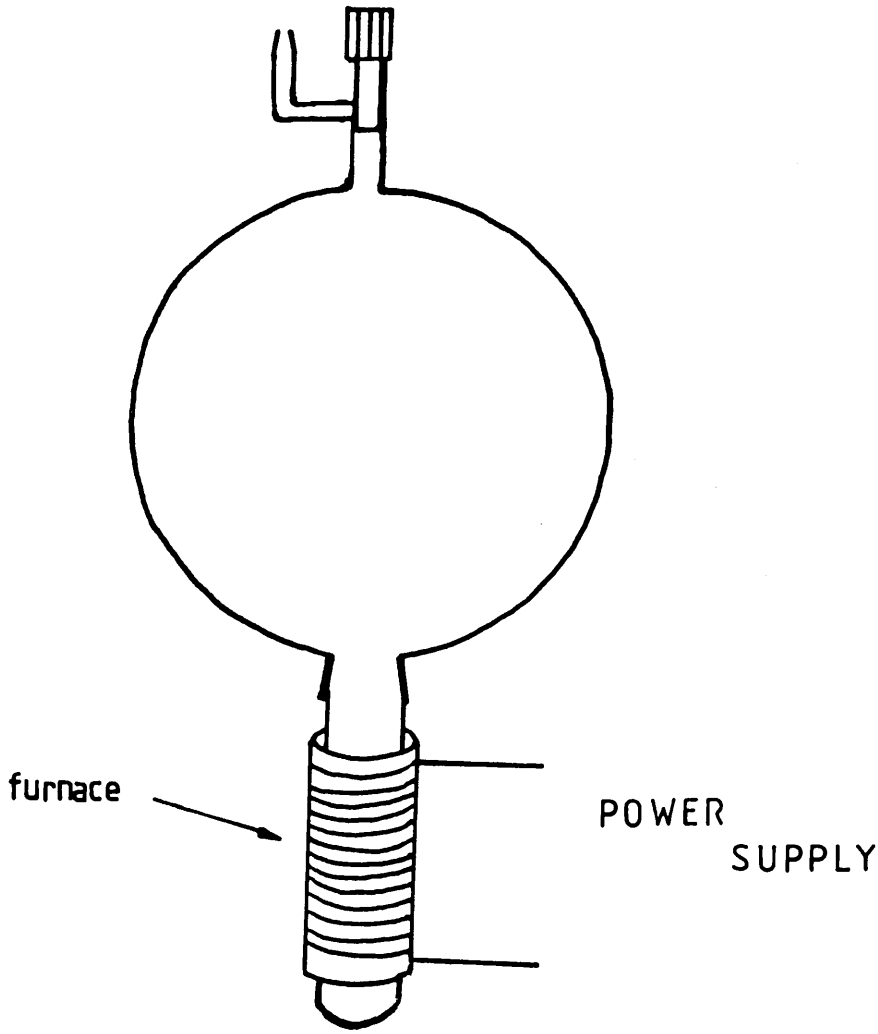

calibrated furnace (a tungsten wire wound around a 2.5 inch diameter Pyrex glass cylinder). The vessel was joined with greased joints to a round-bottomed flask in which it was attached to the vacuum line.

Purified phosphorus pentoxide was collected from the flask, crushed, then accurately weighed (4.34 gm) and transferred into one limb of the evacuable vessel shown in figure 2.2b, the amount of water (1.65 gm) needed for a stoichiometric reaction was added to the second limb. 1,1,3-Trichlorotrifluoroethane (5 cm^3) was added to the phosphorus pentoxide then the mixture was cooled to just below room temperature whilst water was added by distillation by heating with a hot air gun.

This procedure was used for two reasons: firstly, it had been observed that the reaction was very exothermic and could produce an explosion, and secondly, phosphorus pentoxide was found to "skin" with a mixture of metaphosphoric acids formed as intermediate products. After reaction the trichlorotrifluoroethane was removed by vacuum distillation to leave colourless solid.

Orthophosphoric acid was prepared, in the third procedure, according to the equation:-

$$POCl_3 + 3H_2O \rightarrow H_3PO_4 + 3HCl \qquad (2.5)$$

Phosphorus oxychloride was hydrolysed using the apparatus described in section 1.1.3.1. Water (4.4 cm^3) was added dropwise through stopcock S2 on the phosphorus

Figure 2.2.b The evacuable Pyrex glass vessel used to prepare orthophosphoric acid.

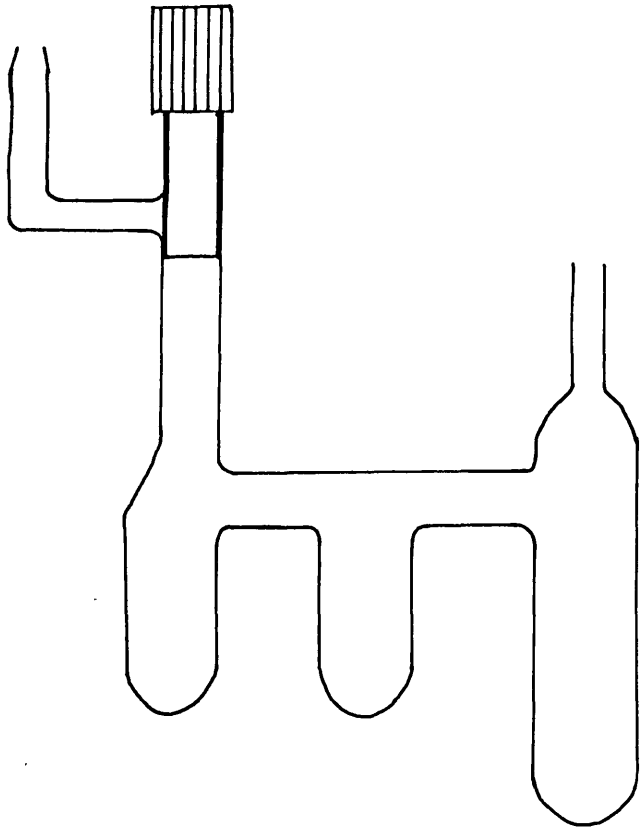

oxychloride (7.6 cm^3), the mixture was brought to 90°C and stirred magnetically for 2 h. The product was allowed to cool and dried under vacuum. Over a period of 5 days the acid solidified to a colourless crystalline mass. This method was also employed to prepare [^{2}H]-hydrogen labelled orthophosphoric acid. In an analogous procedure to that described above, [^{2}H]-hydrogen labelled water (6.85 cm^3) was added to phosphorus oxychloride (11.62 cm^3), the mixture was heated to 80°C and stirred for 2.5 h whereupon the resulting product was a colourless solid. Subsequently, the acid was allowed to cool and dried under vacuum. It was observed to form a colourless crystalline substance within 3 days. The ordinary and [^{2}H]-hydrogen labelled orthophosphoric acids were characterized by infrared and Raman spectroscopy, and were in agreement with the literature.[124,122,123] The fundamental frequencies of infrared and Raman spectra for ordinary and [^{2}H]-hydrogen labelled orthophosphoric acids are listed in Table 2.3.

2.1.4 Preparation of the hydrogen-exchanged waveguides.

The hydrogen-exchange reactions[47] were carried out under two different sets of conditions which were: (a) in an ambient atmosphere, and (b) under N_2 atmosphere. In case (a), the $LiNbO_3$ sample was placed in a PTFE holder (inner diameter 1.5 cm, height 3 cm) which, in turn, was placed in a covered silica glass beaker containing the acid. The PTFE holder was perforated with a number of holes (diameter 4 mm) enough to provide an even flow of the

Table 2.3 Infrared and Raman fundamental frequencies of ordinary and [^{2}H]-hydrogen labelled orthophosphoric acid.

Infrared Frequencies	
orthophosphoric acid	[^{2}H]-hydrogen labelled orthophosphoric acid
482 (s)	
	880 (w)
	935 (w)
	1052 (br)
1074 (br)	
	1750 (br)
1780 (br)	
2370 (m)	
	2940 (br)
3000 (v.br)	
Raman Frequencies	
390 (m)	
	467 (w)
	486 (w)
525 (w)	
	901 (s)
925 (vs)	
2380 (br)	
	2530 (w)

acid around the sample. The PTFE holder and the silica beaker are shown in figure 2.3. In case (b), the hydrogen-exchange reactions were performed in sealed double limb Pyrex glass vessels with large glass stopcocks.

The acid and the sample were transferred separately into each limb of the vessel inside the glove box to ensure a well-controlled environment during all stages of wave-guide preparation.

The weight of the acid was determined using an Oertling LA 164 electronic balance, by weighing the vessel prior to and after filling with the acid. The vessel, later, was sealed and filled with nitrogen after evacuation using the vacuum line. The nitrogen was dried using a gas drying line in which the gas passed through two traps filled with liquid paraffin then through two traps cooled to (-80 to -90^{o}C) using a bath of dichloromethane and dry ice; subsequently the gas passed through a U-shaped tube filled with silica gel and 4^{o}A molecular sieve to capture any moisture. The excess gas escaped through a T-junction passing through two liquid paraffin filled traps. The gas drying line is illustrated in figure 2.4.

The hydrogen-exchange reactions were carried out in a high temperature oil bath with the temperature controlled to ± 0.25^{o}C. The oil bath was covered to provide a thermally isolated environment and the oil was circulated to ensure an even heat distribution. The acid temperature and the oil temperatures were both calibrated using a

Figure 2.3 The silica glass covered beaker and the perforated PTFE holder used for the hydrogen-exchange reaction undertaken in ambient air.

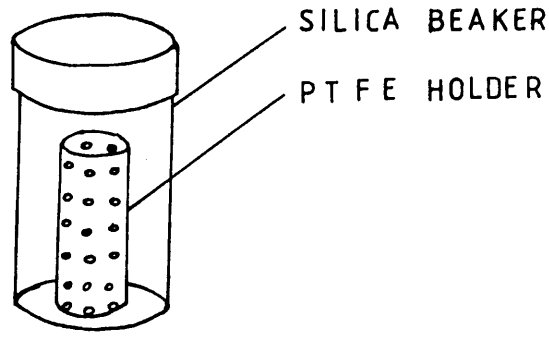

Figure 2.4 The gas drying line used to dry the nitrogen and argon gases which were used as an atmosphere for some of the [^{1}H]- and [^{2}H] hydrogen-exchange reactions.

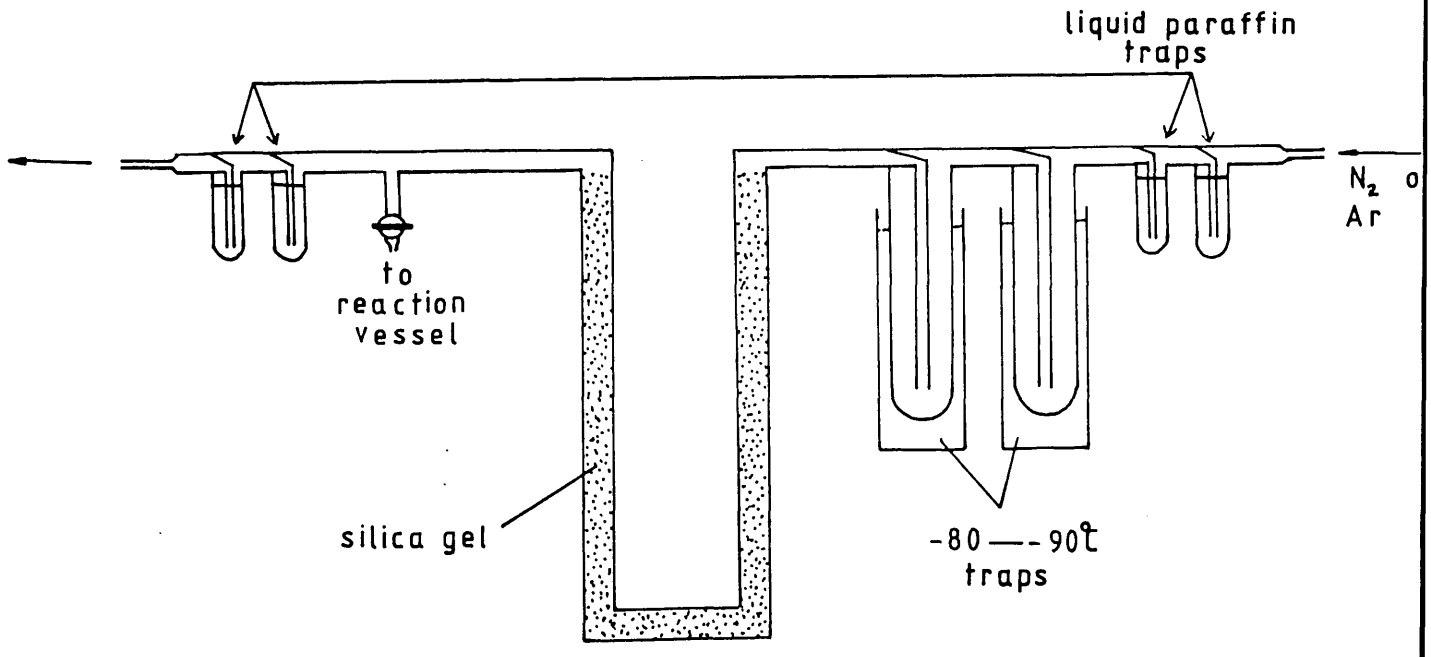

Pt-13% Rh/Pt thermocouple with a $0^{o}C$ reference junction. The difference was $10^{o}C$. All temperatures quoted in this study are the acid temperatures and these were used to calculate diffusion coefficients and the depth of the waveguides. The reaction time is defined as the time interval between the total immersion and removal of the sample from the bath. Following the exchange reaction, the samples were cleaned of the residual acid using chloroform or carbon tetrachloride. The acid was retained after the reaction for lithium analysis by atomic absorption spectroscopy.

2.2 ANNEALING OF THE WAVEGUIDES.

The annealing process [125] was undertaken in a cylindrical furnace with the temperature controlled to $\pm 2^{o}C$, the furnace was temperature-profiled to determine the "hot spot". Annealing was carried out under a flowing "wet oxygen" atmosphere maintained by bubbling the oxygen through a water column (10 cm) which was heated to $70^{o}C$. The flow rate was 1.5 ℓ min^{-1}. The waveguides were mounted on a stainless steel holder designed to ensure even flow of the vapour over the sample surface. The samples were introduced slowly to the hot spot over a period of 3 min to prevent thermal shock. The annealing time is defined as the time interval between reaching and subsequent removal of the samples from the "hot spot".

2.3 DETERMINATION OF LITHIUM IN THE ACID AFTER REACTION BY ATOMIC ABSORPTION SPECTROSCOPY.

2.3.1 Preparation of standard and analyte solutions for atomic absorption spectroscopy.

Due to the difference in the physical properties of benzoic and phosphoric acid, the standard and analyte solutions were prepared as follows. For benzoic acid, the standard solutions were prepared by serial dilution of aqueous lithium nitrate. Accurately weighed portions of AnalaR benzoic acid were dissolved in absolute alcohol (50 cm^3) and added to the solutions, thereafter, the solutions were made up to 100 cm^3 with distilled water. The concentrations of lithium in the standard solutions used were 0(blank), 0.03, 0.05, 0.08, 0.1, 0.3, 0.5, 0.8, 1, 1.5 and 2 $\mu g\ cm^{-3}$.

The analytes were prepared similarly, by dissolving portions of the acid (1.0000± 0.0001g.) in absolute alcohol (50 cm^3) and the solutions were made up to 100 cm^3 with distilled water.

For phosphoric acid samples, the higher solubility of the acid in water eliminated the need to use alcohol. The standards were prepared by dissolving accurately weighed portions of AnalaR orthophosphoric acid (1.0000± 0.0001g.) in distilled water (40 cm^3). Lithium solutions prepared as described above, were added to the standard solutions, and, they were made up to 100 cm^3 with distilled

water. The analytes were prepared by dissolving portions of the reacted acid (1.0000±0.0001g) in distilled water (100 cm^3). Two separately prepared analytes of each individual acid were analysed in each case, the absorbance of each analyte was measured 8 - 10 times.

2.3.2 Determination of lithium in the acid after the exchange reaction.

The lithium present in the acid after the hydrogen-exchange reactions was determined using a Perkin Elmer 306 Atomic Absorption spectrometer in the absorbance mode. The light source was a lithium hollow cathode lamp (λ = 0.678μm) The measured absorptions of the standard solutions were used to produce a calibration curve from which the unknown concentration of the analyte solutions were read off; figure 2.5 shows a typical calibration curve. Errors were calculated for the concentrations using estimated errors in weighing of acid ($\pm 10^{-4}$ g), the solution volumes (± 0.12) and the standard deviation of absorbances.

In order to determine whether the lithium distribution in the acid after reaction was homogeneous, especially in the case of benzoic acid, two lithium niobate samples were exchanged for the same time and temperature. Sample (X1) was [^{1}H] hydrogen-exchanged in air while sample (X2) was [^{2}H] hydrogen-exchanged under nitrogen atmosphere. Six aliquots were prepared separately from each acid and the lithium concentration of each aliquot was calculated as

described above. The 95% reliability intervals[126] were calculated for each acid sample and are presented in Table 2.4. The results indicated that the lithium distribution in the benzoic acid after reaction is uniform and that the concentrations can be determined with a precision between (4.6% and 6.3%). The weight of lithium present in 1 gm of the acid after exchange reaction was calculated by the equation:-

$$W_{Li} = C \times 100 \times \frac{1}{W'} \qquad (2.6)$$

where C = the concentration of lithium for the portion of acid dissolved in 100 cm^3 solution, and W' is the weight of the acid portion dissolved in the analyte solution (Table 2.4).

Figure 2.5 Typical calibration curve of the standard solutions prepared for the atomic absorption spectroscopy.

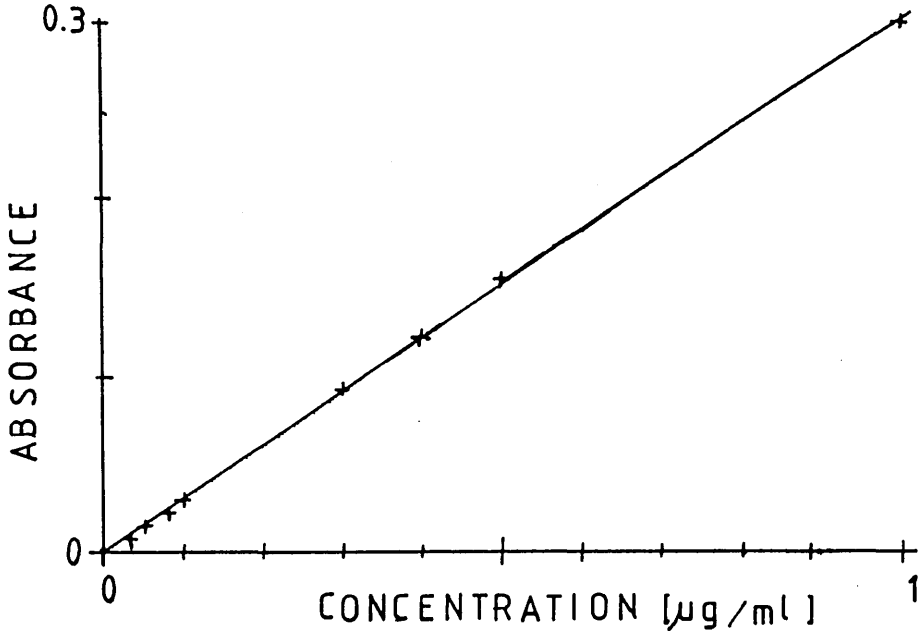

Table 2.4 Reliability interval and Li concentrations in 1gm of acid used to fabricate samples X1 and X2 calculated from atomic absorption spectroscopy results.

Sample	number of replicates	weight of analysed sample (gm)	Li concent. ($\mu g\ cm^{-3}$)	Li concent. Per 1gm of analysed acid	mean (σ) (μgLi/gm acid)	reliability interval (μgLi/gm acid)
X1	6	1.0015	0.08193	0.08180	0.08544	0.08915 -
		1.0000	0.08407	0.08407	(2.687E-3)	0.081730
		1.0008	0.08836	0.08829		
		1.0007	0.08407	0.08402		
		1.0007	0.08878	0.08871		
		1.0004	0.08580	0.08576		
X2	6	1.0000	0.12047	0.12047	0.13019	0.13793-
		1.0015	0.12989	0.12969	(5.177E-3)	0.12245
		1.0008	0.13032	0.13021		
		1.0007	0.13203	0.13193		
		1.0016	0.13417	0.13395		
		1.0010	0.13503	0.13489		

2.4 INFRARED SPECTROSCOPY.

2.4.1 Sample mounting and arrangements for infrared spectroscopic measurements.

A standard brass holder was used for experiments carried out in air and a specially designed gas cell was used for reactions involving moisture sensitive compounds. The evacuable infrared gas cell had CaF_2 windows at each end and a B14 cone connected to a stopcock; figure 2.6, illustrates the infrared gas cell. The waveguide sample was placed on a L-shaped holder with a narrow groove on the inner side where the sample was held. The gas cell was supported by an aluminium holder to ensure reproducible positioning in the spectrometer.

The infrared spectroscopy measurements were carried out using a Perkin Elmer 983 spectrometer with a data station so that the initial spectrum of each sample prior to exchange could be subtracted from that obtained after reactions (see section 1.5.1).

2.4.2 [^{1}H]- and [^{2}H]-hydrogen isotopic-exchange in the infrared gas cell.

A set of hydrogen isotopic-exchange experiments was performed on [^{2}H] hydrogen-exchanged, X- and Z- cut waveguides fabricated in [^{2}H]-hydrogen labelled benzoic and phosphoric acids. The isotopic exchange reactions were carried out in the infrared gas cell where the sample was exposed to water vapour in the ambient atmosphere for a period of time

Figure 2.6 The evacuable gas infrared cell.

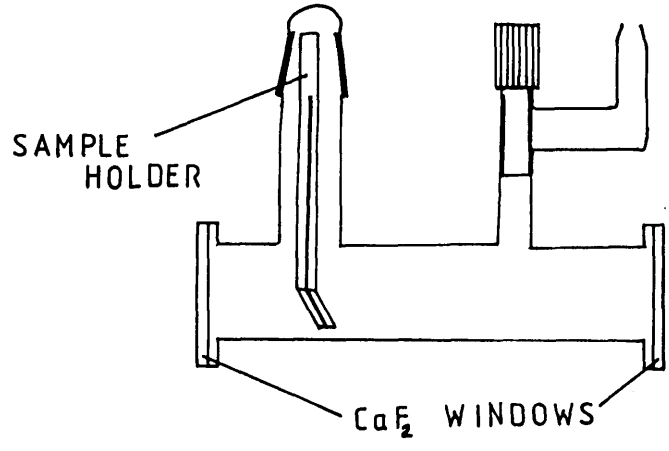

during which infrared spectra were obtained. The reverse isotopic exchange involved exposing [^{2}H] hydrogen-exchanged waveguide to [^{2}H]-hydrogen labelled water vapour. The [^{2}H]-hydrogen labelled water was degassed on the vacuum line using three freeze-pump-thaw-cycles. The sample was exposed to the [^{2}H]-hydrogen labelled water vapour by attaching the infrared gas cell to the manifold containing the ^2H_2O reservoir. Later, ^2H_2O vapour was removed from the gas cell by pumping prior to each infrared measurement.

2.4.3 Polarisation infrared measurements on the [^{2}H] hydrogen -exchanged waveguides.

Polarised infrared radiation was employed in the characterization of [^{2}H] hydrogen-exchanged waveguides. The radiation was polarized linearly by using a gold wire-grid infrared polarizer. The relationship between the polarization direction of the infrared beam and the axes of the waveguides was determined by recording the infrared spectra of the nematic liquid crystal p-n-butyl-N-(p'-methyl-benzylidene)aniline (MBBA), oriented normal to the horizon, with the polarizer set at 0^o and 90^o. Only certain absorption bands were present depending on the incident polarization. Comparison of the spectrum of MBBA with the literature spectra [127] enabled the incident polarization to be determined. The isotropic and linear dichrosim infrared spectra of oriented nematic MBBA are shown in figure 2.7.

Figure 2.7 The Isotropic (---) and the linear dichroism (——) infra red spectrum of oriented numatic MBBA (Dudley et al[127]).

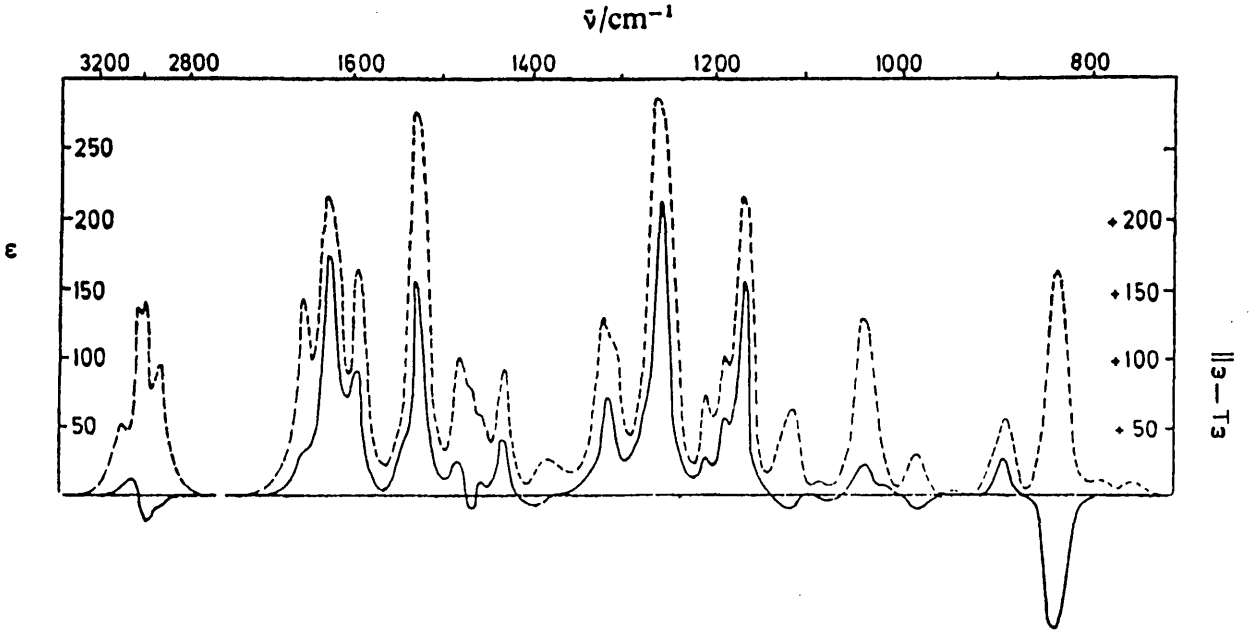

2.5 OPTICAL CHARACTERISATION OF [^{1}H]- AND [^{2}H]-HYDROGEN-EXCHANGED WAVEGUIDES BY THE PRISM-COUPLING TECHNIQUE AT λ = 0.6328 μm

2.5.1 Propagating mode angle measurements and determination of the refractive index profile by the inverse WKB method[128] and the step-index program.[56,129].

A standard prism-coupling technique [113] was employed to assess the optical characteristics of the optical waveguides formed, using single crystal rutile prisms (N_e = 2.8719, N_o = 2.5837) at the wavelength λ= 0.6328 μm of a He-Ne laser. The waveguide was cleaned using methanol, carefully lined up and clipped to the input prism. The prism was fitted on a U-shaped aluminium holder with a plastic screw for clipping the waveguide to minimize the air gap between the prism and the waveguide. The prism holder was fitted onto a prism-coupling rig with (X,Y,Z,Θ, Ø) movements. The X,Y,Z movements were used to position the waveguide and the prism with respect to the input laser beam, Θ rotation movement was used to change the angle of the input laser beam and allow for excitation of different propagating modes. The Ø movement was used to set the waveguide plane normal to the input beam. The prism coupling rig was connected to a digital read-out to measure the synchronous coupling angle of the excited mode. The resolution of the digital read out (accuracy in measuring the mode angles) was 0.01°, which corresponded to a change of $\Delta n = 7 \times 10^{-5}$ in the refractive index of the waveguide. The laser beam was

fired at the input prism, propagated in the waveguide and launched out of the waveguide through the output prism and observed on the screen as a mode line (m-line). A schematic diagram of the apparatus is shown in figure 2.8.

The intensities of the mode lines were optimized by fine tuning of X,Y,Z,Θ movements and the measured angles were put in to a computer program to calculate the effective refractive indices of the modes, the effective depths of the propagating modes, the depth of the waveguide and the surface refractive index of the waveguide (see section 1.5.3).

Figure 2.8 The prism coupling arrangement used to characterize the hydrogen-exchange waveguides. The film represents the waveguiding layer (Tien[3]).

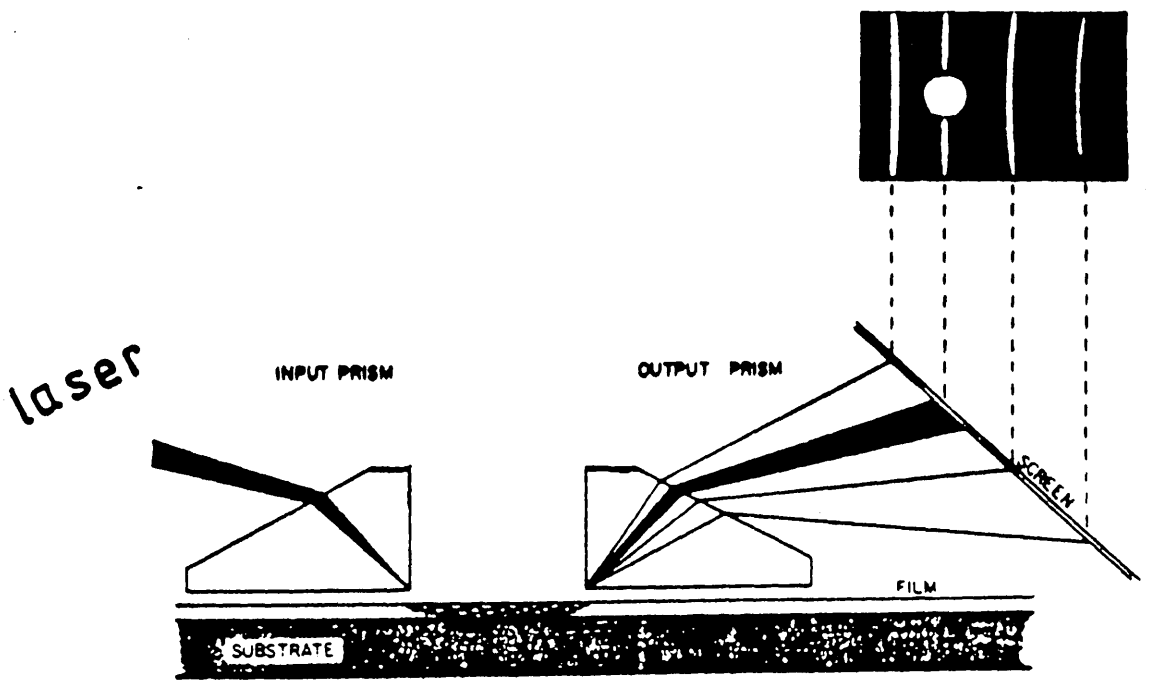

CHAPTER THREE

PREPARATION OF [^{1}H]-/[^{2}H]-HYDROGEN ISOTOPICALLY-EXCHANGED WAVEGUIDES IN X-AND Z-CUT LITHIUM NIOBATE. CHARACTERISATION BY INFRARED SPECTROSCOPY AND THE PRISM-COUPLING TECHNIQUE. DETERMINATION OF LITHIUM BY ATOMIC ABSORPTION SPECTROSCOPY.

3.1 [^{1}H] Hydrogen-exchange of X- and Z-cut lithium niobate single crystals in benzoic acid.

Single crystal x- and z-cut $LiNbO_3$ samples were prepared and cleaned as described in section 2.1.2. The samples were fabricated in sets under different atmospheres (Ar, N_2 and air) to investigate the effect of atmosphere on the extent of the reaction in benzoic acid. The $LiNbO_3$ samples were [^{1}H] hydrogen-exchanged, as described in section 2.1.4, and the conditions under which the samples were exchanged are listed in table 3.1.

Infrared spectra of the waveguides were recorded and they confirmed what was previously reported in the literature.[55,57,129] Typical infrared spectra of x- and z-cut (F5 and F8 respectively) are depicted in figure 1.8a and b.

Spectra of samples fabricated for the same reaction time and temperature but under different atmospheres, for example N_2 and Ar, the samples F3 and F5 (both x-cut) showed no significant differences.

The optical properties of the [^{1}H] hydrogen-exchanged waveguides were characterized at wavelength λ = 0.6328 μm by the prism-coupling technique. The angles of the TE modes in x-cut material and TM modes in z-cut material were measured.

Table 3.1 Fabrication temperatures, times and atmospheres of the x- and z-cut $LiNbO_3$ [^1H] hydrogen-exchanged waveguides fabricated in benzoic acid.

Sample	Crystal cut	Fabrication temperature (°C)	Fabrication time (h)	Fabrication atmosphere
F1	X	163	9	N_2
F2	X	185	5	air
F3	X	200	3	N_2
F4	X	200	3	air
F5	X	200	3	Ar
F6	Z	230	4	Ar
F7	X	235	4	air
F8	Z	235	6	N_2
F9	Z	235	6	N_2

The light propagated along the Y-axis of each sample. The anomalous side-shift in the mode lines spectra reported in the literature[130] was observed on both faces of the $LiNbO_3$ waveguides but it was clearer in x-cut material.

The refractive index/depth profiles of these waveguides were calculated using the inverse WKB program (section 2.5). They showed a step-like profile which is a characteristic feature of the hydrogen-exchanged waveguides. The change in the extraordinary refractive index was Δn_e = 0.1205 ± 0.0021 for x-cut $LiNbO_3$, which agreed with the literature.[55] Optical properties of the waveguides F3 and F5 were identical, therefore, either N_2 or Ar can be used equally well as an atmosphere for the exchange reaction . A typical refractive index/depth profile of a hydrogen-exchanged waveguide is depicted in figure 1.11. The maximum changes in the refractive indices and the waveguide depths of the [^{1}H] hydrogen-exchanged waveguides are presented in Table 3.2.

3.2 [^{2}H] Hydrogen-exchange of x- and z-cut lithium niobate single crystal in [^{2}H]-hydrogen labelled benzoic acid.

[^{2}H]-Hydrogen labelled benzoic acid, freshly prepared as described in section 2.13.2, was used to [^{2}H] hydrogen-exchange x- and z-cut $LiNbO_3$ crystals. The exchange conditions and atmospheres are listed in Table 3.3. Samples FD2 and FD3 (x- and z-cut respectively) were exchanged under an Ar atmosphere.

Table 3.2 Maximum changes in the refractive index and the waveguide depths of [^{2}H] hydrogen-exchanged waveguides calculated by the inverse WKB program.

Waveguide	No. of propagating modes	maximum Δn_e	waveguide depth (μm)
F2	3	0.1147	0.8244
F3	4	0.1214	1.7842
F4	4	0.1199	1.6210
F5	4	0.1188	1.7576
F6	6	0.1487 *0.1235	2.6584 *2.5204
F7	7	0.1420 *0.1292	3.3748 *3.2817

* calculated by the step-index program.

Table 3.3 Fabrication temperatures, times and atmospheres of the X- and Z-cut [^{2}H] hydrogen-exchanged $LiNbO_3$ waveguides fabricated in [^{2}H]-hydrogen labelled benzoic acid.

Sample	Crystal Cut	Fabrication temperature (^{0}C)	Fabrication time (h)	Fabrication atmosphere
FD1	X	235	3.5	air
FD2	X	225	4	Ar
FD3	Z	225	4	Ar
FD4	X	235	4	N_2
FD5	X	235	4	air
FD6	X	225	4	N_2

Infrared spectra of the samples recorded immediately after the reaction showed strong bands in the [^{2}H]-hydroxyl stretching region,while weak bands were present in the [^{1}H]-hydroxyl stretching region. The superimposed spectra of the [^{2}H] hydrogen-exchanged waveguides FD2 and FD3 are depicted in figures 3.1 and 3.2 respectively.

The samples FD4 and FD5, both x-cut, were fabricated at 235^{o}C for 4h under nitrogen and ambient air respectively. The infrared spectra of FD5, unlike that for FD4 showed intense bands in the [^{1}H]-hydroxyl stretching region due to the incorporation of hydrogen from the air (see figures, 3.3 and 3.4 respectively).

3.3 THE [^{1}H-^{2}H] ISOTOPIC EXCHANGE OF [^{2}H] HYDROGEN-EXCHANGED WAVEGUIDES IN [^{1}H]-HYDROGEN WATER AND [^{2}H]-HYDROGEN LABELLED WATER VAPOURS.

3.3.1 Exposure of x- and z-cut [^{2}H] hydrogen-exchanged waveguides to water vapour in air.

The [^{2}H] hydrogen-exchanged waveguides FD1, FD2 and FD3 were exposed to ambient air following the procedure described in section 2.4.2. The infrared spectrum of the waveguide FD1 ([^{2}H] hydrogen-exchanged at 235^{o}C for 3.5h in air) was recorded frequently over a total period of 502h of exposure to the water vapour present in the ambient atmosphere. The superimposed infrared spectra of the

waveguide FD1 are shown in figure 3.5. The spectra showed a sharp intense band at 2588 cm^{-1}, overlapping a broad band centred at 2410 cm^{-1} in the [^{2}H]-hydroxyl stretching region. These bands exhibited a progressive decrease during exposure of the waveguide to the ambient atmosphere.

A small band consisting of two overlapping maxima at 3500 and 3470 cm^{-1} and a band at 3275 cm^{-1} were present in the [^{1}H]-hydroxyl stretching region. These bands showed a continuous increase during the course of exposing the waveguide to water vapour in the ambient air. The high frequency band at 3500 cm^{-1} dominated the band at 3470 cm^{-1} after 141h of exposure to water vapour in the air and also showed a shift in frequency to 3505 cm^{-1}.

The band at 3505 cm^{-1} overlapped the broad band which possessed a distinct maximum at 3275 cm^{-1} unlike the broad smooth contoured, band in the spectra of waveguides originally [^{1}H] hydrogen-exchanged (see figure 1.8a for example). The waveguide FD3 ([^{2}H] hydrogen-exchanged at 225^{o}C for 4h in an Ar atmosphere) was exposed to water vapour in air for a total period of 9600h.

The infrared spectra showed similar features to the spectra of FD1. The superimposed spectra were illustrated in figure 3.1. The infrared spectra recorded before exposing the waveguide to air showed two well-resolved small maxima at 3515 and 3465 cm^{-1}. These maxima were in agreement with that reported in $LiNbO_3$ crystals and in

Figure 3.1 Infrared spectra of x-cut lithium niobate [^{2}H] hydrogen-exchanged waveguide FD2, superimposed as a function of the exposure time of the sample to water vapour in air. The exposure time was a: t = 0, b:t = 72h, c:t = 96h, d:t = 480h and e:t = 9600h (The waveguide was fabricated in [^{2}H]-hydrogen labelled benzoic acid at 225^{o}C for 4h in Ar atmosphere).

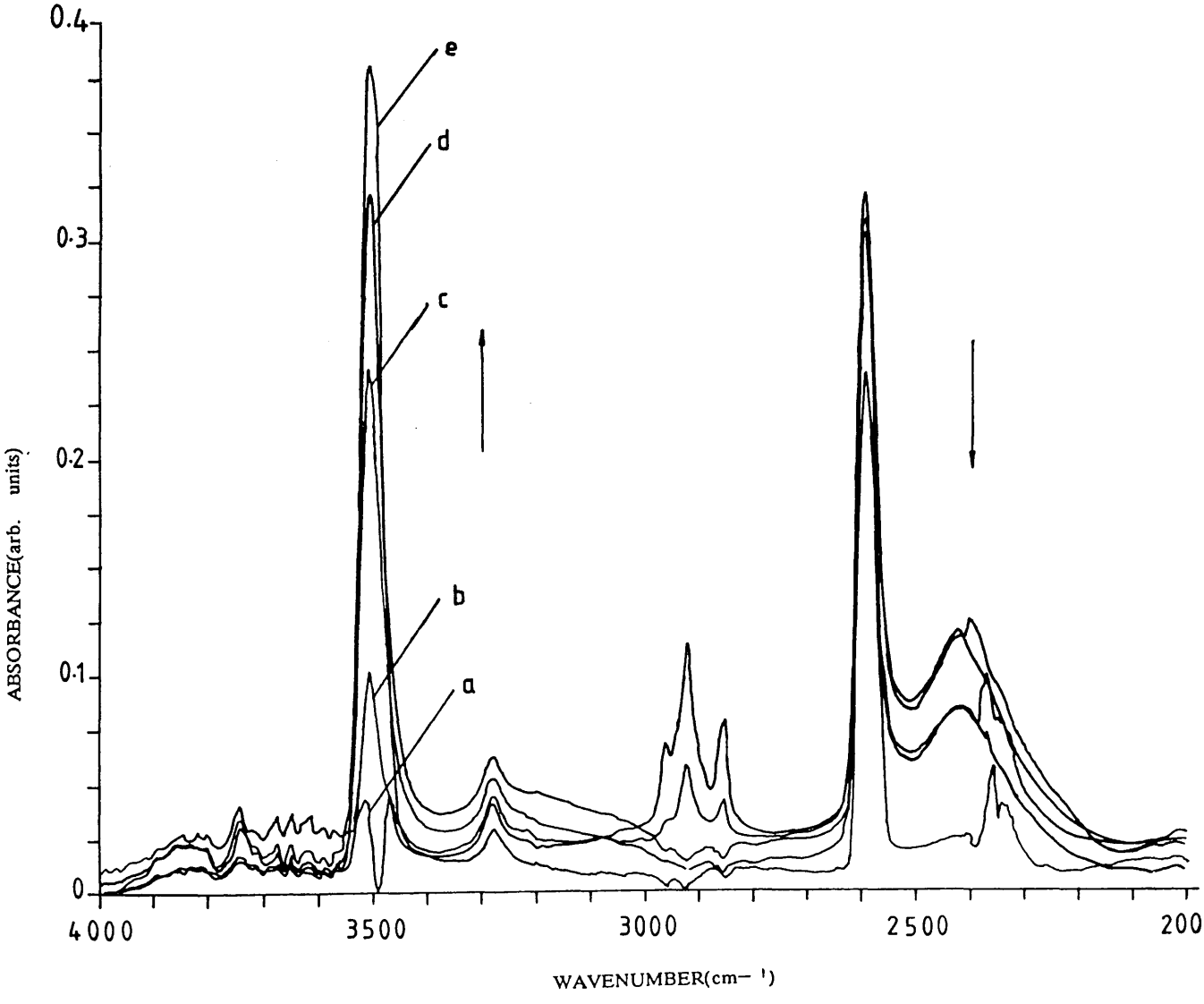

Figure 3.2 Infrared spectra of z-cut lithium niobate [^{2}H] hydrogen-exchanged waveguide FD3, superimposed as a function of the time of exposure of the sample to water vapour in air. The exposure time was: a:t = 0, b:t = 24h, c:t = 72h, d:t = 97h and e:t = 480h. (The waveguide was fabricated using [^{2}H]-hydrogen labelled benzoic acid at 225 for 4h in Ar atmosphere).

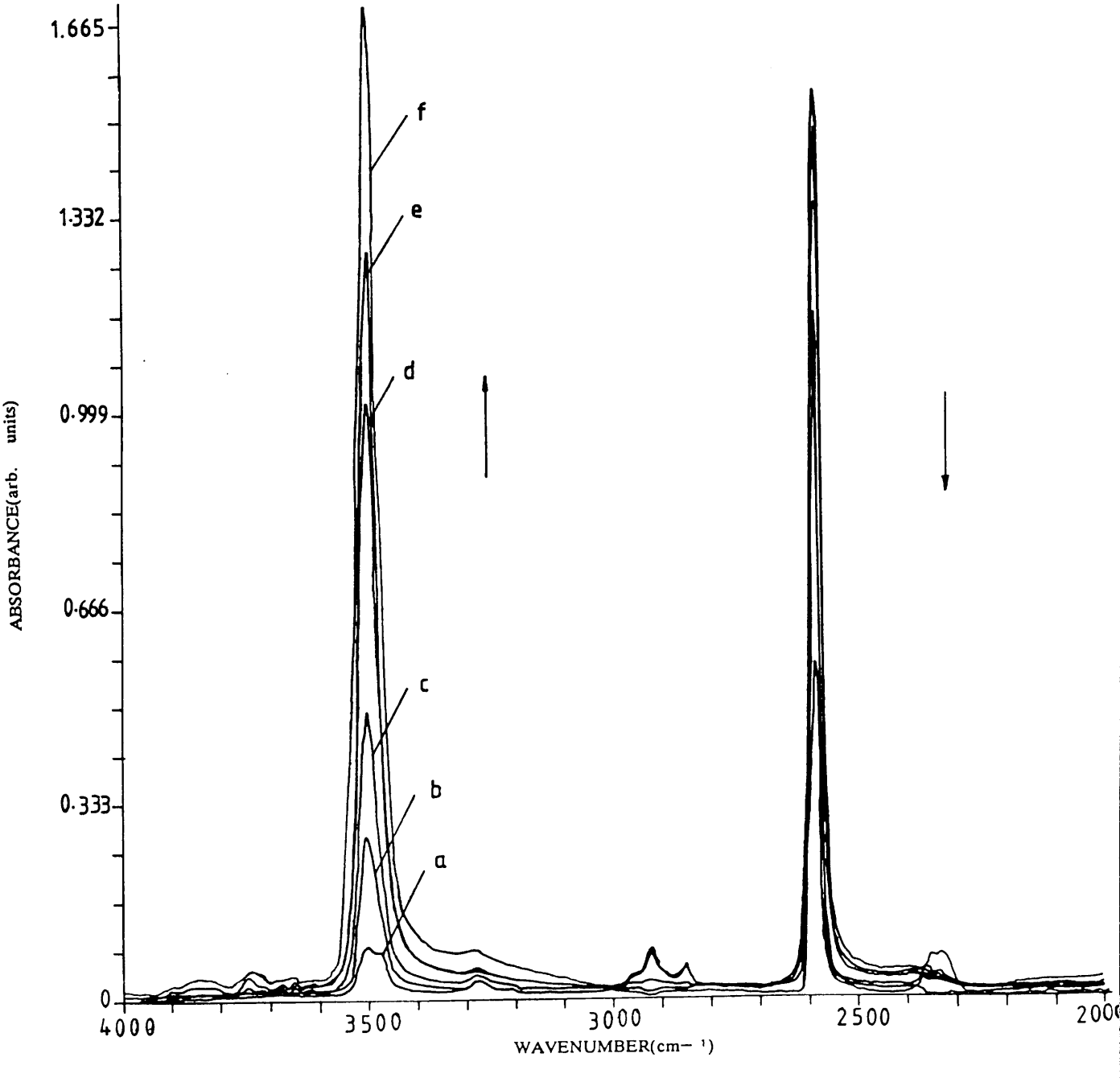

Figure 3.3 Infrared spectrum of [^{2}H] hydrogen-exchanged waveguide FD5 (The waveguide was fabricated using [^{2}H]-hydrogen labelled benzoic acid at 235^{o}C for 4h in air).

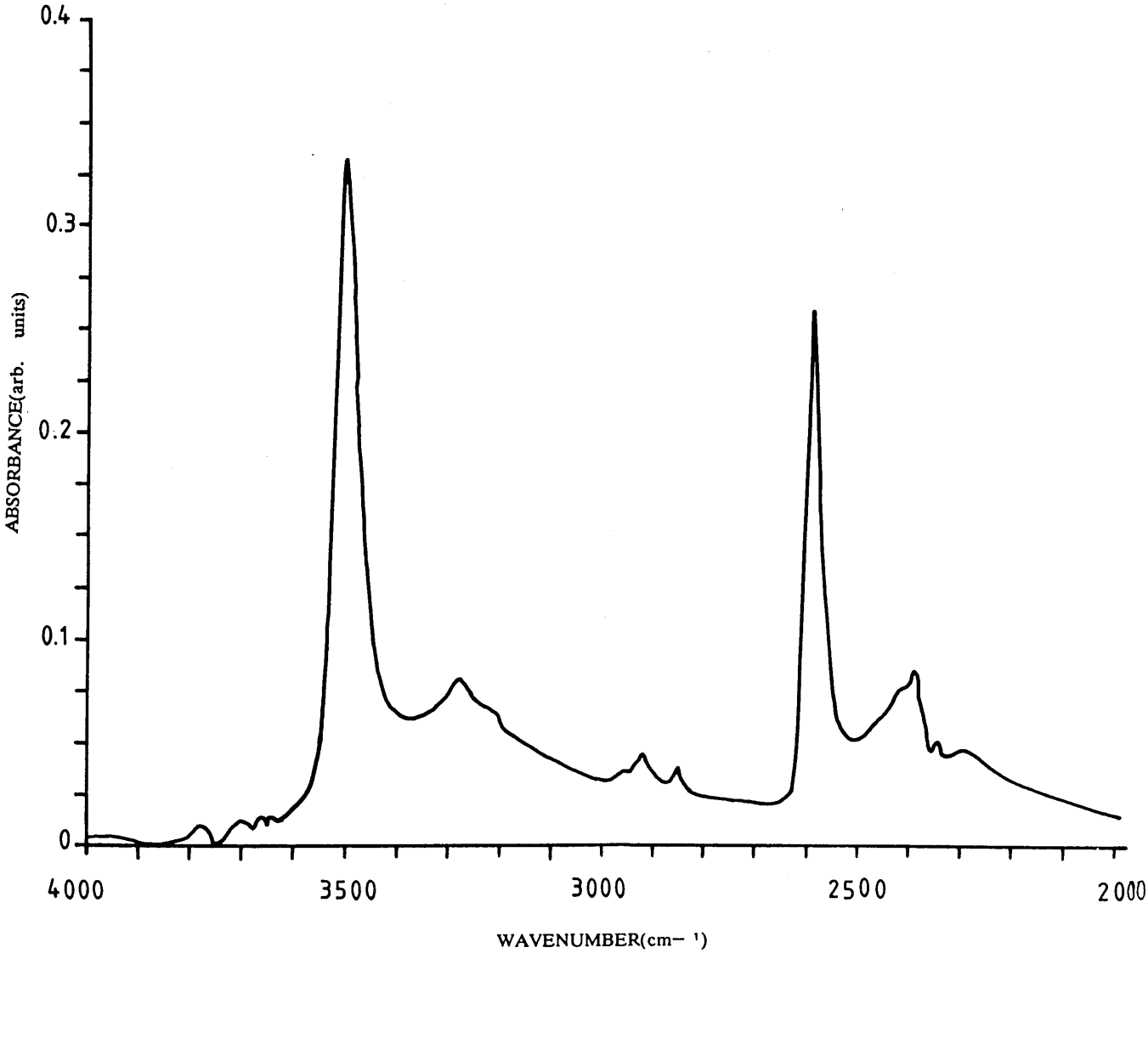

Figure 3.4 Infrared spectrum of [^{2}H] hydrogen-exchanged waveguide FD4. (The waveguide was fabricated using [^{2}H]-hydrogen labelled benzoic acid at 235^{o}C for 4h under N_2 atmosphere).

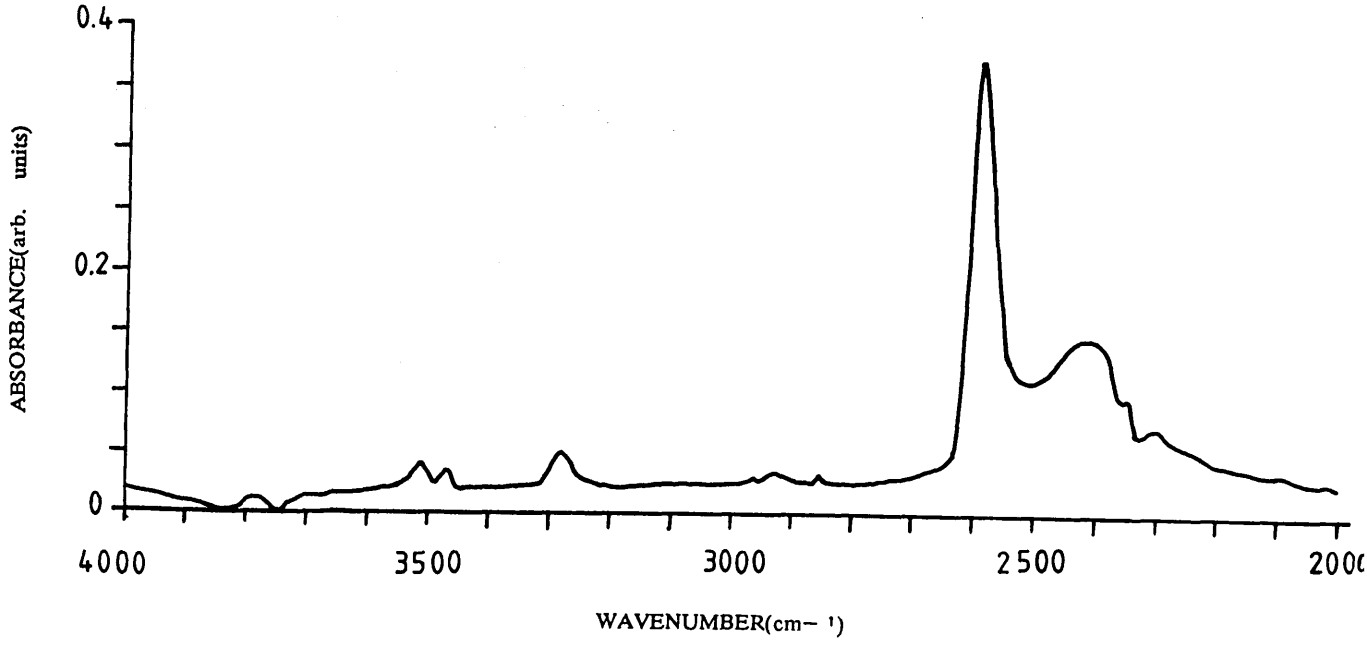

Figure 3.5 Infrared spectra of [^{2}H] hydrogen-exchanged waveguide FD1 superimposed as a function of the time of exposure of the waveguide to water vapour in air. The exposure time was: a:t = 14h, b:t = 21h, c:t = 45.5h, d:t = 141h, e:t = 190h, f:t = 214h and g:t = 502h. (The waveguide was fabricated using [^{2}H]-hydrogen labelled benzoic acid at 235^{o}C for 3.5h in air).

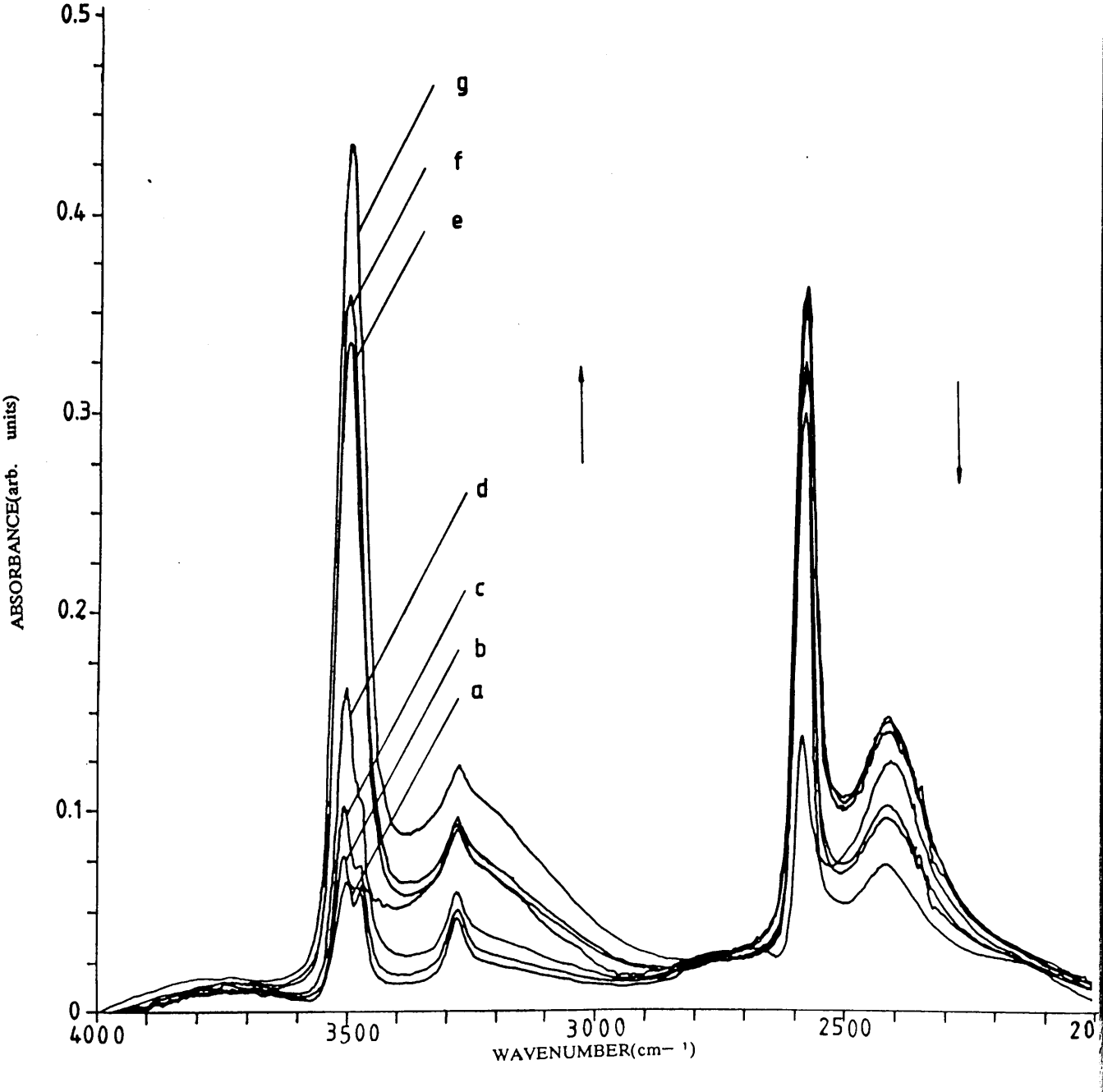

[^{2}H] hydrogen-exchanged waveguides in the literature.[107,78,131] The high frequency maximum dominated and shifted to 3505 cm^{-1} during the course of exposure to air.

A group of three bands at 2958, 2920 and 2850 cm^{-1} was observed in these spectra. These bands decayed and eventually vanished after 96h of exposing the waveguide to water vapour in air. The spectrum recorded after 9600h, showed a strong sharp band at 3505 cm^{-1} and a weak band centred at 3280 cm^{-1} in the [^{1}H]-hydroxyl stretching region. The spectrum also showed a weak sharp band at 2588 cm^{-1} and a new distinct maxima at 2360 and 2340 cm^{-1} in the [^{2}H]-hydroxyl stretching region.

In order to compare the behaviour of the z-cut $LiNbO_3$ with that of the x-cut material towards the exposure to air, the waveguide FD3 ([^{2}H] hydrogen-exchanged at 225^{o}C for 4h in Ar atmosphere) was exposed to water vapour in ambient air for a total period of 9888h. The superimposed spectra of the waveguide FD3 were depicted in figure 3.2.

The spectrum recorded immediately after reaction, before exposure to air, showed an intense band at 2588 cm^{-1} overlapping a weak broad band from the low frequency side in the [^{2}H]-hydroxyl stretching region. This intense band exhibited a steady decrease as the exposure of the waveguide to air proceeded. The spectrum also showed a very weak band with two maxima at 3505 and 3475 cm^{-1}. The high frequency

band dominated later during exposing the waveguide to the ambient air.

A weak broad band centred at 3280 cm^{-1} can also be seen in the [^{1}H]-hydroxyl stretching region. The three bands at 2958, 2920 and 2850 cm^{-1}, previously observed in the x-cut material (figure 3.1) were observed to disappear completely after 96h of exposure to the air. Both the sharp bands at 3505 and 2588 cm^{-1} showed a shoulder from the low frequency side.

The final spectrum recorded for waveguide FD3 (z-cut) showed a decreased sharp band at 2475 cm^{-1} overlapping a very weak maxima at 2360 and 2340 cm^{-1} in the [^{2}H]-hydroxyl stretching region. A strong band at 3505 cm^{-1} overlapping a weak broad band centred at 3280 cm^{-1} was observed.

3.3.2 Exposure of [^{2}H] hydrogen-exchanged waveguides to [^{2}H]-hydrogen labelled water vapour at room temperature.

The possibility of restoring the [^{2}H]-hydrogen lost from the [^{2}H] hydrogen-exchanged waveguide during the exposure to ambient air was investigated using the method described in section 2.4.2. The waveguide FD2 (x-cut) was exposed to water vapour in ambient atmosphere first for a period of 480h (section 3.3.1).

The waveguide was then exposed to [^{2}H]-H_2O water vapour for a period of 118h. Spectra recorded during the

course of exposing FD2 to $[^2H]$-H_2O water vapour are superimposed in figure 3.6.

The spectra showed a little decrease in the absorption intensity of the sharp band at 3505 cm^{-1} (6.8% of the initial absorbance) and lesser reduction of the broad band at 3280 cm^{-1} in the $[^1H]$-hydroxyl stretching region. The band at 3505 cm^{-1} did not decrease after 54h of exposure of the waveguide to $[^2H]$-H_2O water vapour. The maximum absorption intensity of the sharp band at 2588 cm^{-1} showed significant increase (11% of the initial absorbance) whereas the broad band at 2410 cm^{-1} increased to a lesser extent.

This behaviour of the $[^2H]$ hydrogen-exchanged waveguide towards exposure to $[^2H]$-hydrogen labelled water vapour is not identical to that reported in the literature [78] in which a $[^1H]$ hydrogen-exchanged waveguide has been exposed to $[^2H]$-H_2O water vapour at room temperature and then restored all the $[^1H]$ content when exposed to H_2O water vapour.

3.3.3 Exposure of the $[^2H]$ hydrogen-exchanged waveguides to $[^2H]$-hydrogen labelled water vapour at elevated temperatures : The annealing process.

The $[^2H]$ hydrogen-exchanged waveguides FD3 (z-cut) FD2,FD4 and FD5 (all x-cut) were annealed after a period ranging between 5780 to 9888h of exposure to water vapour in ambient

Figure 3.6 Infrared spectra of x-cut lithium niobate [^{2}H] hydrogen-exchanged waveguide FD2, superimposed as a function of the time of exposure of the sample to [^{2}H]-hydrogen labelled water vapour. The exposure time was : a:t = 5h, b:t = 53h, and c:t = 118h. (The waveguide was fabricated using [^{2}H]-hydrogen labelled benzoic acid at 225^{o}C for 4h in Ar atmosphere).

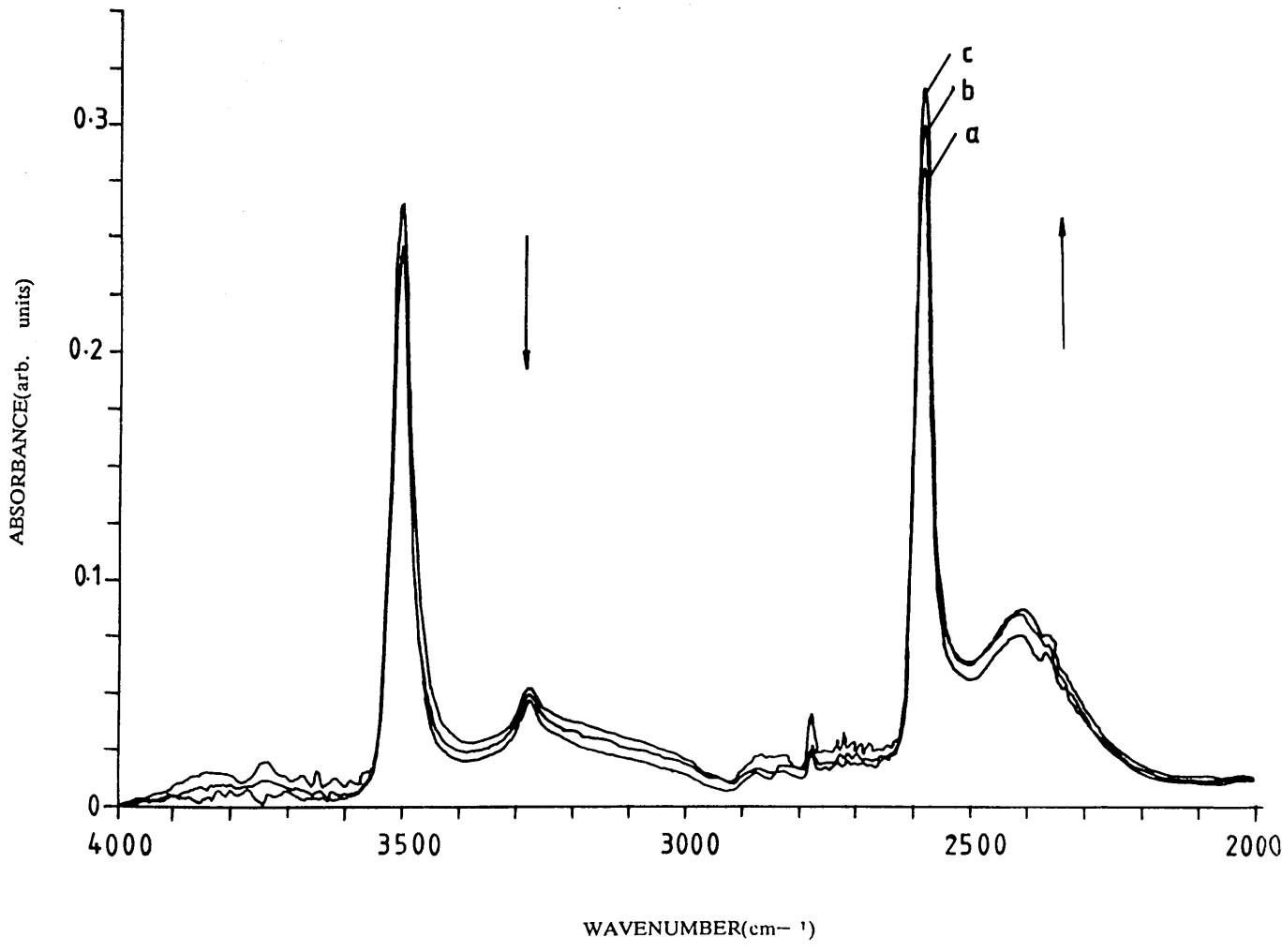

air. According to the procedure described in section 2.3, the waveguides were annealed at 365°C for 20 min. The oxygen flow was 0.2 $lmin^{-1}$ and was bubbled through a 10cm column of [^{2}H]-hydrogen labelled water heated to 85°C.

All samples showed a substantial reduction in both bands of the [^{1}H]-hydroxyl stretching region accompanied by an increase in absorbance in the [^{2}H]-hydroxyl bands. The infrared spectra of the samples are depicted in figure 3.7a, b,c. The [^{1}H]-hydroxyl content of the waveguide FD3 (z-cut exchanged at 225°C for 4h) figure 3.7a was greatly reduced while the bands at the [^{2}H]-hydroxyl stretching region have increased in absorbance as a result of the annealing.

The x-cut samples FD2 and FD4, showed a reduction in the absorbance of the bands at 3505 and 3280 cm^{-1} at the [^{1}H]-hydroxyl stretching region. This reduction was accompanied by a small increase in the absorbance of the bands at the [^{2}H]-hydroxyl stretching region, figure 3.7b.

The spectrum of the waveguide F7, originally [^{1}H] hydrogen-exchanged at 235°C for 4h, recorded after annealing in [^{2}H]-H_2O water vapour showed an increase in the [^{2}H]-hydroxyl region, confirming A. Loni's previous results,[57] figure 3.7c.

To examine the effect of annealing a [^{2}H] hydrogen-exchanged waveguide in water vapour (H_2O/O_2) wet oxygen, the waveguide FD6 ([^{2}H] hydrogen-exchanged at 225°C for 4h under

Figure 3.7.a Infrared spectra of z-cut lithium niobate [^{2}H] hydrogen-exchanged waveguide FD3, (a) before annealing (b) after annealing in ($^2H_2O/O_2$) [^{2}H]-hydrogen labelled water vapour oxygen. (The waveguide was annealed at 365^{o}C for 20 min).

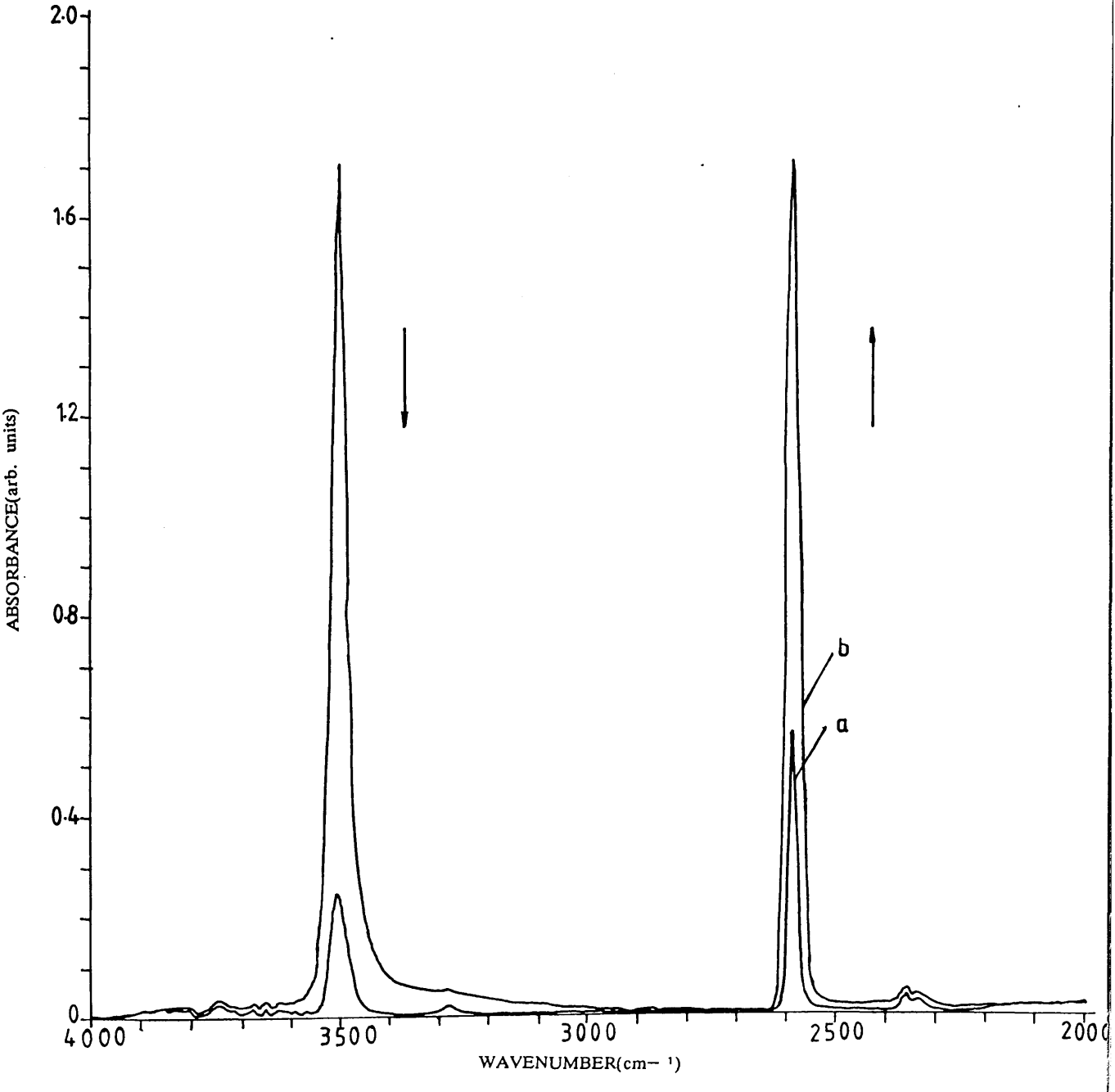

Figure 3.7. b. Infrared spectra of x-cut lithium niobate [^{2}H] hydrogen-exchanged waveguide FD4 (a) before annealing (b) after annealing in ($^2H_2O/O_2$) [^{2}H]-hydrogen labelled water vapour oxygen. (The waveguide was annealed at 365^{o}C for 20 min).

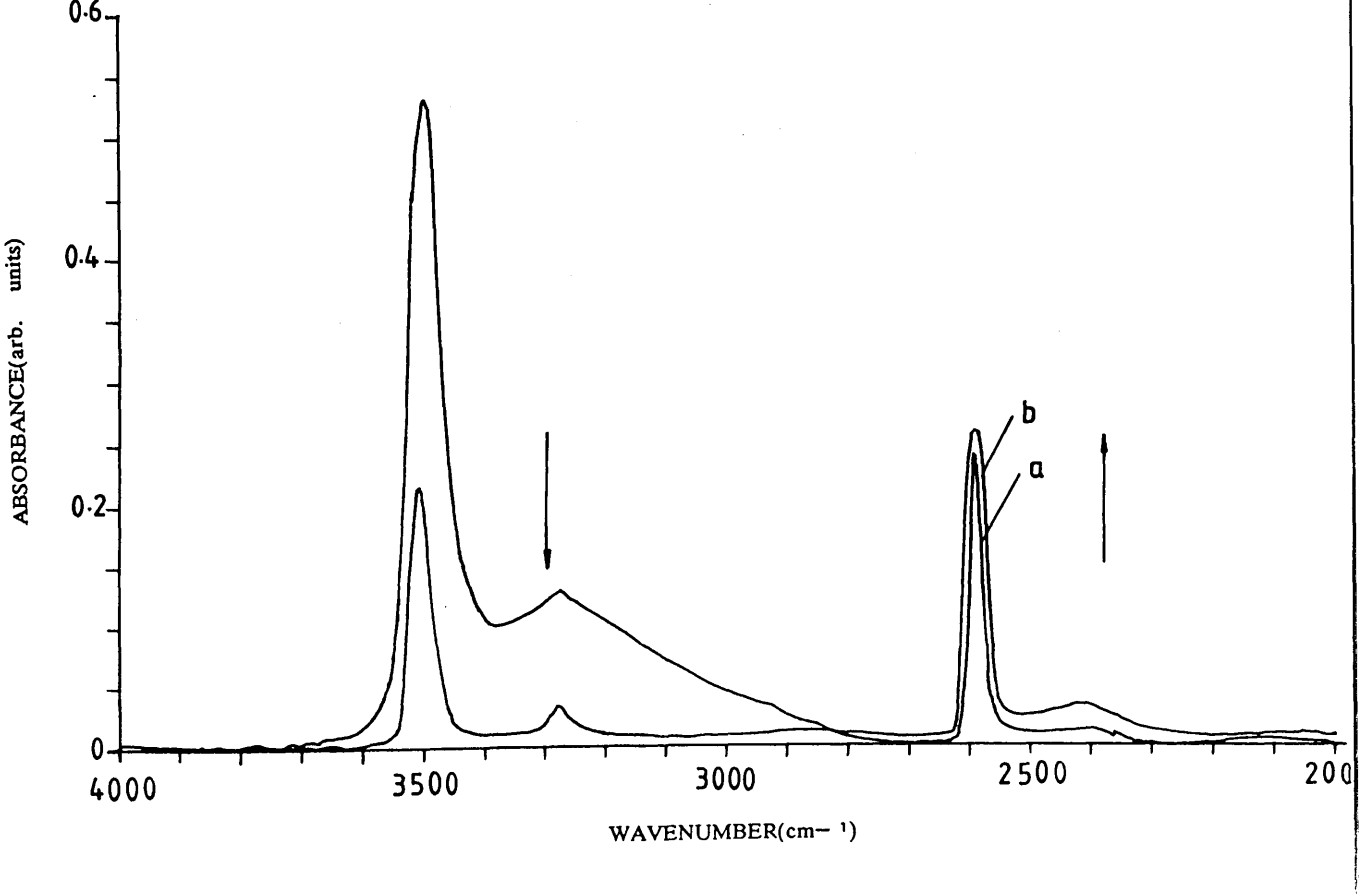

Figure 3.7.c Infrared spectra of x-cut lithium niobate [^{2}H] hydrogen-exchanged waveguide F7 (a) before annealing (b) after annealing in ($^2H_2O/O_2$) [^{2}H]-hydrogen labelled water vapour oxygen. (The waveguide was annealed at 365^{o}C for 20 min).

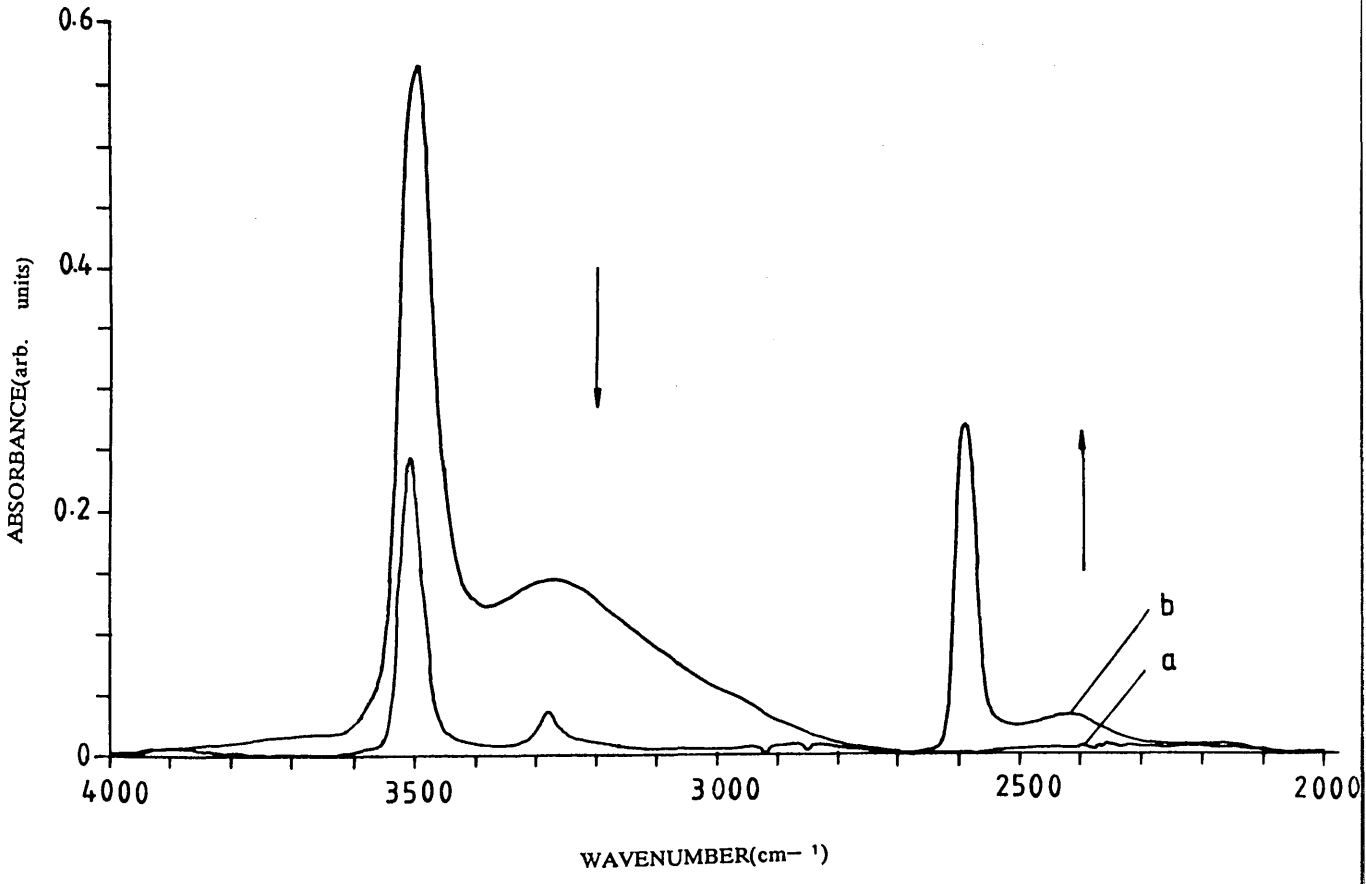

N_2 atmosphere) was annealed at 365°C for 20 min in water vapour (H_2O/O_2) wet oxygen.

The infrared spectrum of the waveguide recorded after annealing showed an intense sharp band an 3505 cm^{-1} overlapping a broad band centred at 3280 cm^{-1}. In the [^{2}H]-hydroxyl stretching region, the overlapping sharp and broad bands at 2588 and 2410 cm^{-1} respectively, existing in the spectra recorded prior to annealing, have completely vanished from the spectrum recorded after the annealing. The superimposed infrared spectra of FD6 (x-cut) prior to and after annealing are depicted in figure 3.8.

Further annealing of the waveguide FD2 (x-cut) under comparable annealing conditions resulted in further reduction of the bands at the [^{1}H]-hydroxyl region and an increase in the bands in the [^{2}H]-hydroxyl region.

3.4 CHARACTERISATION OF THE [^{2}H] HYDROGEN-EXCHANGED WAVEGUIDES BY POLARIZED INFRARED SPECTROSCOPY.

3.4.1 Polarized infrared spectra of x-cut lithium niobate waveguides.

The polarized infrared spectra of the waveguides FD1, FD2, FD4 and FD5 were determined during the [^{1}H-^{2}H]-hydrogen isotopic exchange which occurred while exposing the waveguides to the ambient air. When the polarization direction was parallel to the y-axis (0° polarization, see

Figure 3.9 Spectrum for infrared radiation polarized along the y-axis (0^{o} polarization) of [^{2}H] hydrogen-exchanged waveguide FD1. The insert is an expansion of the sharp band at the [^{2}H]-hydroxyl stretching region.

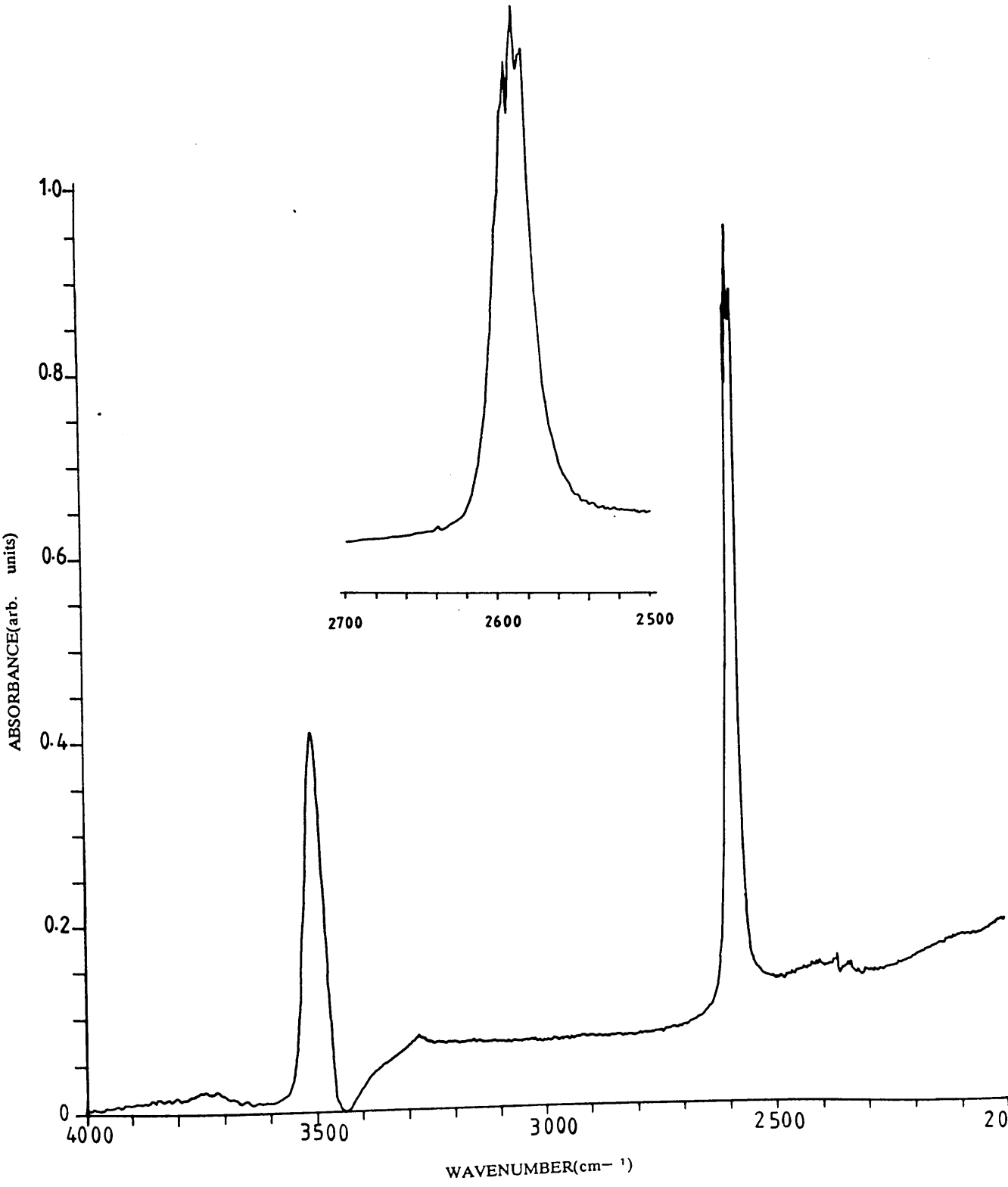

Figure 3.8 Infrared spectra of x-cut lithium niobate [^{2}H] hydrogen-exchanged waveguide FD6 (a) before annealing (b) after annealing in [H_2O/O_2] water vapour oxygen (The waveguide was annealed at 365^{o}C for 20 min).

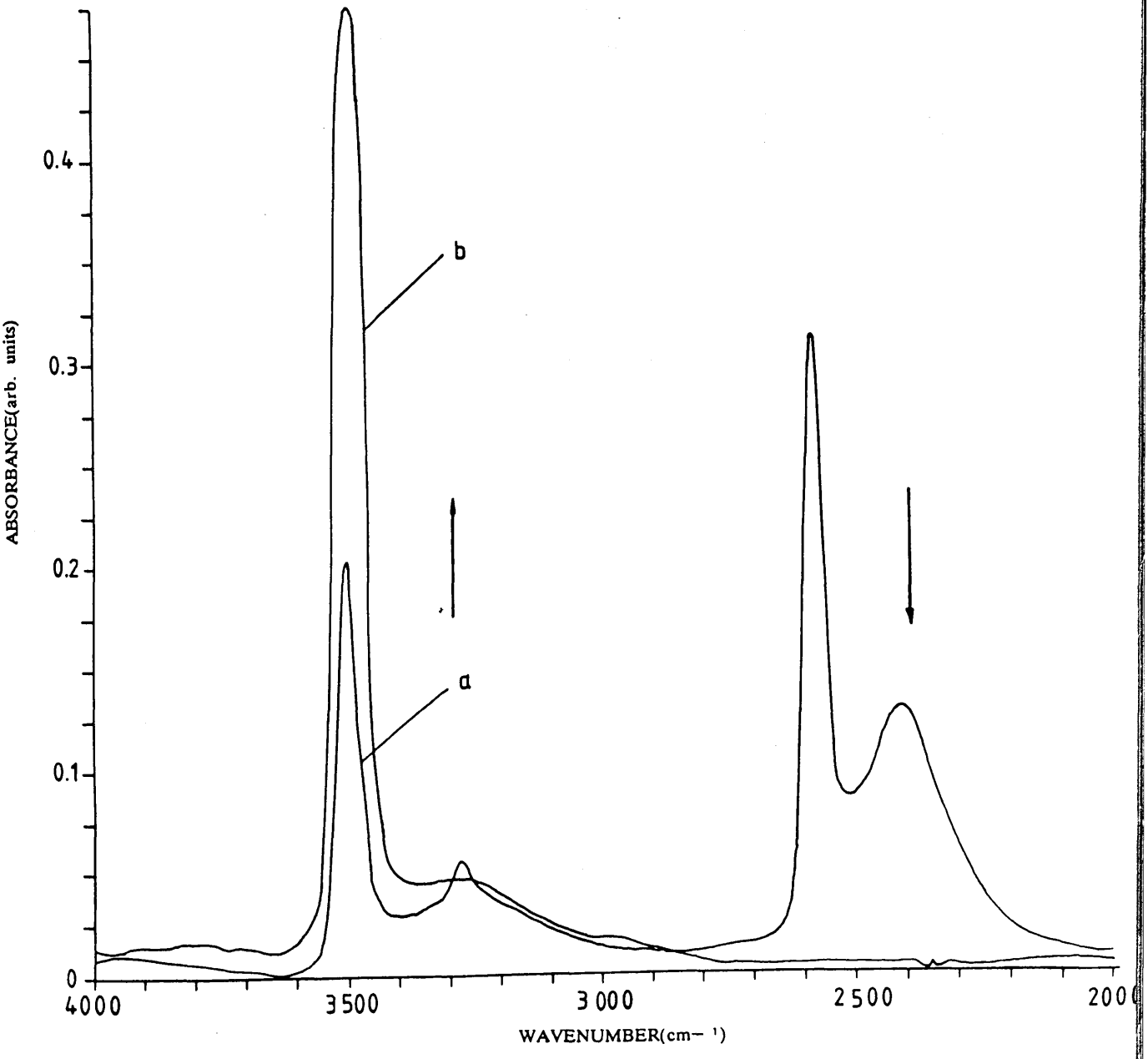

section 2.4.3), the spectra of FD1 showed a sharp intense band overlapping a very weak broad band in the [^{2}H]-hydroxyl stretching region. The sharp band consisted either of two maxima and a shoulder, or three maxima at 2575, 2545 and 2515 cm^{-1}. This feature was observed in all the 0^{o} polarization spectra of the x-cut [^{2}H] hydrogen-exchanged waveguides.

A well-resolved sharp band at 3505 cm^{-1} overlapping a very weak broad band at 3280 cm^{-1} were also observed in the [^{1}H]-hydroxyl stretching region. The spectrum of waveguide FD1 polarized along the y-axis (0^{o} polarization) and an expansion of the sharp band in the [^{2}H]-hydroxyl stretching region are shown in figure 3.9.

The spectra of waveguides FD1 recorded with the polarization direction along the z-axis (90^{o} polarization) exhibited a broad band at 2410 cm^{-1} overlapping a sharp weak band at 2588 cm^{-1}. In the [^{1}H]-hydroxyl stretching region, the bands possessed different features. Here, the broad band exhibited a distinct maximum at 3280 cm^{-1} and overlapping weak broad band from the high frequency side. The superimposed spectra of FD1 polarized along z-axis (90^{o} polarization) are shown in figure 3.10.

3.4.2 Polarized infrared spectra of z-cut lithium niobate waveguides.

Polarized infrared spectra were implemented for

Figure 3.9 Spectrum for infrared radiation polarized along the y-axis (0^{o} polarization) of [^{2}H] hydrogen-exchanged waveguide FD1. The insert is an expansion of the sharp band at the [^{2}H]-hydroxyl stretching region.

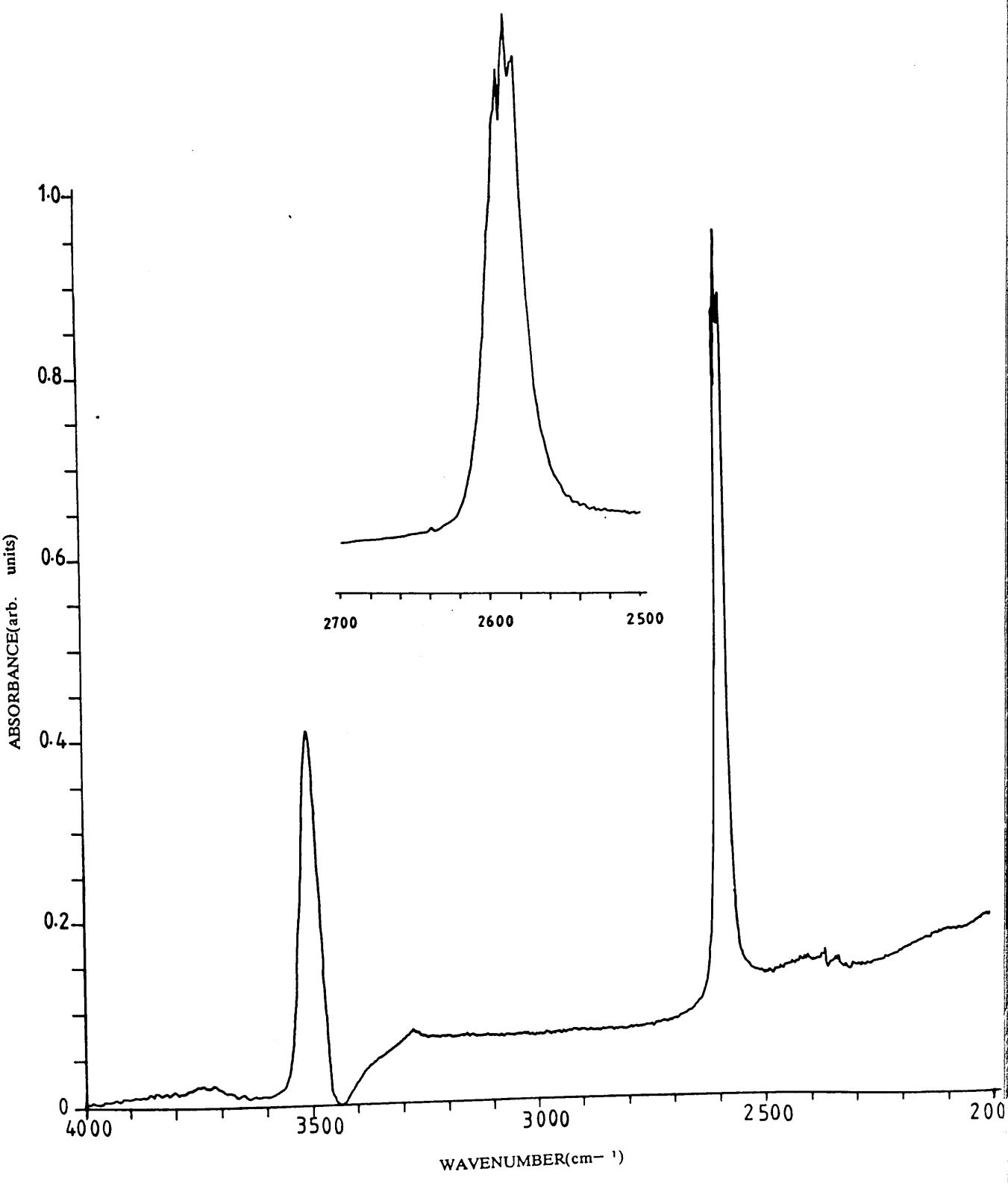

Figure 3.10 Spectra of infrared radiation polarized along the z-axis (90^{o} polarization) of x-cut lithium niobate[^{2}H] hydrogen-exchanged waveguide FD1, superimposed as a function of exposure of the sample to water vapour in air. The exposure time was : a:t = 14h, b:t = 21h, c:t = 45.5h, d:t = 141h, e:t = 190h, f:t = 214h, and g:t = 502h.

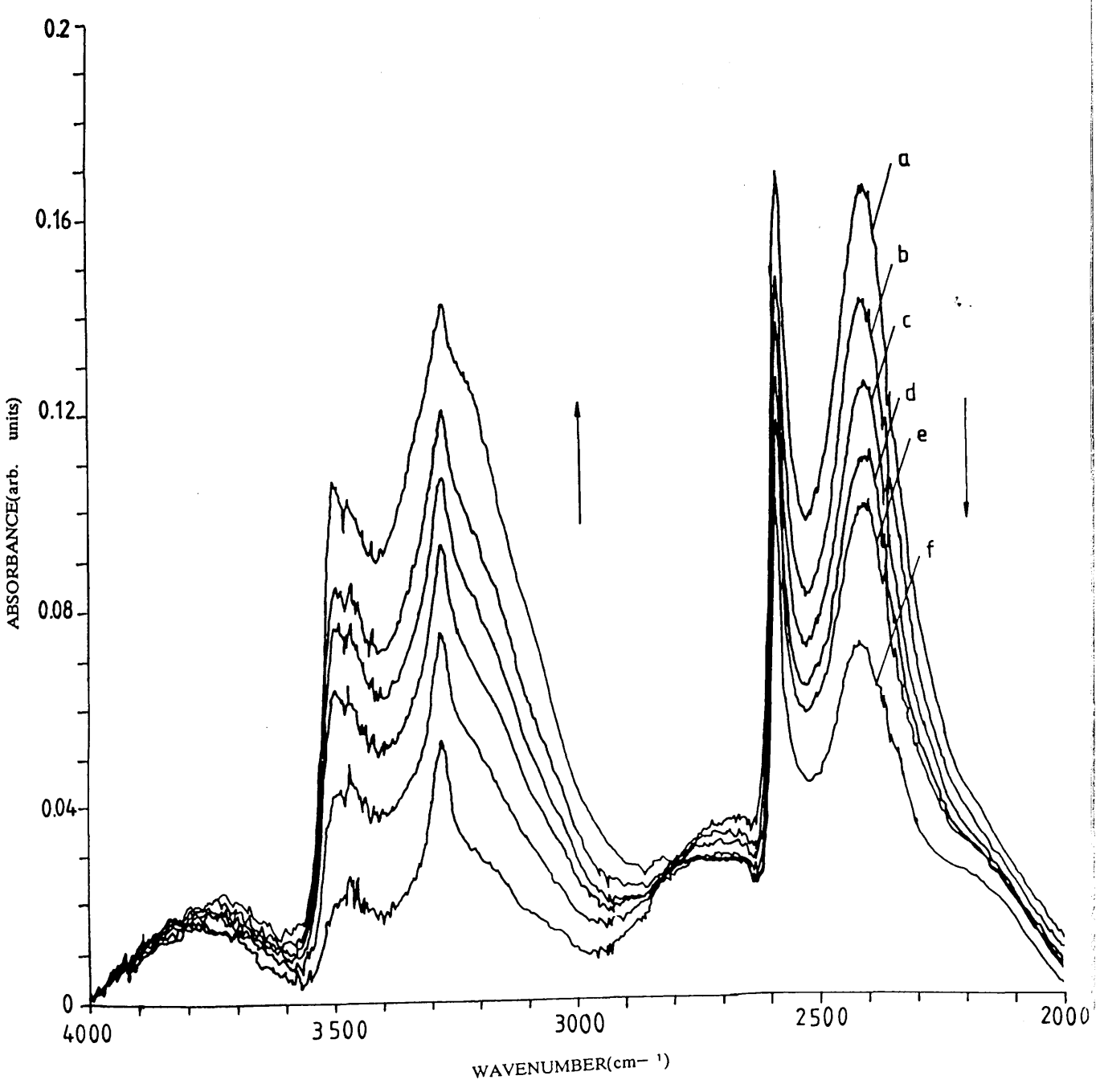

waveguide FD3 (z-cut $[^2H]$ hydrogen-exchanged at 225°C for 4 hours in Ar atmosphere) during the period of exposure to water vapour in ambient air. The 0° polarization spectra, figure 3.11 showed two sharp bands at 3505 and 2588 cm^{-1} in the $[^1H]$- and $[^2H]$-hydroxyl stretching regions respectively. Both sharp bands overlapped very weak broad bands from the low frequency side.

The spectra recorded when the polarization direction was along the x-axis of the crystal (90° polarization) were identical to those described above.

Finally, the width at half hight of the sharp bands in the $[^1H]$-hydroxyl stretching region was approximately double that of the corresponding bands at the $[^2H]$-hydroxyl stretching region.

3.5 THE OPTICAL PROPERTIES OF THE $[^2H]$ HYDROGEN-EXCHANGED WAVEGUIDES.

The optical properties of the $[^2H]$ hydrogen-exchanged waveguides were assessed by the Prism-Coupling technique at wavelength λ = 0.6328 μm. They exhibited a step-like refractive index/depth profile, very similar to that of the $[^1H]$ hydrogen-exchanged waveguide, which is in agreement with the literature.[78]

The maximum change in refractive index and the waveguide depths of some of the waveguides are listed in

Figure 3.11 Spectrum for infrared radiation polarized along the y-axis (0^{o} Polarization) of z-cut lithium niobate [^{2}H] hydrogen-exchanged waveguide FD3.

The insert is an expansion of the sharp band in the [^{2}H]-hydroxyl stretching region.

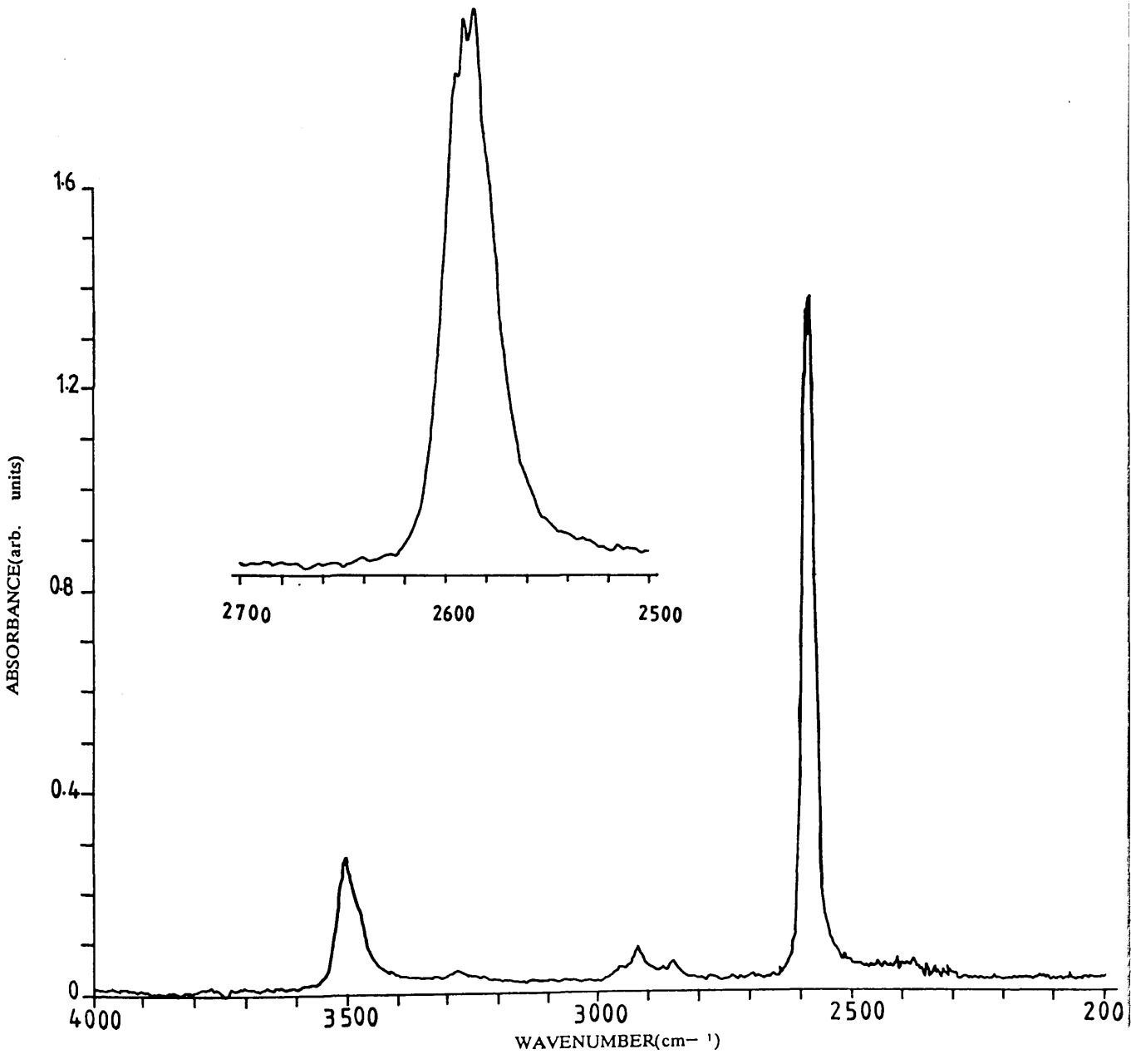

Table 3.4. The change in the refractive index of the [^{2}H] hydrogen-exchanged waveguides was Δn_e = 0.1212 ± 0.0066 for the x-cut $LiNbO_3$ which was in agreement with the literature (Δn_e = 0.127 at wavelength λ= 0.6328 μm)[55] In the case of x- and z-cut waveguide FD2 and FD3 respectively, [^{2}H] hydrogen-exchanged under identical conditions, the waveguide fabricated on x-cut was deeper than that on the z-cut. Consequently, the waveguides on x-cut $LiNbO_3$ supported more propagating modes than on z-cut material.

The effect of annealing the [^{2}H] hydrogen-exchanged waveguides on the optical properties was similar to that when the [^{1}H] hydrogen-exchanged waveguides were annealed.[51,131] In all the waveguides annealed, the number of modes supported after annealing had increased from the case before annealing, and the waveguide depths were also increased. Meanwhile, the maximum change in the refractive index had decreased. This was in agreement with the literature.[131]

Further annealing caused a tail to form in the index profile at the waveguide substrate boundary indicating a change to a more graded-index profile. The refractive index/depth profile of FD2, x-cut, [^{2}H] hydrogen-exchanged and annealed twice is depicted in Figure 3.12. The maximum change in refractive index and the depths of the annealed waveguides are presented in table 3.5.

Table 3.4 Maximum change in refractive indices and the waveguide depths of the [^{2}H] hydrogen-exchanged waveguides calculated using the step-index and the inverse WKB computer programs.

		Step-index program		Inverse WKB Program	
waveguide	no of propagating modes	maximum ΔN_e	waveguide depth (μm)	maximum ΔN_e	waveguide depth (μm)
FD1	9	0.1235	3.5204	0.1487	3.6584
FD2	8	0.1207	3.3163	0.1369	3.4847
FD3	6	0.1240	2.5226	0.1481	2.7859
FD4	10	0.1173	4.4789	0.1342	4.3497
FD5	7	0.1291	2.7788	0.1442	2.9709

Figure 3.12 Pefractive index/depth profiles of x-cut lithium niobate [^{2}H] hydrogen-exchanged waveguide FD2 (a) before annealing (b) after the first annealing (c) after the second annealing (The annealing was undertaken at 365^{o}C for 20 min in($^{2}H_{2}O/O_{2}$) [^{2}H]-hydrogen labelled water vapour oxygen).

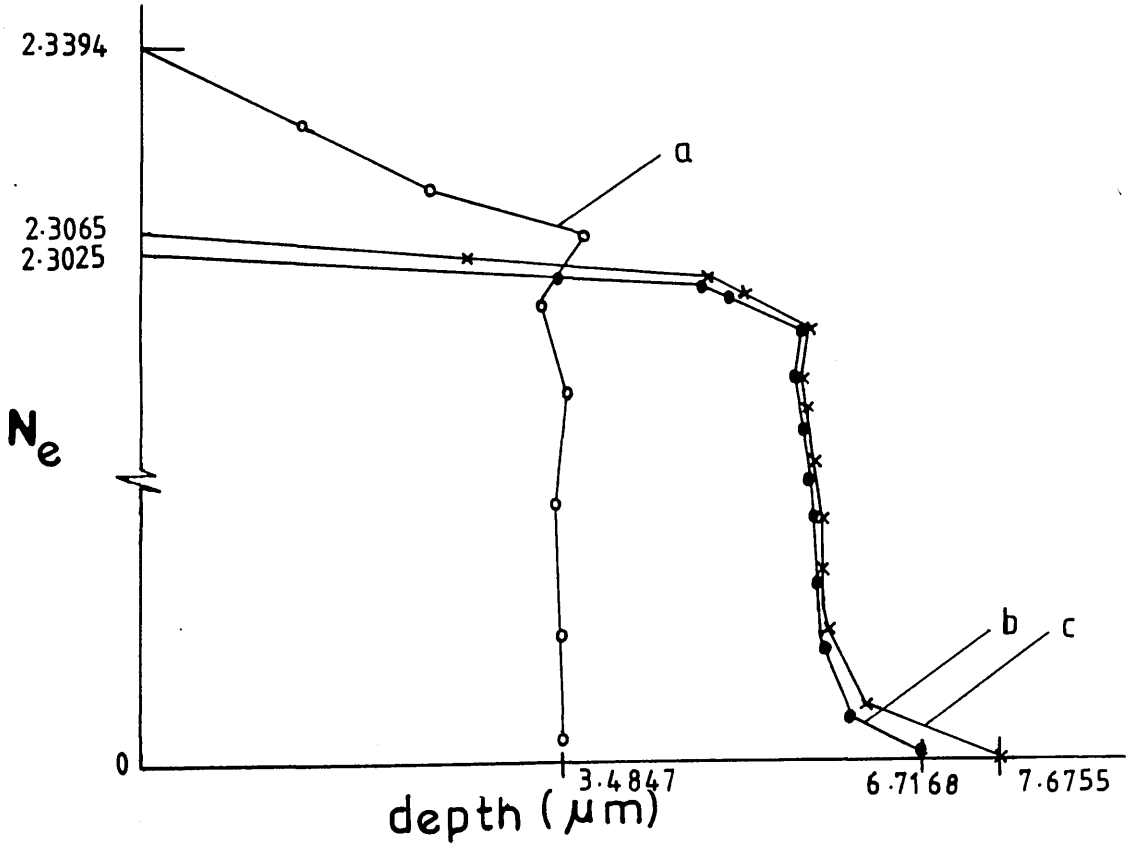

Table 3.5 Maximum change in refractive indices and the waveguide depths of the annealed [^{2}H] hydrogen - exchanged waveguides calculated by the inverse WKB program. Annealing was undertaken at 365^{o}C for 20 mins.

waveguide	maximum ΔN_e	waveguide depth (μm)	remarks
FD2	0.1040	6.7168	1st annealing
	0.1000	7.6755	2nd annealing
FD3	0.1137	4.8158	
FD4	0.1110	7.3481	

The stability of the refractive index of the [^{2}H] hydrogen-exchanged waveguides was monitored during exposure of the waveguide FD2 to ambient air. The mode angles of the first four modes were measured and the effective refractive indices were calculated for these modes on both faces of the waveguide. These indices were plotted against the time of exposure of the waveguide to ambient air and are shown in Figure 3.13.

3.6 DETERMINATION OF LITHIUM IN THE ACID AFTER THE REACTION BY ATOMIC ABSORPTION SPECTROSCOPY.

3.6.1 Determination of lithium in the benzoic acid used to fabricate the [^{1}H]- and [^{2}H] hydrogen-exchanged waveguides.

The lithium content in the acid retained after the exchange reaction was determined following the procedure described in section 2.3. The results are tabulated in table 3.6. In the acid used for the [^{1}H] hydrogen-exchange reactions, greater quantities of lithium were detected for the x-cut sample F7, than for the z-cut sample exchanged in comparable conditions, F6.

The same trend was observed for the [^{2}H] hydrogen-exchanged samples FD1, FD2, FD4 and FD3 respectively. Calculation of the ratio x in the formula $Li_{1-x}H_xNbO_3$ in the waveguiding layer based on the atomic absorption analyses

Figure 3.13 Variation of the effective refractive indices of the first four propagating modes of the waveguide FD1. The effective refractive indices were measured on both faces of the waveguide. (The waveguide was [^{2}H] hydrogen-exchanged using [^{2}H]-hydrogen labelled benzoic acid at 235 for 3.5h in air).

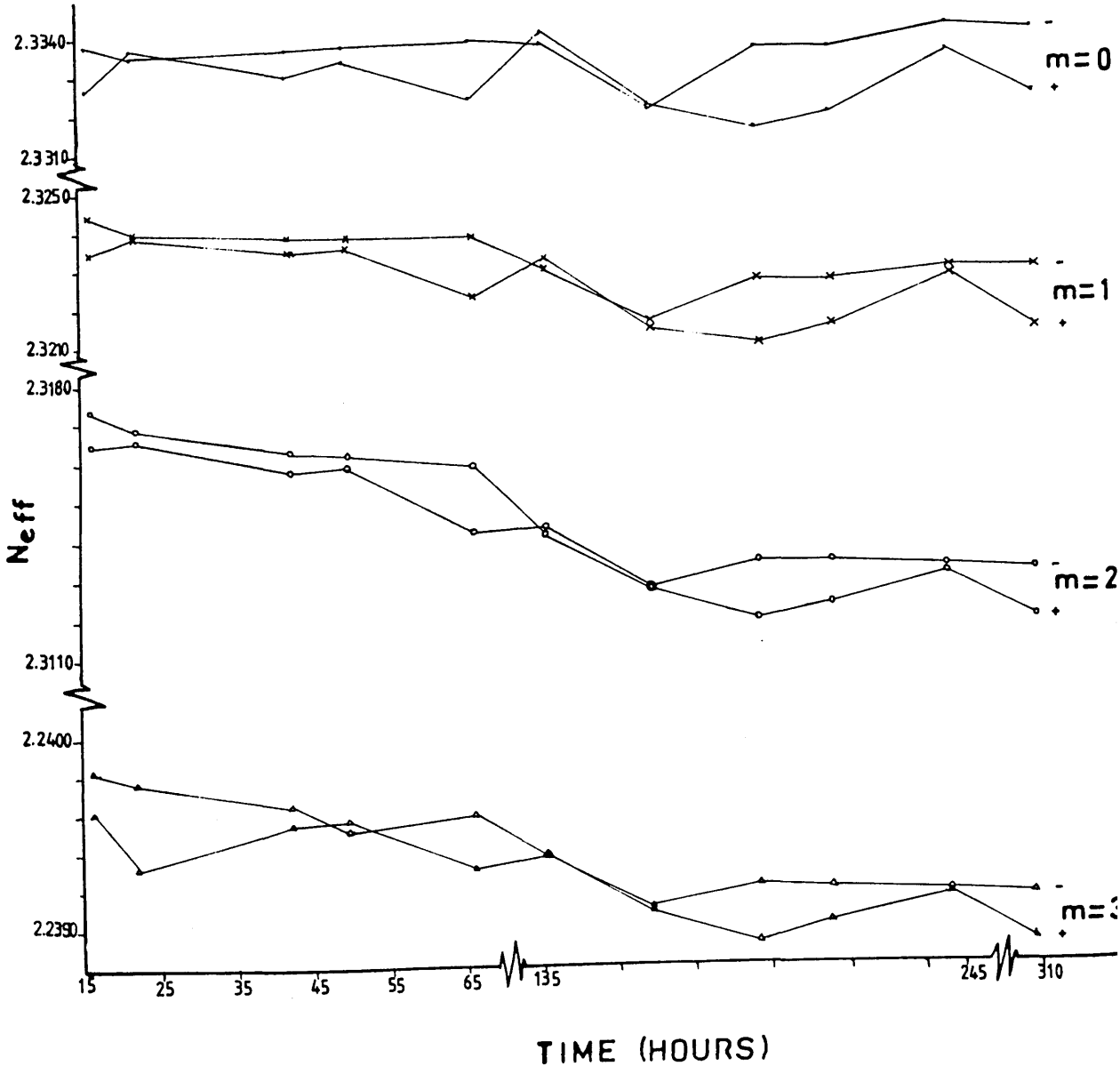

Table 3.6 Concentrations of lithium, weight of lithium per aliquot and total amount of lithium detected in the benzoic acid used for the [^{1}H]-and [^{2}H] hydrogen-exchange reactions of lithium niobate crystals determined by atomic absorption spectroscopy (AAS).

waveguide	total weight of acid (g)	acid used for the (AAS) (g)	absorbance ($\sigma \times 10^{-3}$)	concentration of lithium (PPM)	Lithium per aliquot (µg)	Total Lithium detected in the acid (µg)
F1	15.6530	1.0240	0.032(2.7)	0.04	4.0	59.4
F2	15.4689	1.0045	0.052(1.9)	0.08	8.2	127.0
F6	6.1935	1.0077	0.029(2.0)	0.17	17.1	105.4
F7	19.7358	1.0007	0.041(2.3)	0.08	8.8	175.0
FD1	5.5421	0.9997	0.021(1.7)	0.02	2.1	11.8
FD2	4.6758	0.9744	0.090(4.2)	0.02	2.3	11.2
FD3	5.6056	1.0002	0.069(3.4)	0.17	1.7	10.0
FD4	12.4060	1.0066	0.062(3.2)	0.16	16.3	203.0
FD5	22.5066	1.0094	0.030(1.8)	0.14	14.1	314.2

determined values of x = 0.35 for the [^{1}H] hydrogen-exchanged waveguides compared with x = 0.05-0.085 for the [^{2}H] hydrogen-exchanged waveguides; the maximum value which has been determined using the same technique, x = 0.33.[57] Other values for x determined using nuclear analysis ranged between x = 0.65-0.75, Canal et.al[53] and Rice et al.[48]

The results obtained by atomic absorption spectroscopy suggested that only part of the lithium exchanged was detected in the acid melt after the reaction and loss of lithium may occur during the waveguide fabrication stages.

In order to investigate the possibility that lithium was lost from the solution, for example by adsorption or evaporation during the exchange reactions, series of analyses were undertaken. In the first set, four identical weights of benzoic acid were mixed with small quantities of lithium benzoate. The mixture was heated for 4 hours, 25 min. at 235^{o}C using covered silica glass beakers with PTFE holders inside, but without $LiNbO_3$ crystals.

Two portions of each acid sample were analysed separately. The weight of lithium present in the portion of acid, determined by the analyses was calculated using the equation:

$$W_{Li} = \text{Concentration PPM}(\mu g ml^{-1}) \times 100 \text{ (ml)} \qquad (3.1)$$

This value was compared to a value calculated from the molality of lithium benzoate present in the portions,

the weight of lithium benzoate, number of moles of lithium benzoate and finally the weight of lithium present in the portion analysed as follows:

$$\text{Molality of lithium benzoate } M = \frac{Wx1000}{Wxm} \qquad (3.2)$$

$$\text{Weight of lithium benzoate in the portion } W' = \frac{Mms}{(Mm+1000)} \qquad (3.3)$$

$$\text{Moles Lithium benzoate} = w \times \frac{1}{m} \qquad (3.4)$$

$$\text{Moles Lithium} \times m_{Li} = \text{Weight of lithium} \qquad (3.5)$$

where w is the weight of lithium benzoate, W is the weight of benzoic acid, m is the molecular weight of lithium benzoate (m = 108) s is the weight of the portion analysed and m_{Li} is the molecular weight of lithium (m_{Li} = 6.941).

The results presented in table 3.7a,b indicated that, for low concentration, the lithium detected in the acid was lower than the calculated values, while the lithium amounts detected were in agreement, within the experimental error, with the calculated values if relatively higher concentrations were used.

In the second set of analyses, nine acid samples were mixed with larger amounts of lithium benzoate. Every pair of acid samples contained the same quantity of lithium

benzoate but one of them only contained the PTFE holder. The ninth acid sample (e) was mixed thoroughly with lithium benzoate then analysed without any heating involved. This sample was prepared to test whether the lithium losses could occur in any other than at the heating stage. The quantities of lithium determined and calculated for the portions analysed are presented in tables 3.8a,b.

The results showed good agreement between the determined and calculated values of lithium present within the experimental error limits, and showed no significant differences between the "C" samples (samples without PTFE holder) and the "D" samples (samples with the PTFE holder). The lithium determined for the sample (e) was in agreement with the calculated value.

3.6.2 The effect of the acid quantity on the extent of the exchange reaction.

In order to investigate the effect that the quantity of acid used in the reaction had on the extent of the exchange reaction, two z-cut $LiNbO_3$ waveguides F8 and F9 were hydrogen-exchanged at T = 235°C for 6h under N_2 atmosphere. The waveguides had identical geometric areas (1.085 cm^2). They were reacted in 24.985 and 2.9457 g of benzoic acid respectively, corresponding to 0.2048 and 0.02413 moles of acid. Two aliquots were prepared and analysed from each acid sample.

Table 3.7a Weights of total acid and total lithium benzoate used for atomic absorption spectroscopy (AAS) and the lithium benzoate molal calculated for the first set of analyses.

Sample	Total Weight of Acid (g)	Total Weight of Lithium Benzoate (g)	Lithium Benzoate molal
1	20.0000	9×10^{-4}	4.16×10^{-4}
2	20.0000	2.8×10^{-3}	1.30×10^{-3}
3	20.0000	6.1×10^{-3}	2.82×10^{-3}
4	20.0001	1.01×10^{-2}	4.67×10^{-3}

Table 3.7b. Determined weights of lithium by atomic absorption spectroscopy and the calculated weights of lithium from the lithium benzoate molal of the first set of analyses.

Sample	Weight of Portion used for AAS (g)	Concentration of lithium (ppm)	Weight of lithium determined per portion by AAS (µg)	Weight of lithium calculated per portion (µg)
1a	1.0368	6.3×10^{-4}	0.06	3
1b	1.0403	4.8×10^{-4}	0.05	3
2a	1.0088	0.03	3.13	9
2b	1.0188	0.03	3.20	9.1
3a	1.0591	0.28	28.60	20.7
3b	0.9963	0.26	26.00	19.5
4a	1.0471	0.31	31.60	33.9
4b	1.0373	0.30	30.40	33.6

Table 3.8b Determined weight of lithium by atomic absorption spectroscopy and the calculated weights of lithium from the lithium benzoate molal of the second set of analyses.

Sample	Weight of portion used for AAS (g)	Concentration of lithium (PPM)	Weight of lithium per portion determined by AAS. (µg)	Weight of lithium calculated per portion. (µg)
1c	1.0034	0.444	44.4	38.3
1d	1.0014	0.507	50.7	37.1
2c	1.0004	0.753	75.3	75.4
2d	1.0000	0.800	80.0	81.7
3c	1.0014	1.274	127.4	117.3
3d	1.0004	1.036	103.6	108.1
4c	1.0006	1.676	167.6	171.0
4d	1.0003	1.540	154.0	171.2
e	1.0000	0.572	57.2	65.5

The results of the atomic absorption analysis are presented in table 3.9. They indicated that the acid of the sample F8, exchanged in the large quantity of acid, contained a greater amount of lithium than the samples exchanged in the small weight of acid, F9. The band areas of the infra red spectra integrated for the samples in the range 3600 - 3000 cm^{-1} showed a larger peak area for F8 than for F9 which also implied that the extent of reaction was higher in the case of F8.

Table 3.9 Total Li weight, number of Li moles and infrared band areas of the acid used for the samples F8, F9 determined by atomic absorption spectroscopy acid weight was 24.985g for F8 and 2.9457g for F9 and the exchange reaction was performed at 235^{o}C for 6h under N_2 atmosphere.

Sample.	Acid Portion used for the (g)	Li concentration PPM($\sigma \times 10^{-3}$)	Total Li weight detected (μg)	Number of Li moles detected. (μmoles)	Infrared peak area (arb. unit)
1F8	1.0008	0.13 (5.5)	309.3	25.04	123.753
2F8	1.0011	0.12 (10.18)			
1F9	1.0012	0.60 (28.4)	173.8	44.55	100.017
2F9	1.0013	0.58 (11.01)			

CHAPTER FOUR

PREPARATION OF [^{1}H]-/[^{2}H] HYDROGEN ISOTOPICALLY-EXCHANGED WAVEGUIDES IN Z- AND X-CUT LITHIUM NIOBATE USING PHOSPHORIC ACID. CHARACTERISATION BY INFRARED SPECTROSCOPY AND THE PRISM-COUPLING TECHNIQUE. DETERMINATION OF LITHIUM BY ATOMIC ABSORPTION SPECTROSCOPY.

4.1 [^{1}H] HYDROGEN-EXCHANGE OF Z- AND X-CUT LITHIUM NIOBATE IN PHOSPHORIC ACID.

4.1.1 [^{1}H] Hydrogen-exchange of z-cut lithium niobate in phosphoric acid.

Recently, Yamamoto et al[92] have reported the fabrication of superior waveguides with a large change in the refractive index (Δn_e = 0.145) on z-cut $LiNbO_3$, using pyrophosphoric acid. In order to investigate the properties of waveguides prepared using phosphoric acid, two sets of z-cut $LiNbO_3$ crystals were hydrogen-exchanged at 215^{o}C in phosphoric acid. The first set was exchanged in orthophosphoric acid (85%) whereas the second was prepared using pyrophosphoric acid (97%). The temperatures and times at which the waveguides were exchanged in ortho and pyrophosphoric acid are listed in table 4.1.

The infrared spectra of the waveguides fabricated in ortho and pyrophosphoric acids were very similar and identical to that of z-cut [^{1}H] hydrogen-exchanged waveguides fabricated under the same conditions using benzoic acid.

The spectra consisted of a strong sharp band at 3505 cm^{-1} overlapping a very weak broad band on the low-frequency side. The superimposed spectra of the z-cut waveguides fabricated in orthophosphoric acid (85%) are shown in Figure 4.1. The figure indicates that the extent of the reaction increases as the time of reaction increases.

Table 4.1 Reaction temperatures and times of waveguides fabricated using ortho and pyrophosphoric acids in air.

Waveguide	Fabrication temperature (°C)	Fabrication time (h,min)
OF1	215	0,10
OF2	215	0,25
OF3	215	0,40
OF4	215	1,0
OF5	215	2,0
OF6	215	3,0
OF7	215	4,25
OF8	215	6,0
PF1	215	0,25
PF2	215	3,0
PF3	215	6,0
PF4	235	6,0
PF5	235	6,0

*The "OF" waveguides were fabricated using orthophosphoric acid (85%).

**The "PF" waveguides were fabricated using pyrophosphoric acid (97%).

Figure 4.1 Superimposed infrared spectra of z-cut lithium niobate waveguides fabricated using orthophosphoric acid at 215^{o}C in air. Fabrication time was : a:t = 25 min b:t = 40 min, c:t = 1h, d:t = 2h, e:t = 3h, f:t = 4h 25min and g:t = 6h.

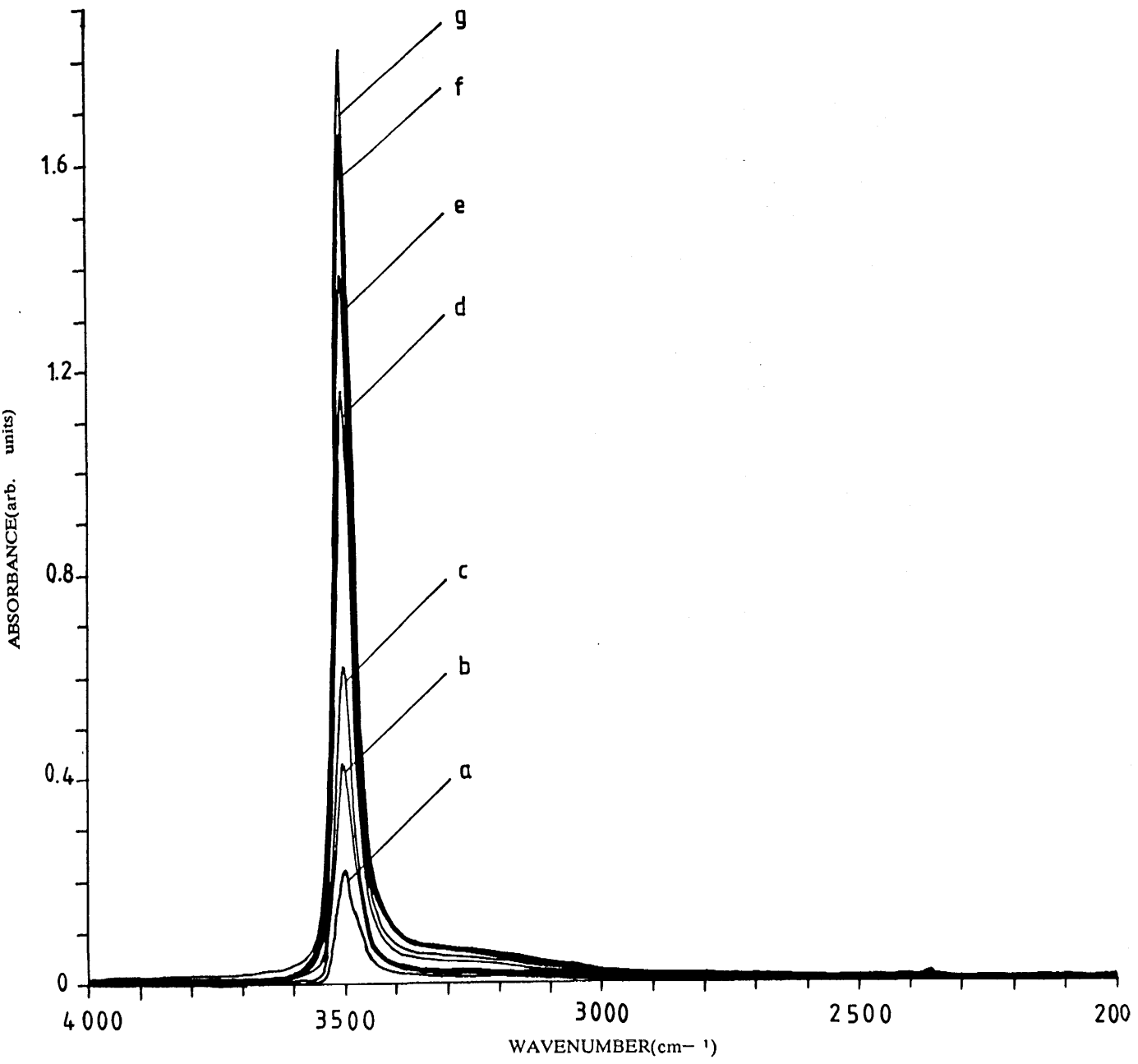

The areas of the infrared bands were integrated for the orthophosphoric acid waveguides over the region from 3650 to 2900 cm^{-1} and when plotted against the square root of the reaction time, gave a straight line represented by the equation:

$$(\text{band area}) = 45.788\ t^{\frac{1}{2}}\ (h)^{\frac{1}{2}} - 0.064 \qquad (4.1)$$

This may be compared to an equation that has been calculated for z-cut $LiNbO_3$ waveguides fabricated in benzoic acid at the same temperature:[57]

$$(\text{band area}) = 40.189\ t^{\frac{1}{2}}\ (h)^{\frac{1}{2}} - 1.080 \qquad (4.2)$$

The plot of the infrared band areas versus the square root of the exchange time for the waveguides fabricated in orthophosphoric acid is depicted in figure 4.2.

Concentrated orthophosphoric acid prepared as described in sections 2.1.2.3, 2.1.2.4 and 2.1.2.5 was used to fabricate four z-cut $LiNbO_3$ samples at 230^{o}C for 4h under an argon atmosphere. The infrared spectra of the waveguides were identical to the spectra shown in figure 4.1. The integrated band areas of the various waveguide spectra are presented together with the reaction conditions for each waveguide in table 4.2. All the waveguides had comparable band areas except for the waveguide CF3 which had an area which was insufficient to be measurable.

Figure 4.2 Infrared band area as a function of $t^{\frac{1}{2}}$ for z-cut hydrogen-exchanged lithium niobate waveguides fabricated in orthophosphoric acid at 215°C.

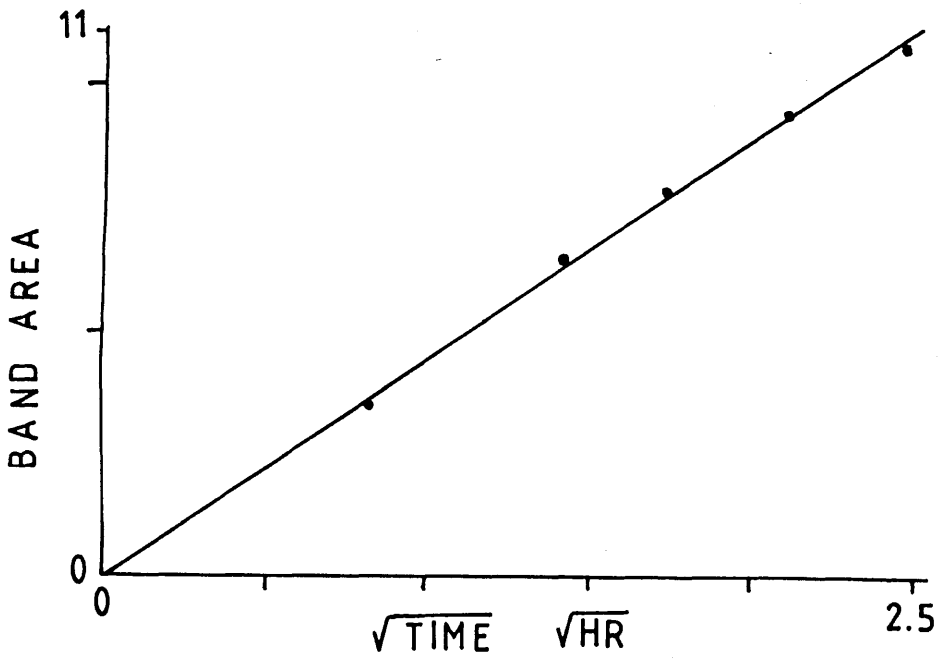

Table 4.2 Method of acid preparation and the integrated infrared band areas of z-cut $LiNbO_3$ waveguides fabricated in concentrated orthophosphoric acid at 230°C for 4h under Ar atmosphere.

Waveguide	Acid	IR band area (arb.units)
CF1	85% orthophosphoric acid.	99.20
CF2	97% pyrophosphoric acid.	112.56
CF3	acid prepared by hydrolysis of pyrophosphoric acid. (Section 2.1.2.3).	-
CF4	acid prepared by hydrolysis of P_2O_5 (Section 2.1.2.4).	101.20
CF5	acid prepared by hydrolysis of P_2O_5 (Section 2.1.2.4).	111.07
CF6	acid prepared by hydrolysis of $POCl_3$ (Section 2.1.2.5).	110.50

4.1.2 [^{1}H] Hydrogen-exchange of x-cut lithium niobate in phosphoric acid.

It has been reported in the literature[92] that the use of pyrophosphoric acid for the fabrication of waveguides in $LiNbO_3$ is limited to z-cut material. X- and z-cut $LiNbO_3$ crystals were fabricated at 230°C for 3.5h in air using orthophosphoric acid (85%). The reaction produced a deep waveguide in the z-cut material but severely damaged the x-cut material. Micrographs of the x-cut $LiNbO_3$ waveguide taken in a scanning electron microscope showed a very rough surface as shown in figure 4.3.

A set of experiments attempting to fabricate optical waveguides on x-cut $LiNbO_3$ was performed using phosphoric acid but at lower temperature and for shorter times. Mono-mode waveguides were successfully fabricated, for the first time by hydrogen-exchange in pyrophosphoric acid with x-cut $LiNbO_3$ at a temperature of 200°C for times ranging from 2 to 30 min. The waveguides and the times of reaction are presented in table 4.3.

The infrared spectra of these waveguides were similar to the spectra of x-cut $LiNbO_3$ waveguides prepared using benzoic acid. They consisted of a sharp strong band at 3505 cm^{-1} overlapping a broad band at 3260 cm^{-1}. The superimposed spectra of the x-cut waveguides fabricated using pyrophosphoric acid are depicted in figure 4.4. The areas of the infrared bands were integrated over the range

Figure 4.3 Micrographs taken by scanning electron microscope in different magnifications for a damaged x-cut lithium niobate waveguide fabricated in orthophosphoric acid at 230^{o}C for 3.5h.

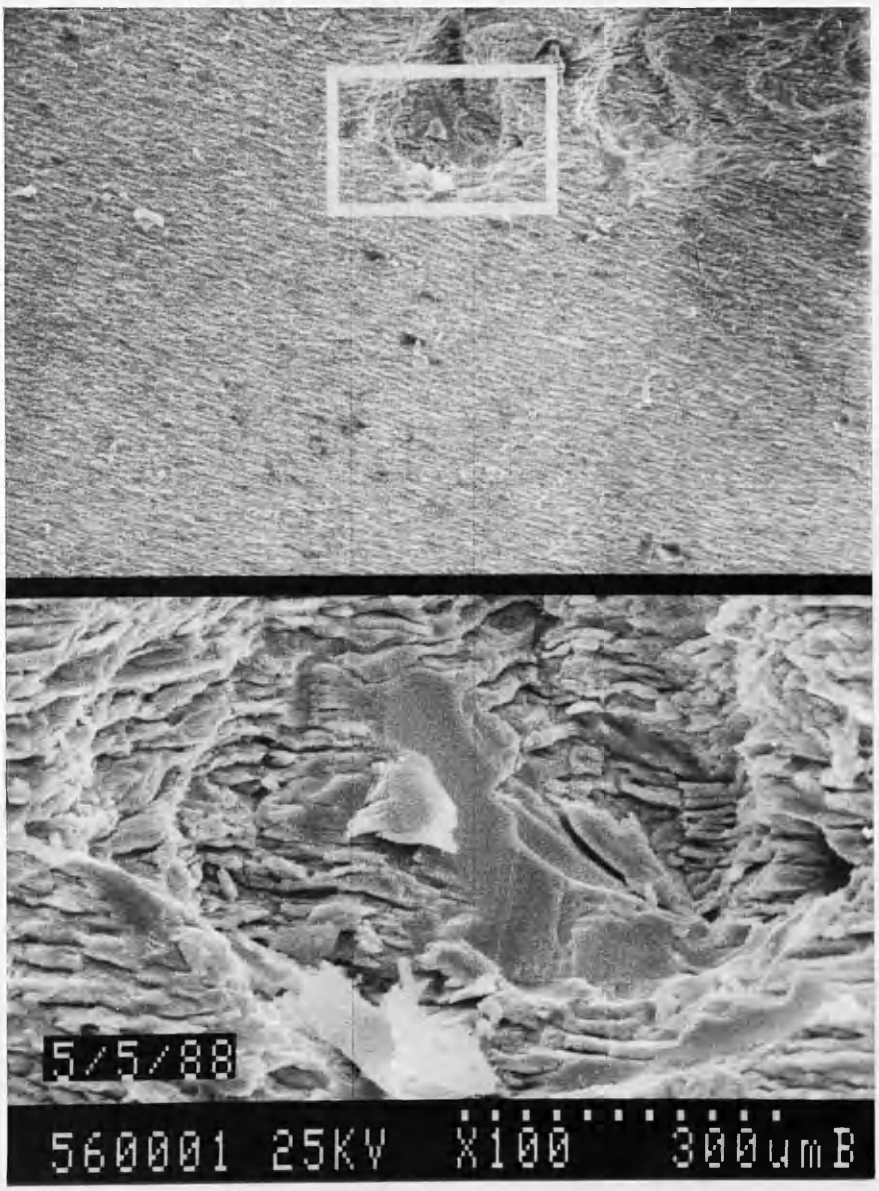


5/5/88
560000 25KV X1.50K 20.0um

Table 4.3 The reaction times of the waveguides fabricated on the x-cut $LiNbO_3$ using pyrophosphoric acid at 200°C in air.

Waveguide	Fabrication Time (min)
XP1	2
XP2	4
XP3	6
XP4	8
XP5	10
XP6	15
XP7	30

Figure 4.4 Superimposed infrared spectra of x-cut hydrogen-exchanged lithium niobate waveguides fabricated using pyrophosphoric acid at 200°C in air. Fabrication time was : a:t = 2 min, b:t = 4 min, c:t = 6 min, d:t = 8 min, e:t = 10 min, f:t = 15 min and g:t = 30 min.

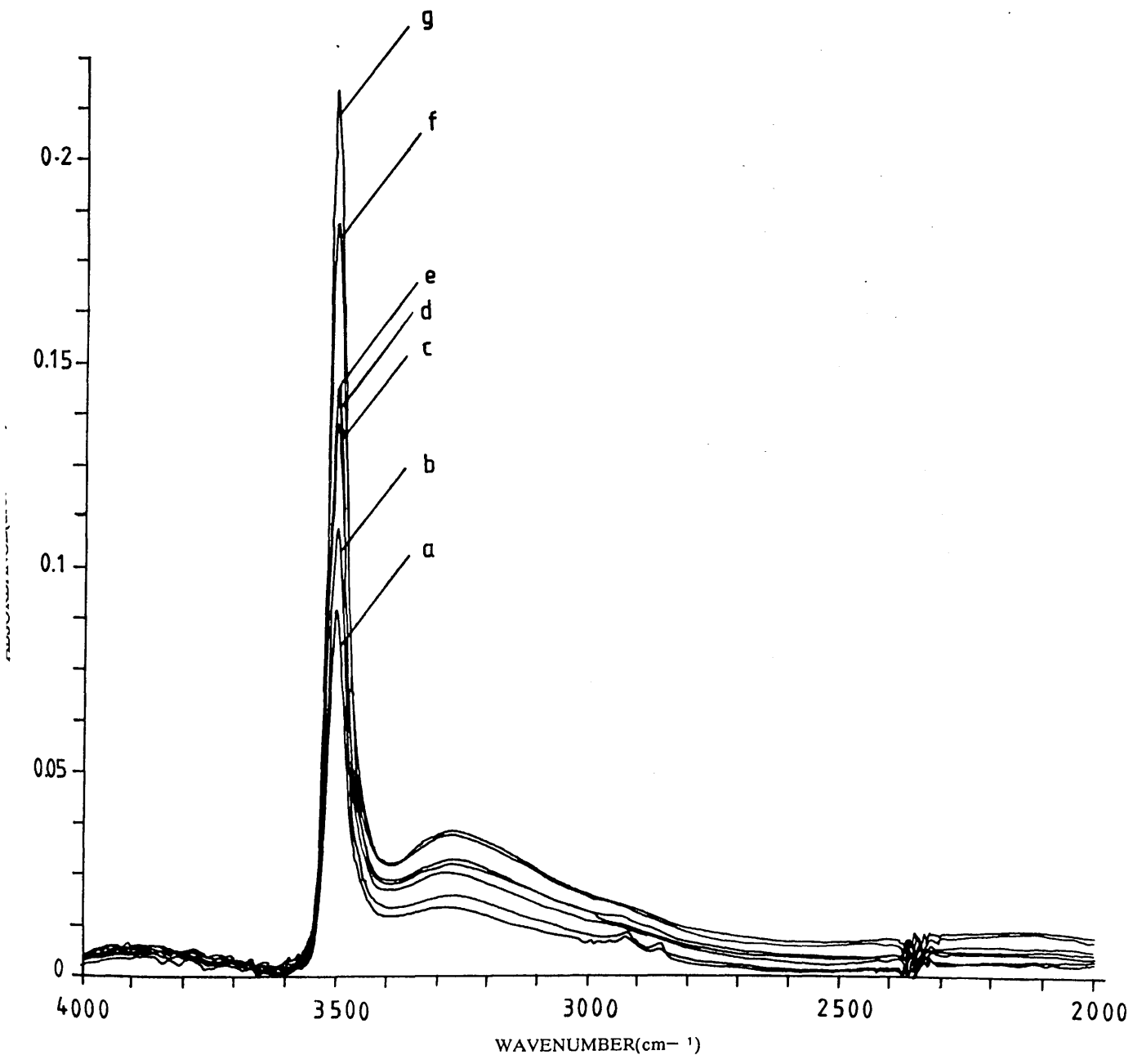

from 2600 to 3600 cm^{-1}. These areas when plotted against the square root of the reaction time, gave a straight line of the form:

$$(\text{band area}) = 31.4928\ t^{\frac{1}{2}}\ (h)^{\frac{1}{2}} + 0.9390 \qquad (4.3)$$

This may be compared to the results reported in the literature[57] for x-cut $LiNbO_3$ waveguides fabricated in benzoic acid at 198.7°C for times up to 3.5h which was of the form:

$$(\text{band area}) = 31.914\ t^{\frac{1}{2}}\ (h)^{\frac{1}{2}} \qquad (4.4)$$

The plot of the band areas versus the square root of the reaction times for x-cut $LiNbO_3$ waveguides fabricated in pyrophosphoric acid is shown in figure 4.5.

4.2 OPTICAL CHARACTERISATION OF WAVEGUIDES FABRICATED ON Z-CUT LITHIUM NIOBATE IN PHOSPHORIC ACID BY THE PRISM-COUPLING TECHNIQUE AT WAVELENGTH λ = 0.6328 μm.

The optical properties of waveguides fabricated on z-cut $LiNbO_3$ using phosphoric acid were characterised utilizing the prism-coupling technique at a wavelength of λ = 0.6328 μm. The waveguides showed a step-like refractive index/depth profile similar to that of hydrogen-exchanged waveguides fabricated in benzoic acid. Surface refractive indices and waveguide depths were calculated using the inverse WKB and the step-index computer programs.

Figure 4.5 Infrared band area as a function of $t^{\frac{1}{2}}$ for x-cut hydrogen-exchanged lithium niobate waveguides fabricated in pyrophosphoric acid at 200°C.

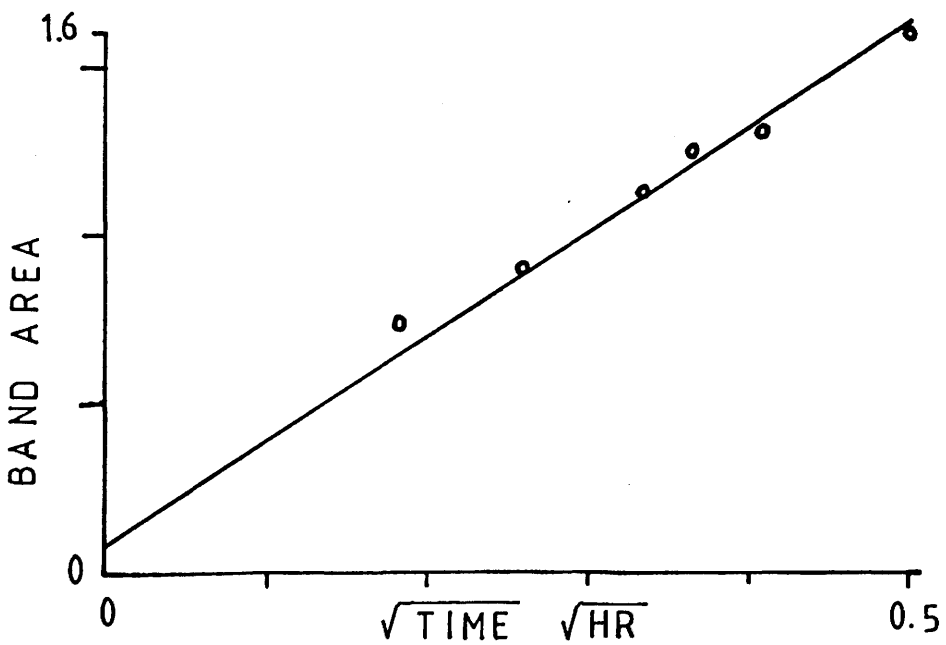

The number of modes supported, surface refractive indices and the waveguide depths of the waveguides fabricated in ortho and pyrophosphoric acids calculated by the step-index program are presented in tables 4.4 and 4.5 respectively. A typical refractive index/depth profile is presented in figure 4.6. The maximum changes in the extraordinary refractive index calculated by the step-index program was $(\Delta n_e)_{max}$ = 0.1324 for waveguide OF7 and 0.1284 for waveguide PF7 which were fabricated using ortho and pyro phosphoric acid respectively.

By plotting the waveguide depths against the square root of the exchange time, straight lines of the form:

$$\text{depth}(\mu m) = 0.9343\ t^{\frac{1}{2}}\ (h)^{\frac{1}{2}} - 0.044 \qquad (4.5)$$

$$\text{depth}\ (\mu m) = 0.9619\ t^{\frac{1}{2}}\ (h)^{\frac{1}{2}} + 0.0185 \qquad (4.6)$$

were obtained for waveguides fabricated in ortho and pyro-phosphoric acids respectively, which are presented in figures 4.7 and 4.8 respectively.

By substituting the slope of these plots in equation 1.10, the effective diffusion coefficient $D(t)\ (\mu m^2 h^{-1})$ could be calculated at the exchange temperature (483K) which were 0.2182 and 0.2313 $(\mu m^2 h^{-1})$ for the reactions in ortho and pyrophosphoric acids respectively.

For samples fabricated using concentrated ortho-phosphoric acid, the optical properties were assessed by the

Table 4.4 The number of modes supported, surface refractive index and waveguide depth calculated using the step-index computer program, for the waveguides fabricated on z-cut $LiNbO_3$ using orthophosphoric acid.

Waveguide	No. of supported modes	the surface refractive index (σ)	waveguide depth (μm)
OF1	1	2.2028*	*0.04
OF2	1	2.2787*	*0.38
OF3	2	2.3311 (2.3×10^{-5})	0.683
OF4	2	2.3345 (3.7×10^{-5})	0.856
OF5	3	2.3347 (1.4×10^{-3})	1.267
OF6	4	2.3340 (1.5×10^{-3})	1.570
OF7	5	2.3349 (1.3×10^{-3})	1.949
OF8	6	2.3339 (2.2×10^{-3})	2.249

The extraordinary refractive index of bulk $LiNbO_3$ = 2.2025

*Effective refractive indices calculated using eqn. 1.9 and the effective depths estimated from a plot of N vs. d for these waveguides.

Table 4.5 The number of supported modes, surface refractive index and waveguide depth calculated using the step-index program for waveguides fabricated on z-cut $LiNbO_3$ using pyrophosphoric acid.

Waveguide	No. of Supported modes	Surface refractive index (σ)	Waveguide depth (μm)
PF1	1	2.2699*	-
PF2	3	2.3304 (2.05×10^{-3})	1.342
PF3	5	2.3309 (2.64×10^{-3})	1.981

*Effective refractive index calculated using the equation (1.9).

Figure 4.6 A typical refractive index/depth profile of a z-cut hydrogen-exchanged waveguide fabricated in orthophosphoric acid, determined by the inverse WKB method. (The waveguide OF8 was fabricated for 6h at 215 ^{o}C).

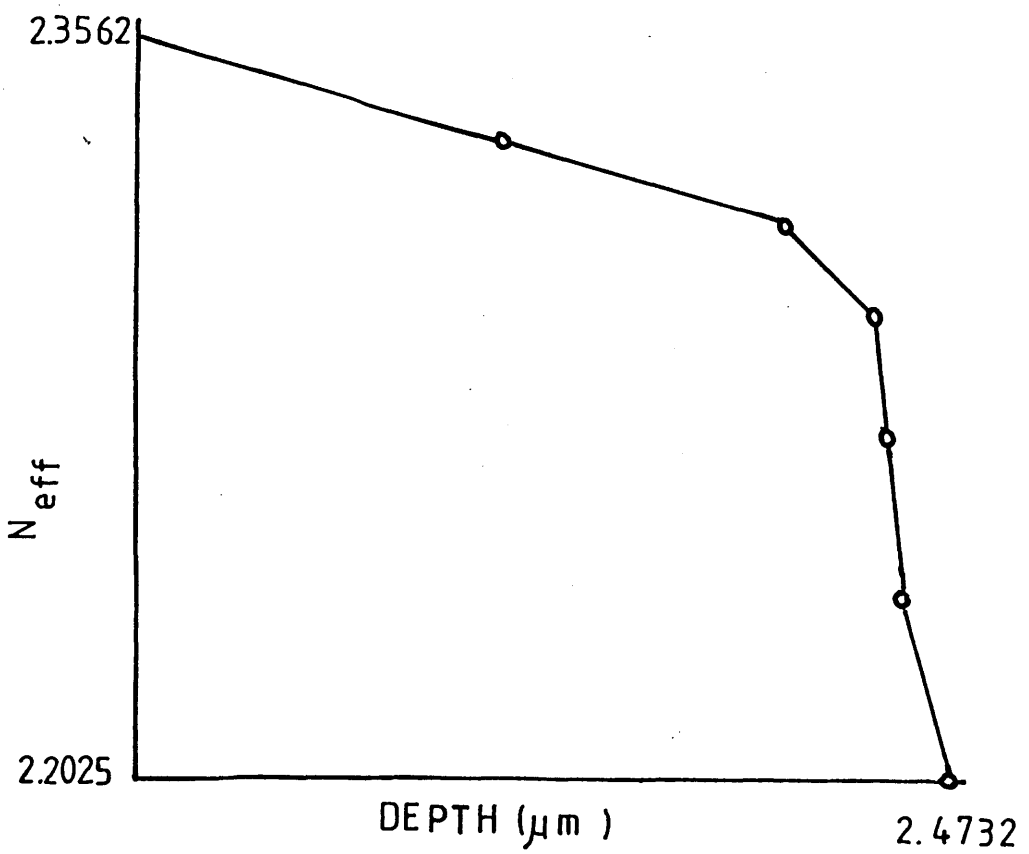

Figure 4.7 Waveguide depth as a function of $t^{\frac{1}{2}}$ for z-cut hydrogen exchanged lithium niobate waveguides fabricated in orthophosphoric acid at 215°C.

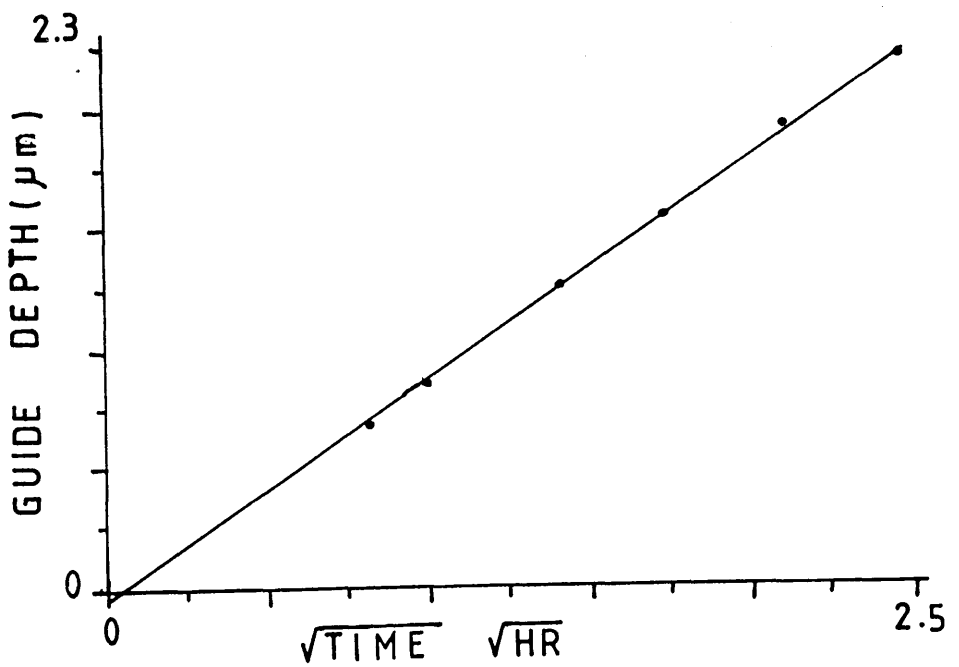

Figure 4.8 Waveguide depth as a function of $t^{\frac{1}{2}}$ for z-cut hydrogen-exchanged lithium niobate waveguides fabricated in pyrophosphoric acid at 215°C.

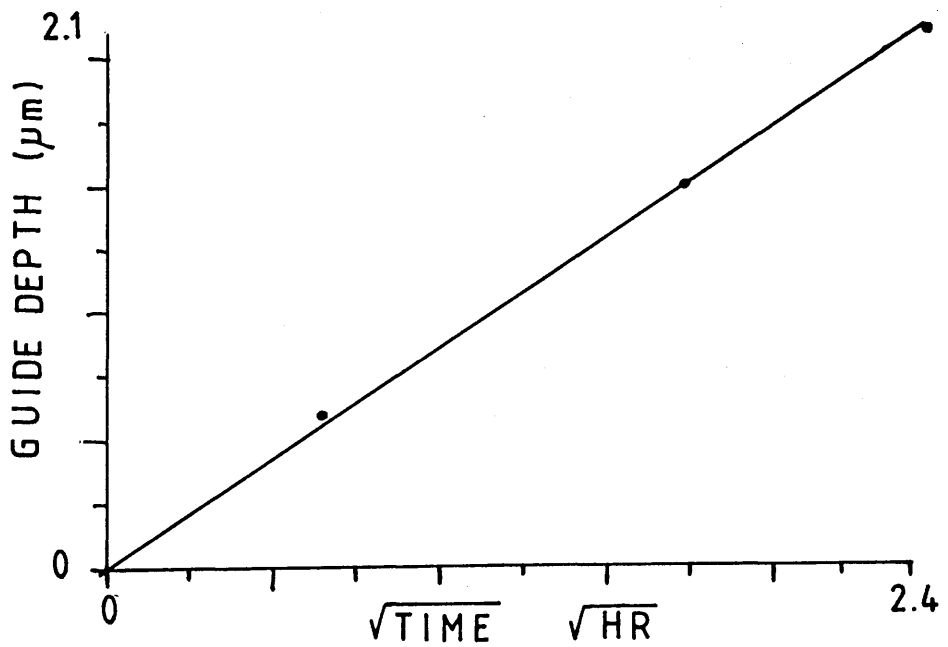

prism-coupling technique at a wavelength λ = 0.6328 μm. The surface refractive indices and waveguide depths, calculated using both the inverse WKB and the step-index programs are presented in table 4.6. The mode angles of the x-cut waveguide were measured and the effective refractive indices are presented in table 4.7, it is not possible to calculate the surface refractive index and the waveguide depth of mono-mode waveguides directly by either method.

4.3 [^{2}H] HYDROGEN-EXCHANGED WAVEGUIDE IN Z-CUT LITHIUM NIOBATE FABRICATED USING [^{2}H]-HYDROGEN LABELLED ORTHOPHOSPHORIC ACID.

4.3.1 Preparation of z-cut [^{2}H] hydrogen-exchanged waveguide and its exposure to water vapour and [^{2}H]-hydrogen labelled water vapour.

The [^{2}H] hydrogen-exchange reaction was carried out in a nitrogen atmosphere using [^{2}H]-hydrogen labelled ortho-phosphoric acid prepared as described in section 2.1.2.6.

The waveguide DZ1 was [^{2}H] hydrogen-exchanged at 225^{o}C for four hours. An infrared spectrum recorded before exposing the waveguide to water vapour in ambient air (t = 0) showed an intense sharp band at 2588 cm^{-1} in the [^{2}H] hydroxyl stretching region. A weak band consisting of two overlapping maxima at 3500 and 3475 cm^{-1} and a weak broad overlapping band at 3280 cm^{-1} in the [^{1}H]-hydrogen

Table 4.6 The surface refractive indices and waveguide depths calculated using the step-index and inverse WKB programs for the z-cut $LiNbO_3$ waveguides fabricated in concentrated orthophosphoric acid.

	Step-index program		Inverse WKB program	
Waveguide	Surface refractive index ($\sigma x10^{-3}$)	Waveguide depth (μm)	Surface refractive index	Waveguide depth (μm)
CF1	2.3286 (4.14)	2.5048	2.3600	2.6839
CF2	2.3288 (5.34)	2.9071	2.3579	2.9614
CF3	2.3314 (3.26)	2.6890	2.3587	2.7892
CF5	2.3307 (3.81)	2.8968	2.3597	3.0675
CF6	2.3331 (2.88)	3.1384	2.3561	3.3281

stretching region were also observed. The waveguide was then exposed to water vapour in ambient air for a total period of 1800 hours.

The superimposed infrared spectra recorded during exposure of the sample DZ1 to ambient air are depicted in figure 4.9. The absorbance of the sharp band in the [^{2}H]-hydroxyl stretching region exhibited a progressive reduction while the bands in the [^{1}H]-hydroxyl region showed a steady increase, to a certain extent, in the absorbance during the exposure of the waveguide to water vapour in ambient air.

The polarised infrared spectra recorded for waveguide DZ1 were very similar to those of FD3 in section 3.4.2. (Z-cut [^{2}H] hydrogen-exchanged in [^{2}H]-hydrogen labelled benzoic acid). The areas under the infrared bands at 3505 and 2588 cm^{-1} were determined by integrating the spectra recorded at a number of times throughout the course of exposure of the waveguide to water vapour in ambient air.

The changes in the percentage ratio:

$$[\{(\text{area at } t=t_1)-(\text{area at } t=0)\}/(\text{area at } t=0)]\times 100\% \qquad (4.7)$$

were calculated for both bands and plotted against the time of exposure as shown in figure 4.10.

In an attempt to investigate the effect of exposure of the waveguide at this stage, to [^{2}H]-hydrogen labelled water vapour at room temperature, the partially exchanged

Figure 4.9 Infrared spectra of z-cut [H] hydrogen-exchanged waveguide DZ1, superimposed as a function of time of exposure of the sample to H_2O water vapour in air. Exposure time was a:t = 0, b:t = 126h, and c:t = 1800h. (The waveguide was fabricated using $[^2H]$-hydrogen labelled orthophosphoric acid at 225°C for 4h in N_2 atmosphere).

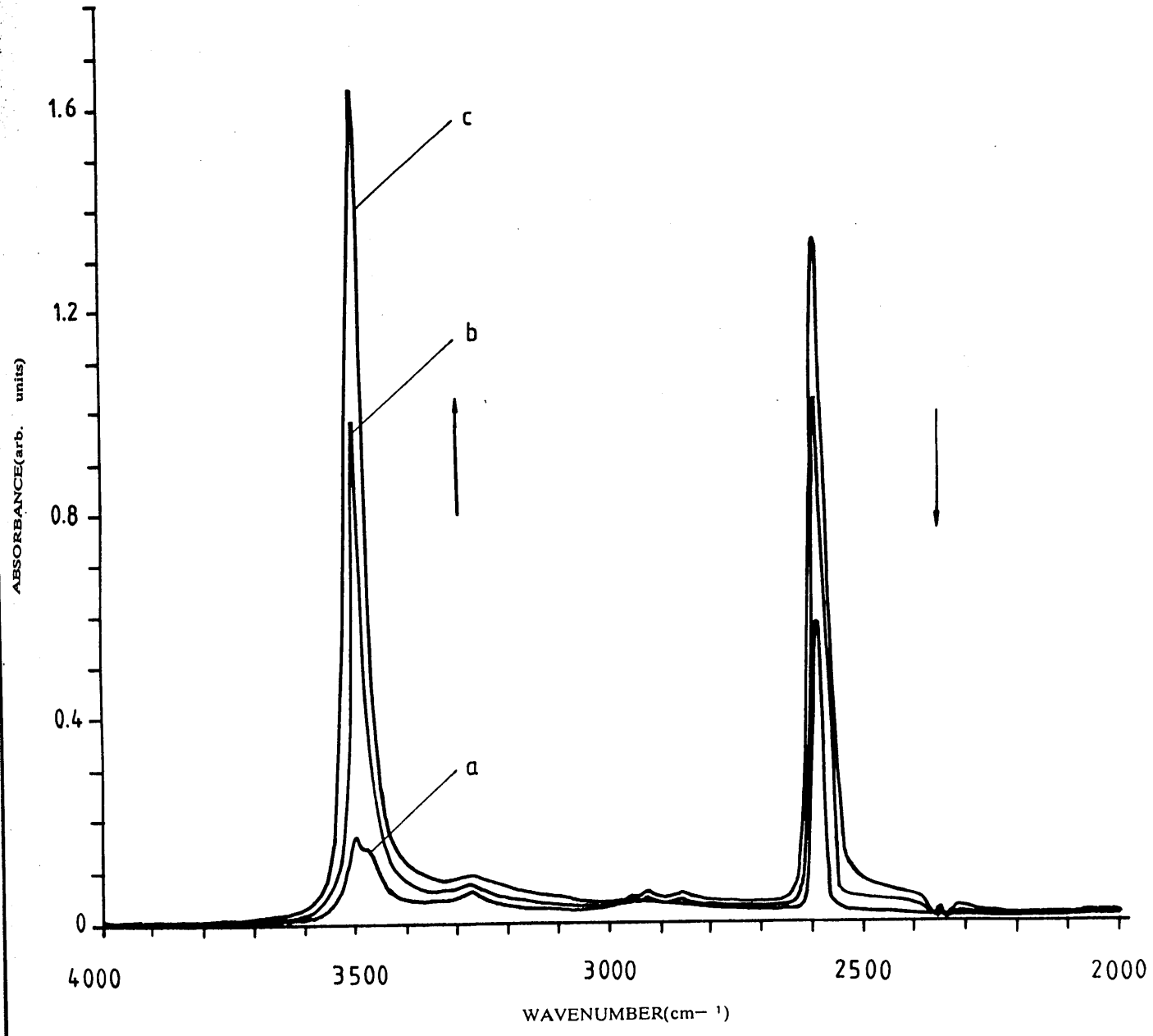

Figure 4.10 Percentage of the infrared band area of the [^{2}H] hydrogen-exchanged waveguide DZ1, as a function of time of exposure of the sample of H_2O water vapour in air. (The waveguide was fabricated using [^{2}H]-hydrogen labelled orthophosphoric acid at 225^{o}C for 4h).

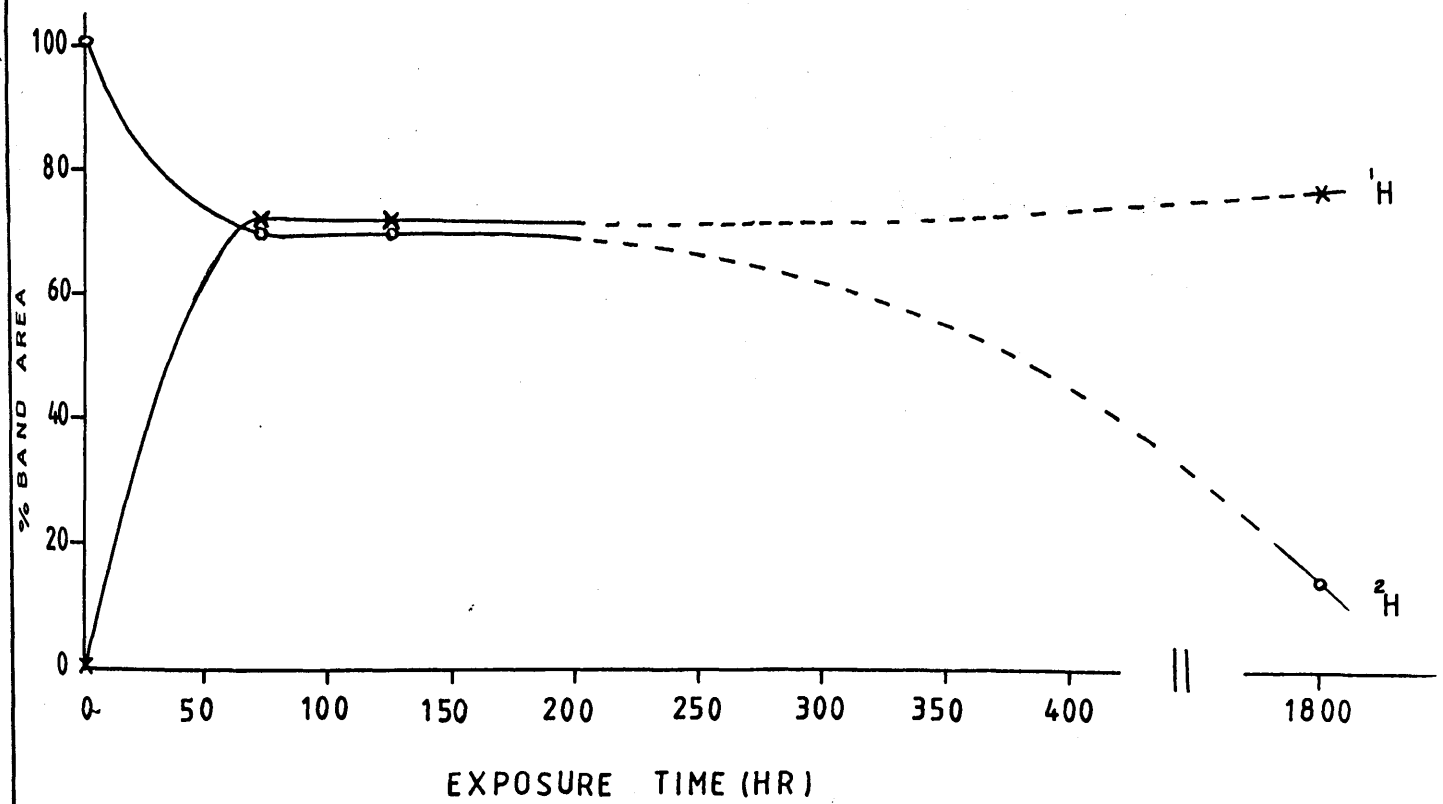

[^{1}H-^{2}H] waveguide derived from DZ1 was exposed to [^{2}H]-hydrogen labelled water vapour according to the procedure described in section 2.4.2 for 91 hours. Its superimposed infrared spectra, figure 4.11, showed an increase of 66% in the area of the sharp band at 2588 cm^{-1} in the [^{1}H]-hydroxyl region.

This behaviour indicates that the [^{1}H-^{2}H] hydrogen isotopic-exchange in z-cut [^{2}H] hydrogen-exchanged samples is essentially a reversible reaction. The observed results were not analogous to x-cut [^{2}H] hydrogen-exchanged waveguides fabricated in [^{2}H]-hydrogen labelled benzoic acid, section 3.2, but were analogous to z-cut [^{1}H] hydrogen-exchanged in benzoic acid.[76]

The areas of the infrared bands at 3505 and 2588 cm^{-1} were integrated several times throughout the course of exposing the waveguide to [^{2}H]-hydrogen labelled water vapour. The percentage ratio of the band areas were plotted against the time of exposure and are presented in figure 4.12.

4.3.2 Exposure of the [^{2}H] hydrogen-exchanged waveguide to [^{2}H]-hydrogen labelled water vapour at elevated temperature : The annealing process.

The effect of annealing of the [^{2}H] hydrogen-exchanged waveguides in [^{2}H]-hydrogen labelled water vapour was investigated at 365^{o}C. The waveguide was annealed

Figure 4.11 Infrared spectra of z-cut [^{2}H] hydrogen-exchanged waveguide LZ1. Superimposed as a function of time of exposure of the sample to [^{2}H] hydrogen labelled water vapour at room temperature. Exposure time was a:t = 0, b:t = 18h, c:t. = 24h and d:t = 91h.

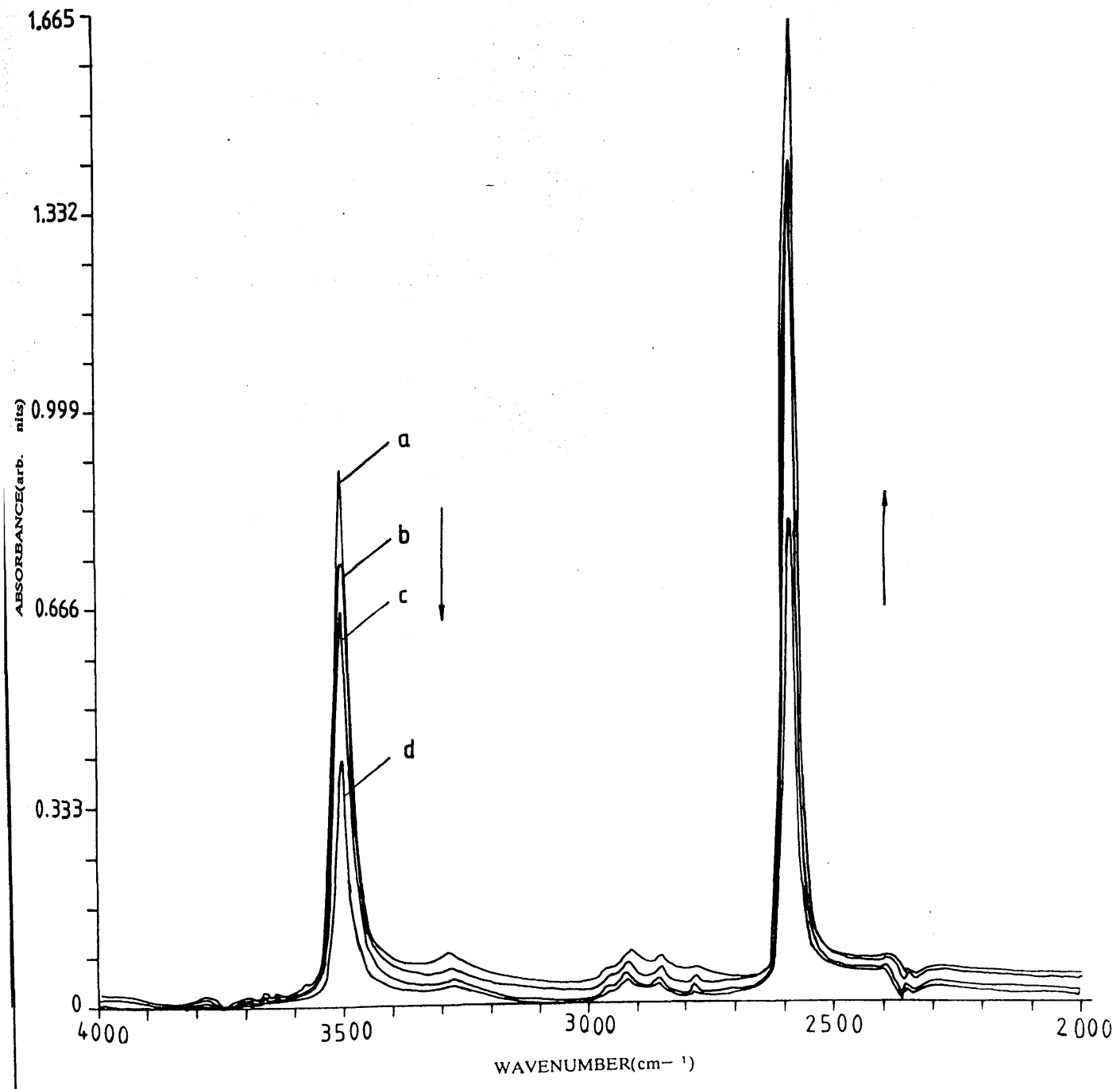

Figure 4.12 Percentage of the infrared band area of the [^{2}H] hydrogen-exchanged waveguide DZ1 superimposed as a function of time of exposure of the sample to [^{2}H] -hydrogen labelled water vapour at room temperature.

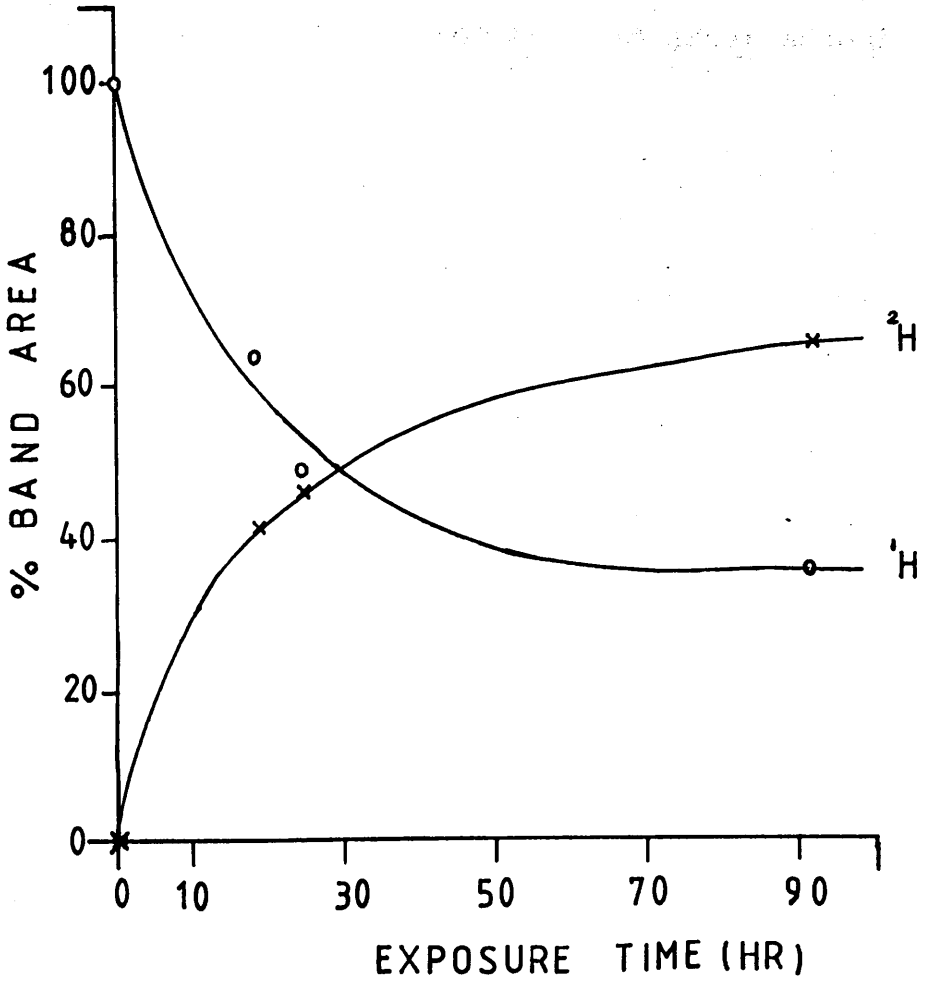

for 20 min. in oxygen flowing at a rate of 0.2 ℓ min^{-1} and bubbled through a 10 cm column of [^{2}H]-hydrogen labelled water heated to 85^{o}C.

The infrared spectra of the annealed sample showed an increase of 247% in the area of the sharp band at 2588 cm^{-1} in the [^{2}H]-hydroxyl stretching region and a decrease of 61% in the area of the sharp band at 3505 cm^{-1} in the [^{1}H]-hydroxyl stretching region. The superimposed infrared spectra of the waveguide DZ1 prior to, and after annealing are depicted in figure 4.13.

4.3.3 The optical properties of the [^{2}H] hydrogen-exchanged waveguides fabricated using [^{2}H]-hydrogen labelled orthophosphoric acid, characterised by the prism-coupling technique at a wavelength of λ = 0.6328 μm.

The optical properties of the [^{2}H] hydrogen-exchanged waveguide DZ1 were assessed during exposure of the waveguide to water vapour in air, by the prism-coupling technique at λ = 0.6328 μm. The waveguide supported six TM modes and possessed a step-like refractive index/depth profile with a surface refractive index of n_{sur} = 2.3598 and waveguide depth of d_g = 2.8276 μm, calculated by the inverse WKB program. The optical properties, when examined after the annealing process, showed that the number of modes supported had increased to eight and that the surface refractive index had decreased to n_{sur} = 2.3145 while the

waveguide depth had increased to 4.2420 μm. The surface refractive index/depth profile of the waveguide DZ1 calculated after the annealing is depicted in figure 4.14.

4.4 DETERMINATION OF THE LITHIUM CONTENT OF PHOSPHORIC ACID AFTER THE EXCHANGE REACTION USING ATOMIC ABSORPTION SPECTROSCOPY (AAS).

4.4.1 Determination of lithium in phosphoric acid used for [^{1}H] and [^{2}H] hydrogen-exchange reactions.

The orthophosphoric acid sample melts used to fabricate waveguides on z-cut $LiNbO_3$ were retained and analysed by atomic absorption spectroscopy in an attempt to determine the amount of lithium out-diffused from the waveguides. The results are presented in table 4.8. The waveguides LX and LZ, x- and z-cut $LiNbO_3$ respectively were hydrogen-exchanged at 230^{o}C for 3·5 hours in orthophosphoric acid (85%). Two aliquots were prepared of each acid and analysed separately.

The results showed that greater amounts of lithium were detected in the acid used to fabricate the x-cut waveguide than in the acid used to fabricate the z-cut waveguide (samples LX and LZ). This agreed with the results presented earlier in this work and in the literature for benzoic acid.[57]

The total quantity of lithium detected in the [^{2}H]-hydrogen labelled orthophosphoric acid used to fabricate DZ1

Figure 4.13 Superimposed infrared spectra of z-cut [^{2}H] hydrogen-exchanged waveguide DZ1 (a) before annealing, (b) after annealing. (The waveguide was annealed at 365^{o}C for 20 min in($^2H_2O/O_2$)[^{2}H]-hydrogen labelled water wet oxygen).

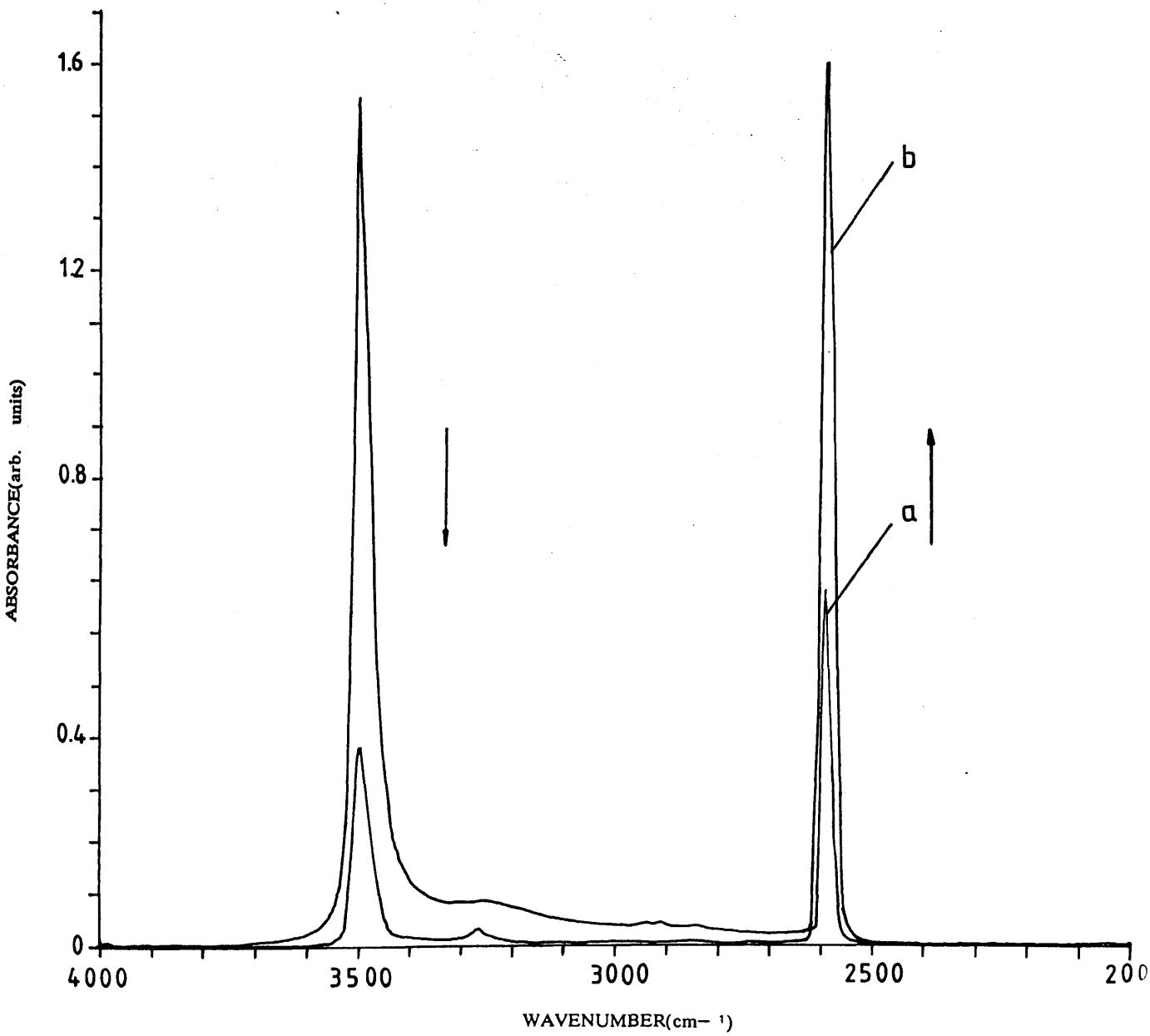

Figure 4.14 Refractive index/depth profile of the z-cut [^{2}H] hydrogen-exchanged waveguide D^{Z1}, (a) before annealing (b) after annealing. (The waveguide was annealed at 365^{o}C for 20 min in($^2H_2O/O_2$)[^{2}H]-hydrogen labelled water wet oxygen).

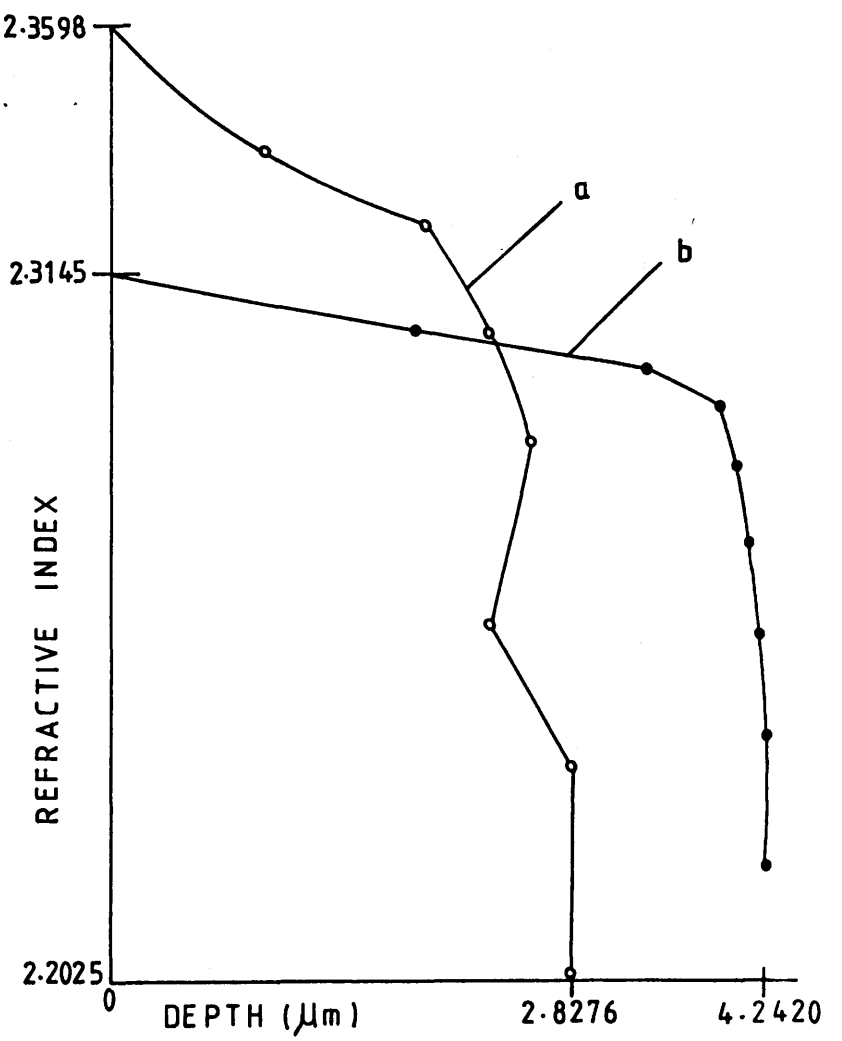

Table 4.8 Weight of Li per lg of the acid and the total weight of Li in the acids used to [^{1}H] and [^{2}H] hydrogen exchange, z- and x-cut $LiNbO_3$ waveguides determined by atomic absorption spectroscopy.

Acid of the sample	Total acid used for reaction (g)	Portion of acid used for the AAS (g)	Li per portion of acid analysed (μg)	Li per lg of the acid (μg)	Total weight of lithium detected (μg)
CF1	13.0333	0.9994	17.4	17.4	227.0
CF2	20.7024	1.0024	8.7	8.6	184.2
CF4	4.5500	1.0028	34.2	34.1	155.4
CF5	5.5521	1.0025	25.9	25.8	143.6
CF6	18.6470	1.0016	16.3	16.2	303.5
DZ1	18.5120	0.9998	14.8	14.8	275.3
LZ	32.5661	1.0030	10.1	10.1	330.0
LX	31.7101	1.0034	14.3	14.2	452.3

was greater than the amount of lithium detected in the [^{2}H]-hydrogen labelled benzoic acid used to fabricate FD3 (section 3.6.1). The total quantity of lithium detected in the acid used to hydrogen-exchange CF6 was higher than in the [^{2}H]-hydrogen labelled used to fabricate DZ1 in which equivalent weights of acid were used and comparable reaction conditions were employed. The greatest weight of lithium detected per 1g of acid was for the orthophosphoric acid prepared by hydrolysis of phosphorus pentoxide [CF4 and CF5] in which the smallest amounts of acid were used in the exchange process.

4.4.2 The effect of the volume of acid on the extent of the exchange reaction.

The effect which the quantity of phosphoric acid had on the extent of the exchange reaction was studied using two z-cut $LiNbO_3$ samples. The waveguides PF4 and PF5 (chosen to have an identical geometric area = 1.085 cm^2) were prepared by hydrogen-exchange at 235^oC for 6 hours under a N_2 atmosphere in pyrophosphoric acid. The acid weights were respectively 34.8469 and 4.1027g which correspond to 0.2048 and 0.0241 moles respectively.

Two aliquots were prepared and analysed for each acid sample. The results of the atomic absorption analysis is presented in table 4.9 and indicated that lithium detected in the acid of the waveguide PF4 is significantly

Table 4.9 Total lithium weight detected and the integrated areas of the infrared bands for PF4 and PF5 (z-cut, hydrogen exchange at 235°C for 6h in 34.846 and 4.1027g of pyrophosphoric acid respectively) determined by atomic absorption spectroscopy (AAS).

Sample	Portion of acid used for AAS (g)	Li concentration per 1g of acid $\mu g ml^{-1}$ (σ x10^{-3})	Li per 1g of of acid (μg)	Total Li detected (μg)	Li detected (μmol)	Infrared peak area (arb.unit
1PF4	1.0041	0.114 (28.7)	11.3			
2PF4	1.0031	0.115 (22.3)	11.5			
			$\bar{x}$: 11.4	397.2	57.3	167
1PF5	1.0007	0.828 (4.63)	83.1			
2PF5	1.0004	0.819 (4.96)	81.9			
			$\bar{x}$: 82.5	338.4	48.4	165

higher than that of waveguide PF5. The peak areas of the infrared bands integrated in the range 3700 to 3000 cm^{-1} were 167 and 165 respectively which was surprising in view of the analytical results described above.

CHAPTER FIVE.

DISCUSSION.

5.1 LITHIUM NIOBATE CRYSTAL GROWTH AND WAVEGUIDE FABRICATION.

The Czochralski technique is used for the growth of lithium niobate crystals since this method is undoubtedly the best for minimizing both the problems associated with the change of stoichiometry during the growth of $LiNbO_3$ and the impurities which affect the properties of the crystal such as the Curie temperature and the optical damage.[16]

The shift in lithium niobate composition from stoichiometric to congruent (lithium deficient side) has been attributed by Carruthers[133] and Peterson[134] as due to the fact that the NbO_6 octahedra possess a substantial degree of covalency. Hence, the lattice can accommodate Li vacancies in an energetically favourable state. The curvature of the free energy surface with composition change is small and the minimum is displaced towards the Nb_2O_5-rich region which allows the shift from stoichiometry towards the congruent composition.

Svaasand et al[13] have demonstrated that a significant amount of the $LiNb_3O_8$ phase is precipitated from the $LiNbO_3$ phase on annealing of congruent crystals for 17 hours at 600 - 700°C. This phase has also been observed during the fabrication of Ti-diffused waveguides in a dry atmosphere (N_2, Ar or air).[135,136] Later, it was shown that fabrication of waveguides in wet oxygen (H_2O/O_2) totally prevented the formation of the $LiNb_3O_8$ phase and gave lower in-plane scattering energy levels.[137]

Hydrogen-exchange "proton-exchange", is a promising new technique in integrated optics technology. The simplicity of the process, by means of which large refractive index difference waveguides have been made. Single-mode waveguides are produced by immersing lithium niobate samples in molten acids for periods of a few minutes, whereas larger times give highly multimode waveguides.

Their considerable immunity against optical damage is an attractive property and has led to increasing attention in a number of research centres. High quality waveguides with very low optical losses and restored electrooptic effects have been reported recently.[75,138,139].

5.2 INFRARED CHARACTERISATION OF THE [^{1}H] AND [^{2}H] HYDROGEN-EXCHANGED WAVEGUIDES FABRICATED USING BENZOIC AND PHOSPHORIC ACIDS.

5.2.1 Characterisation of [^{1}H] hydrogen-exchanged waveguides by infrared spectroscopy.

Benzoic acid has been used as a reaction medium for the hydrogen-exchange technique by many workers, since it is easy to handle at room temperature and produces a large change in the refractive index of the crystal. It also, causes no surface damage to x- and z-cut samples unless otherwise extreme reaction conditions are used.

There is evidence in the literature[83] that exchange reactions performed in stronger acids (phosphoric acid for example) produce changes in the refractive index larger than

that obtained when benzoic acid is used. However, the relationship between the acidity of the medium and the change in the refractive index is not simple because strong acids (sulphuric acid for example) were shown to totally exchange the lithium in $LiNbO_3$ powder resulting in the formation of the cubic phase $HNbO_3$.[45,46]

It is necessary to point out that the results concluded from work carried out on $LiNbO_3$ powder do not necessarily apply for single crystal $LiNbO_3$, since no direct evidence has been observed, to date, for the formation of $HNbO_3$ from single crystal $LiNbO_3$.

It was shown in this study that both Ar and N_2 could be used equally well as an exchange atmosphere. The step-like refractive index/depth profiles, of these waveguides are very similar to those of waveguides fabricated in air using an equivalent reaction time and temperature.

The spectroscopic and optical properties of [^{1}H] hydrogen-exchanged x- and z-cut $LiNbO_3$ waveguides presented in section 3.1 are consistent with the literature.[55,56,57] The infrared spectra of these waveguides showed a sharp intense band at 3505 cm^{-1} in x- and z-cut $LiNbO_3$ which corresponds to a "free" OH group. In the spectra of x-cut $LiNbO_3$ however, a broad band centred at 3250 cm^{-1} could also be seen. This broad band exists in a much weaker form in the spectra of z-cut $LiNbO_3$. Polarised IR spectra of x-cut [^{1}H] hydrogen exchanged waveguides suggest that this broad band possesses a large component along the z-axis and smaller components along the x- and y-axes of the crystal.

This suggestion explains the observation of a weak broad band in the z-cut material, since no matter what the polarization of the infrared radiation is, the stretching vibrations of these bonds are only weakly excited.

In all the infrared spectra of x-cut hydrogen-exchanged waveguides and for both the [^{1}H] and [^{2}H] hydrogen stretching regions, the intense sharp bands at 3505 and 2588 cm^{-1} overlap broad bands centred at 3250 and 2410 cm^{-1} respectively. Such a shift in the frequency is characteristic of the formation of bonded hydrogen i.e. [^{1}H] and [^{2}H] hydrogen are bonded to more than one oxygen anion.

5.2.2 Characterisation of [^{2}H] hydrogen-exchanged waveguides by infrared spectroscopy.

The [^{2}H] hydrogen was used in this study for two purposes; first, to examine how labile the [^{1}H] hydrogen is during and after the exchange reaction. Secondly, to investigate the difference in behaviour between the [^{1}H] and [^{2}H] hydrogen-exchanged waveguides via the isotopic exchange reactions.

The spectra of the [^{2}H] hydrogen-exchanged waveguides recorded directly after the reaction show two well-resolved maxima, figure 3.1, at 3500 and 3470 cm^{-1} in the [^{1}H] hydroxyl stretching region, indicating two different environments for the OH groups.

It has been demonstrated that x- and z-cut [^{1}H] hydrogen exchanged waveguides react with water vapour in ambient

atmosphere via the $[^1H\text{-}^2H]$ isotopic-exchange reaction at room temperature.[78]

X- and z-cut $[^2H]$hydrogen-exchanged waveguides are shown to react with atmospheric water vapour, figure 3.5.

The reduction in the sharp band at 2588 cm^{-1} observed in figure 3.1 and 3.5 was not reported in the work of A. Loni[57,78] since the exposure time in that particular experiment was relatively short (636 hours) compared to the present study (9600 hours) and the change in the absorbance was negligibly small.

It has been shown by Loni et al[78] that $[^1H]$ hydrogen-exchanged waveguides formed on x-cut $LiNbO_3$, when exposed to $[^2H]$-H_2O water vapour, exhibited an almost total hydrogen isotopic-exchange where the $[^1H]$ hydrogen content of the waveguide has been exchanged with $[^2H]$ hydrogen at room temperature. These waveguides showed reversible behaviour when exposed subsequently to water vapour in ambient air (figure 5.1a). Hence, all the $[^2H]$ hydrogen content was exchangeable with $[^1H]$ hydrogen.

In this study a parallel hydrogen isotopic-exchange experiment was undertaken. Starting with the x-cut $[^2H]$ hydrogen-exchanged waveguide FD2 ($[^2H]$ hydrogen-exchanged in $[^2H]$-hydrogen labelled benzoic acid at 225^oC for 4 hours), when exposed to water vapour in ambient air, the $[^1H\text{-}^2H]$ hydrogen forward isotopic-exchange, only a small reduction of the $[^2H]$ hydrogen content had occurred. However a substantial amount of $[^1H]$ hydrogen had been introduced to the waveguide. During the second part of the

Figure 5.1a Infrared spectra of x-cut hydrogen-exchanged waveguide, superimposed as a function of the time of exposure of the sample to [^{2}H]-hydrogen labelled water vapour at room temperature (the waveguide was fabricated at 155^{o}C for 2h), (Loni[78]).

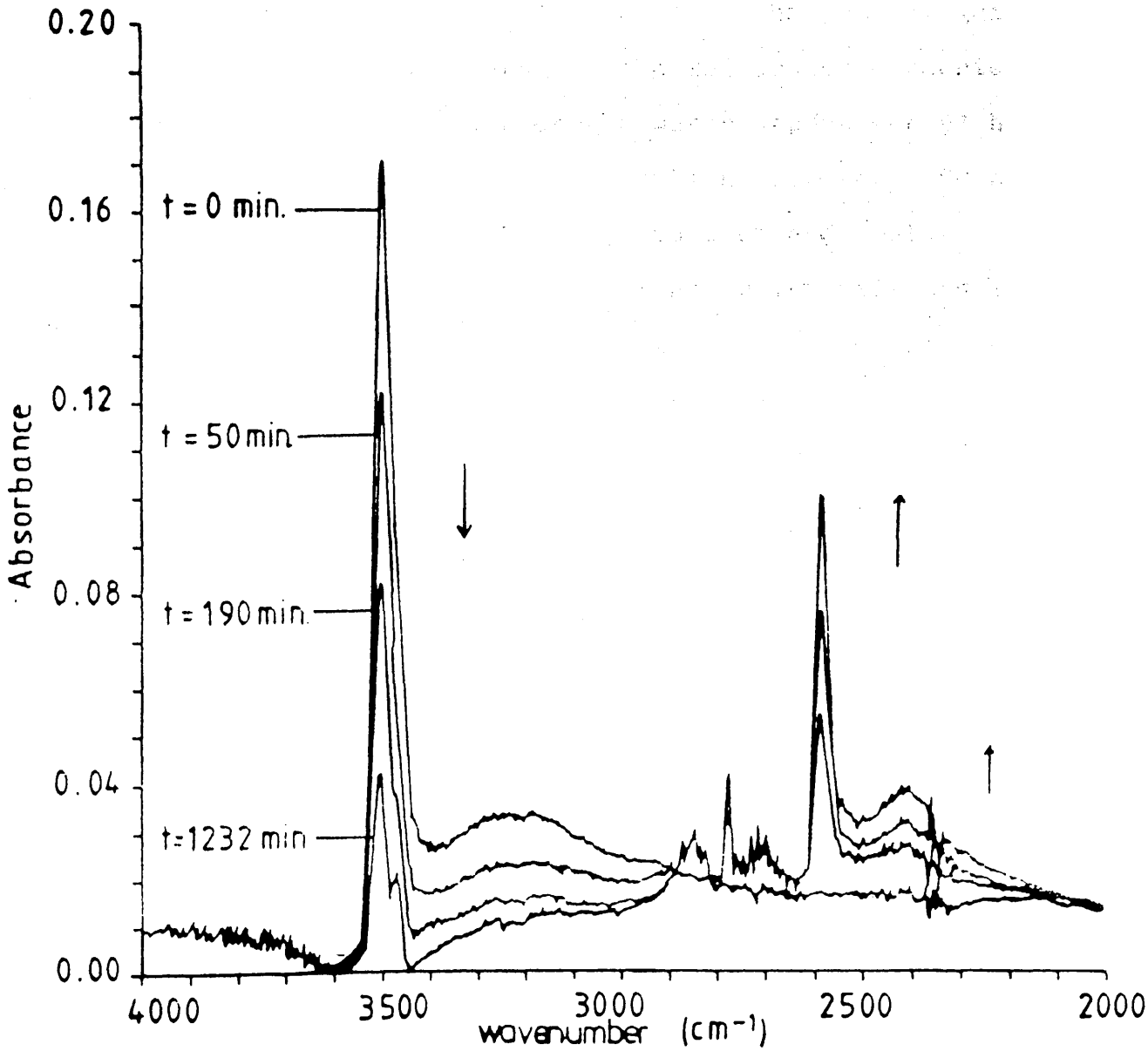

experiment the [^{2}H-^{1}H] hydrogen back isotopic-exchange, both the [^{1}H] and [^{2}H] hydrogen content changed but only slightly.

This indicates that the x-cut [^{2}H] hydrogen-exchanged waveguides behave non-reversibly towards the [^{1}H-^{2}H] hydrogen isotopic-exchange <u>unlike</u> the [^{1}H] hydrogen-exchanged waveguides reported in the literature.[78]

When the z-cut [^{2}H] hydrogen-exchanged waveguide DZ1 (exchanged in [^{2}H]-hydrogen labelled orthophosphoric acid) was exposed to [^{2}H]-hydrogen water vapour for 91 hours, after exposure to water vapour in ambient air for 1800 hours figure 4.11, it retained the [^{2}H] hydrogen and lost a substantial amount of the [^{1}H] hydrogen which diffused in during the period of exposure to water vapour in ambient air. This is identical to the reversible hydrogen isotopic-exchange observed during exposure of z-cut [^{1}H] hydrogen-exchanged waveguide to [^{2}H]-H_2O water vapour and then to water vapour in air[78], see figure 5.1b.

The behaviour of the [^{2}H] hydrogen-exchanged $LiNbO_3$, especially x-cut, towards the isotopic exchange may indicate some form of difference in the detailed microstructure between the [^{1}H] and [^{2}H] hydrogen-exchanged waveguides.

The observed reversible behaviour of z-cut material with respect to the [^{2}H-^{1}H] isotopic-exchange reactions and the non-reversible behaviour of x-cut, originally [^{2}H] hydrogen-exchanged in both cases, can not be attributed solely to the anisotropy of the crystal structure since the behaviour of both x- and z-cut [^{1}H] hydrogen-exchanged waveguides is

Figure 5.1b Infrared spectra of z-cut hydrogen-exchanged waveguide, superimposed as a function of the time of exposure of the sample to [^{2}H]-hydrogen labelled water vapour at room temperature (the waveguide was fabricated at 155^{o}C for 2h), (Loni[78]).

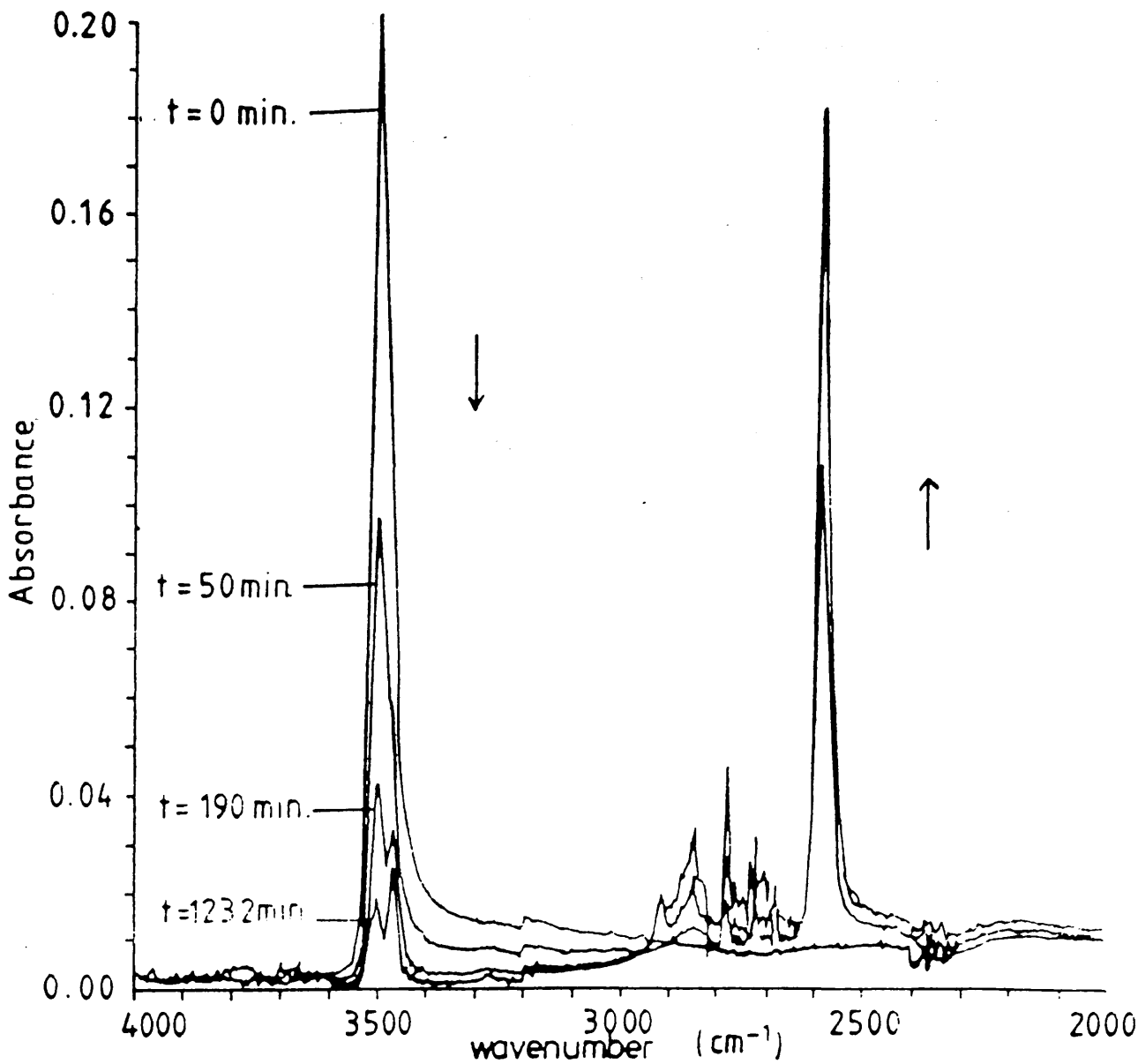

reversible. Neither can the observed behaviour be attributed simply to the isotopic mass effect resulting from the [^{1}H-^{2}H] substitution in the [^{2}H] hydrogen-exchanged $LiNbO_3$. If this is the case, the behaviour of both x- and z-cut $LiNbO_3$ towards the isotopic exchange reactions should be either reversible or non-reversible.

A combination of both factors may be necessary to explain the behaviour observed during the [^{2}H-^{1}H] isotopic exchange reactions.

The infrared spectra of [^{2}H] hydrogen-exchanged waveguides fabricated on z-cut $LiNbO_3$ showed a successive decrease in the sharp band at the [^{2}H] hydroxyl stretching region, as the waveguide was exposed to water vapour in the ambient air, see figure 3.2. Rice and co-workers[76] have stated that exposing the [^{2}H] hydrogen-exchanged waveguides to air at room temperature for several hours caused no increase in the OH absorption of the infrared spectra.

The factors effecting the change in IR spectra band widths due to isotopic exchange are well known[108] and were observed in this study. The full width at half maximum of the sharp band at 3505 cm^{-1} in the [^{1}H]- hydroxyl stetching region is almost double the corresponding band at 2588 cm^{-1} in the [^{2}H] hydrogen stretching region. This effect can be interpreted as showing that the substitution of [^{1}H] hydrogen by [^{2}H] hydrogen increases the anharmonic coupling effects. This in turn increases the effective width of each band of the hydrogen stretching group as a whole.[108]

A distinct maximum at 3275 cm^{-1} can be observed in the broad band at the [^{1}H] hydrogen stretching region in the spectra of [^{2}H] hydrogen-exchanged waveguides on x-cut $LiNbO_3$ after exposure to ambient air, figure 3.1. This maximum is not observed in the originally [^{1}H] hydrogen-exchanged waveguides where the broad band shows a smooth contour, see figure 1.8a for example. This distinct maximum at 3275 cm^{-1} suggests that the [^{1}H]- hydrogen forms a special hydrogen bond in the [^{2}H] hydrogen exchanged waveguides which is more dominant than the case of [^{1}H] hydrogen exchanged waveguides.

This may support the conclusion that the crystal structure of the lithium niobate developed by the [^{2}H] hydrogen-exchange process differs slightly from that for [^{1}H] hydrogen-exchange and therefore, the [^{1}H] hydrogen introduced to the crystal lattices of $LiNbO_3$ developed with [^{2}H] ions ([^{2}H] hydrogen-exchange), may form hydrogen bonds slightly different from the bonds formed by [^{1}H] in originally [^{1}H] hydrogen-exchanged $LiNbO_3$.

The three bands at 2958, 2926 and 2850 cm^{-1} observed in all the spectra of [^{2}H] hydrogen-exchanged waveguides, recorded using the gas infrared cell (section 2.4.2) have been found to be due to the presence of [^{2}H]-hydrogen labelled water vapour in the infrared gas cell, since the spectrum of [^{2}H]-hydrogen labelled water vapour showed bands apparently similar to those identified in the spectra of the waveguides. This spectrum is reproduced from the literature[57] in figure 5.2.

Figure 5.2 Infrared absorption spectrum of [^{2}H]-hydrogen labelled water vapour (Loni[57]).

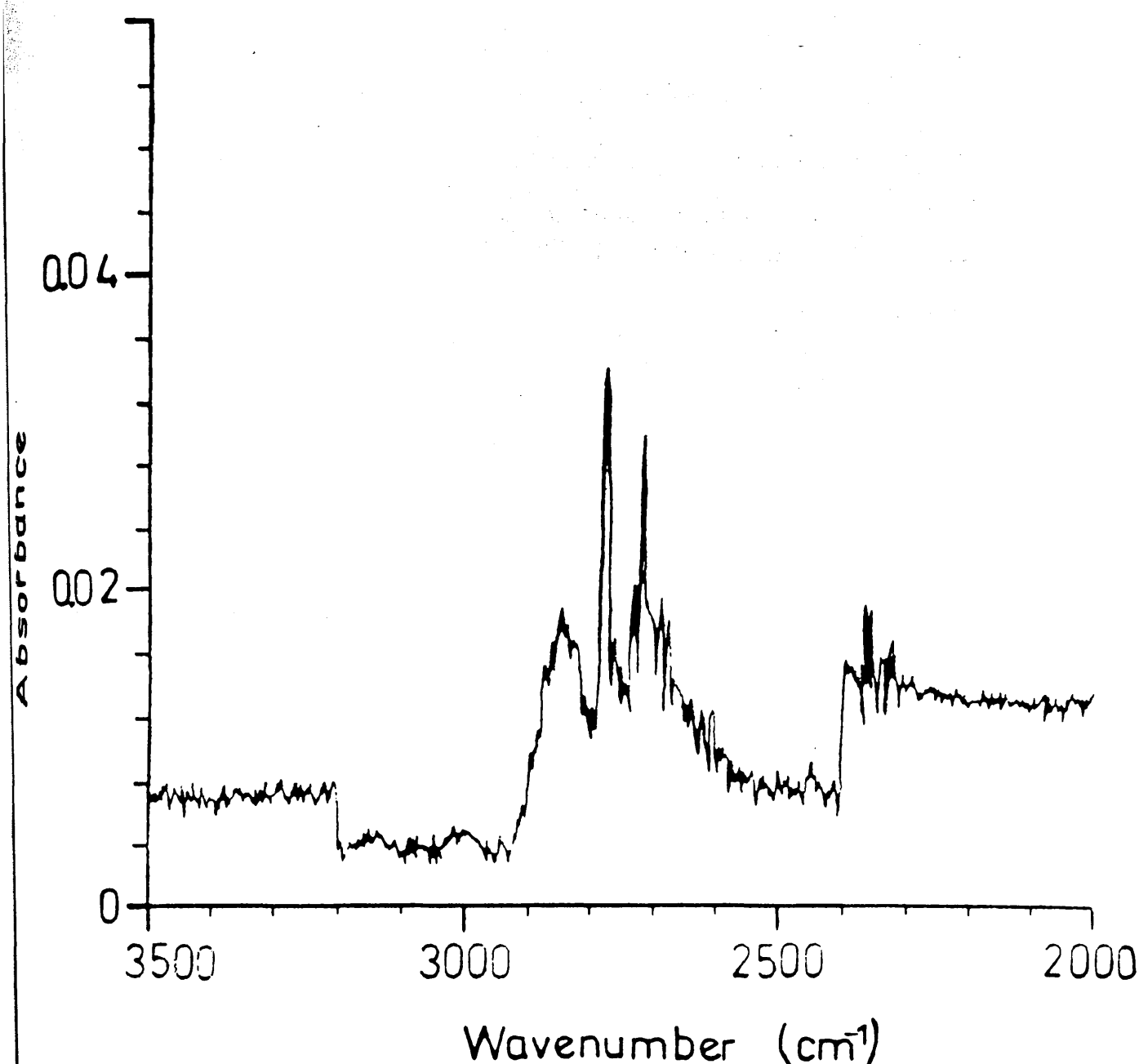

5.2.3 Characterisation of [^{1}H] hydrogen-exchanged waveguides fabricated in phosphoric acid by infrared spectroscopy.

The infrared spectra of [^{1}H] hydrogen-exchanged waveguides on z-cut $LiNbO_3$ fabricated using phosphoric acid were very similar to those produced using benzoic acid. This suggests that the distribution of [^{1}H] hydrogen in the lattice is identical in both cases.

It has been established that the extent of the reaction can be monitored by integrating the area of the infrared band.[131] The relation between the IR absorption band area and the square root of the exchange time is linear consistent with a diffusion governed process.[118,131]

The average band area of the waveguides prepared using the concentrated phosphoric acids, table 4.2 were 107±6 arb. units. The fluctuations in the band area (12% at greatest) were not large enough to interpret as directly determined by a particular type of phosphorus containing acid. The different weight of acids used for the reactions may explain the fluctuations since a spread of lithium weights was detected by atomic absorption spectroscopy, as will be discussed later.

It has been reported that attempts to prepare waveguides on x-cut $LiNbO_3$ using phosphoric acid were unsuccessful.[83] Surface damage was observed for x-cut $LiNbO_3$ samples exchanged at 235°C for 4 hours. However, monomode waveguides were fabricated for the first time in pyrophosphoric acid. The choice of a moderate reaction temperature (200°C) was the key for successful production of the x-cut waveguides.

Equally important, the short reaction times (4 - 30 min) helped to cut down the diffusion of high population of hydrogen.

It has been suggested that high values of "X" in the formula $Li_{1-x}H_xNbO_3$ causes the volume of the exchanged layer to contract.[84] This contraction will exert a strain at the exchanged layer/substrate interface which eventually relaxes leading to crack formation.

Another possible reason for the damage is that some of the lithium ions in the crystal diffuses into deeper layers instead of diffusing out of the crystal. Such a process could change the composition of the crystal from congruent to stoichiometric or even higher lithium content via the mechanism proposed by Abrahams et al.[15] This change in the crystal composition is accompanied by strain in which the nature of a stoichiometric unit cell is 0.1% smaller than the corresponding congruent unit cell.

According to Abraham's model however, Nb^{5+} present at Li sites may migrate back to the Nb empty sites. This process continues from the bulk of the crystal towards the surface. Hence, some of the Nb ions will either diffuse to the surrounding medium or react with the Li_2O vapour in the atmosphere of that particular experiment. For the suggested mechanism, niobium if out diffused, should be detected in the acid used for the exchange reaction.

Bollmann[41] has detected traces of Nb in benzoic acid from exchanged sample by mineralizing the acid in two parts with HF and H_2SO_4 respectively.

5.3 POLARIZED INFRARED CHARACTERISATION AND THE BIFURCATED HYDROGEN BOND MODEL.

The use of polarized infrared spectroscopy at two perpendicular polarisation angles on two different crystal cuts provides data to develop a three-dimensional model of the hydrogen bonds in hydrogen-exchanged $LiNbO_3$ crystals.

A spectrum of the x-cut sample FD1 recorded when the infrared radiation was polarized along the z-axis (90^o polarization), figure 3.10 shows a sharp weak band at 2588 cm^{-1} overlapping the broad band in the [^{2}H]- hydroxyl stretching region. The appearance of this sharp weak band in the [^{2}H]-hydroxyl region only, indicates that some of the "free" OH hydrogen bonds possess a small vibrational component along the z-axis. In the literature[106] for the bulk $LiNbO_3$ crystals it has been concluded that the OH hydrogen bonds are in the x-y plane within $\pm 5^o$.

Spectra of infrared radiation polarized along the x- and y-axes of the [^{2}H] hydrogen-exchanged waveguides fabricated on z-cut $LiNbO_3$ were similar and showed a very weak broad band, figure 3.11. This indicates that the broad band centred at 2410 cm^{-1} has small components along the x- and y-axes. By correlating these spectra with figure 3.10 of x-cut, 0^o polarized (along the z-axis) a three dimensional model of the bonds can be visualized.

The weak broad bands, in the spectra of z-cut hydrogen-exchanged, are due to bonds that have small vibrational components along the x- and y-axes, whereas they have a large vibrational component along the z-axis, figure 3.10. The

resulting vibrational motion is not parallel to the z-axis, otherwise it would not be possible to observe any components along the x- and y-axes in the spectra. Details supporting the case for the asymmetry of these bonds are presented in appendix B.

A careful study of the three-dimensional crystal structure of lithium niobate suggests that these bonds may be formed between the [^{2}H] hydrogen and the oxygen triangles where the Li^+ ions were originally bonded. Therefore, any [^{2}H] hydrogen ion introduced into the crystal forming bonds to more than one oxygen anion may possibly form a bifurcated bond to the three oxygen anions of the triangle, especially in the smallest oxygen triangle case, see figure 5.3.

The suggested bifurcated hydrogen bond in the structure of [^{2}H] hydrogen-exchanged $LiNbO_3$ waveguides is presented in figure 5.4. In crystals containing hydrogen the molecular stoichiometry[103] and the geometrical requirements may conflict with the requirement of linear hydrogen bonds so that the observed packing and the lowest energy configuration may lead to a situation in which a proton donor group [OH] is approximately equidistant from two acceptor groups, oxygen anions.

One of the extensively studied examples of bifurcated hydrogen bonding occurs in violuric acid (5-hydroxylmino-barbituric acid) monohydrate, figure 5.5. The orientation of the water molecule is influenced by all the neighbouring atoms, the bifurcated hydrogen bond occurs between the O^{2}H of water molecule and the O(5) and O(6) of violuric acid.[140]

Figure 5.3 A schematic diagram of the nearest neighbours for an O^{2-} anion in $LiNbO_3$. Dotted circles denote ions below the plane and dashed circles denote ions above the plane. The largest diameter circles denote Nb^{5+} ions, the medium diameter circles denote Li^+ ions, and the small diameter circles denote O^{2-} ions. Each O^{2-} anion in $LiNbO_3$ has the same coordination, though the neighbours may be rotated by an angle of $\pm 120^o$ about the c-axis Note that triangles 1-2-3, 1-4-5, and 1-6-7 are equilateral. (Herrington et al[106]).

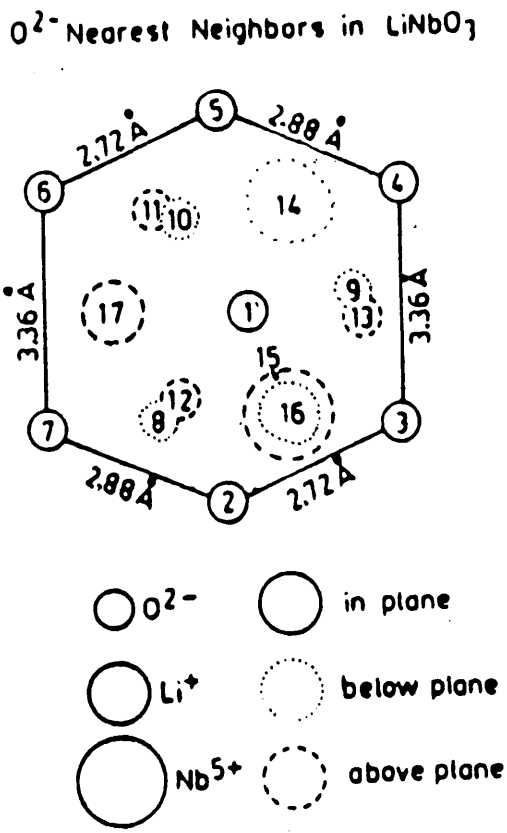

Figure 5.4 The suggested bifurcated [^{2}H] bond in [^{2}H]hydrogen -exchanged waveguides in lithium niobate (a) top view (b) 3-dimensional view, the arrow indicates the direction of vibration.

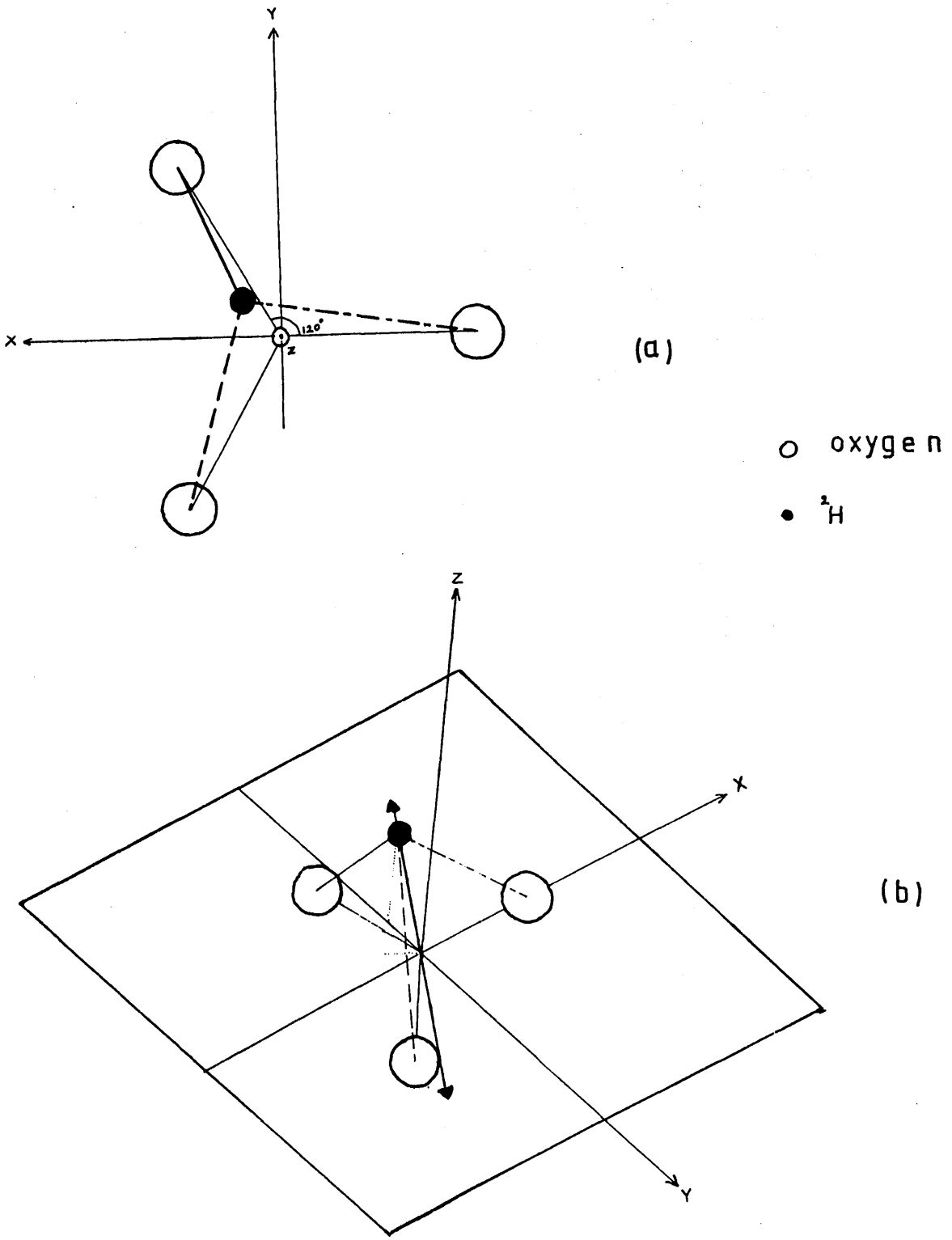

Figure 5.5 The interatomic distances and angles involving deuterium atoms in perdeuterated violuric acid monohydrate. The bifurcated H bond is between the OD of the D_2O molecule and O(6) and O(5) of violuric acid. (Donahue et.al[144]).

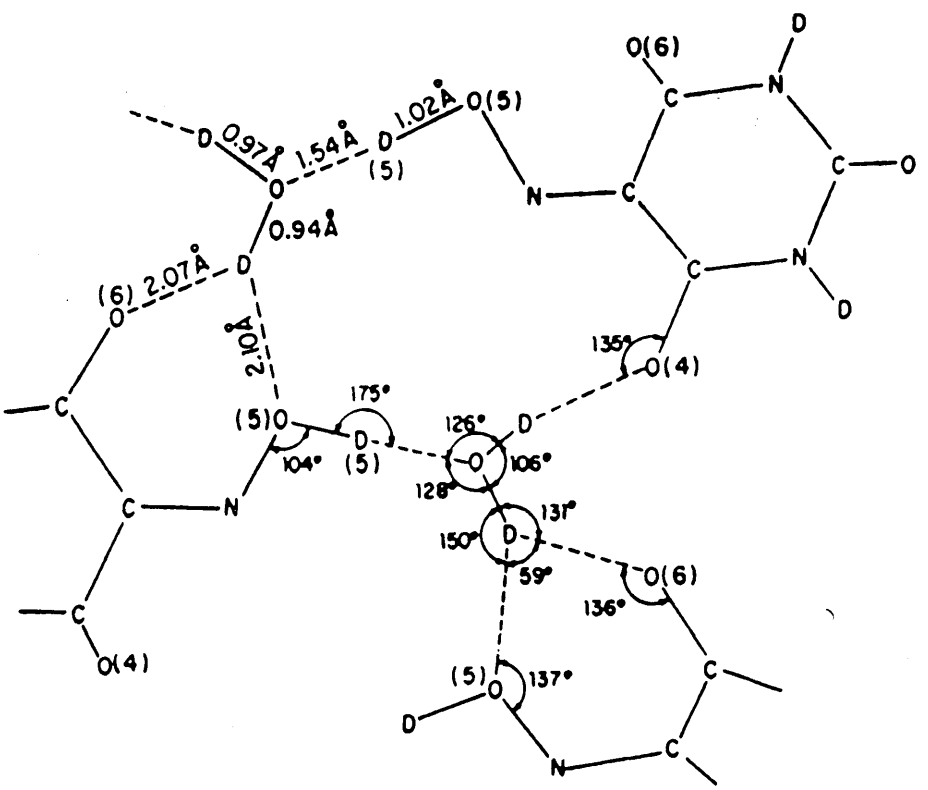

Bifurcated bonds have been reported in number of other crystal structures. Redek et al[141] have observed bifurcated hydrogen bonding in an adenine derivative. Lutz et al[142] have reported a symmetric bifurcated bond in the crystal structure of isotopic $MX_2.H_2O$ where M = Sr,Ba and X = Cl, Br, I, when analysed by infrared and Raman spectroscopy.

The bifurcated hydrogen bond has also been reported in glycine and barium chloride dihydrate in Tutton's salts (double salts MSO_4, $NiSO_4$, $6H_2O$ where M^{II} = Fe,CO or Mg), raurine (2-aminoethylsulfonic acid), magnesium sulfate tetrahydrate and 1,3,5-triamino-2,4,6-trinitrobenzene .[143,144]

More studies for example, using neutron diffraction are necessary to confirm the existance of bifurcated hydrogen bonds in [^{2}H] hydrogen-exchanged $LiNbO_3$.

5.4 OPTICAL CHARACTERISATION OF [^{2}H] AND [^{1}H] HYDROGEN-EXCHANGED WAVEGUIDES IN BENZOIC AND PHOSPHORIC ACIDS.

The optical properties of [^{2}H] hydrogen-exchanged waveguides are very similar to those in [^{1}H] hydrogen-exchanged waveguides reported in the literature.[55,56] The refractive index versus depth profile is step-like, a typical characteristic of the hydrogen exchange waveguides before annealing.

The depth of the x-cut [^{2}H] hydrogen-exchanged waveguides is greater than the counterpart for z-cut waveguides processed under identical conditions.

The refractive index instability of the [^{2}H] hydrogen-exchanged waveguides was monitored during exposure of the waveguide sample FD1 (x-cut [^{2}H] hydrogen-exchanged

at 235^{o}C for 3.5h) to ambient air, figure 3.13. The maximum amplitude in the effective refractive indices, was detected for m = 2 on the positive face of the crystal and was δn_e = 0.005, compared with reported values for [^{1}H] hydrogen-exchanged waveguides which were δn_e = 0.025 [67] and 0.020 [68] for non-annealed samples. The possibility of realizing waveguides with high change in the refractive index was tested using ortho and pyrophosphoric acids. Optical waveguides fabricated on z-cut $LiNbO_3$ using phosphoric acid support TM modes and posses a step-like refractive index versus depth profile. Surface refractive indices obtained using the inverse WKB technique and step-index computer programs were significantly higher than corresponding waveguides fabricated in benzoic acid. The values calculated by the inverse WKB program are comparable with the literature values[83,92] but higher than those produced by the step-index program. However, Yamamoto et al[83],did not specify the method used to produce the published results.

It is known that the inverse WKB is an approximate method in which the experimental data are fitted to a theoretical model to produce the closest refractive index versus depth profile that matches the actual waveguide profile.

The step-index program, on the other hand, is based on the assumption that the refractive index profile is in the form of a step function and the precision of the calculated data is limited by how close the true refractive index profile of the waveguide is to the assumed step function.

However, it should be pointed out that neither of the methods produces an accurate value for the surface refractive index of the waveguides.

A preliminary experiment in which the sample was treated by spin coating of the pyrophosphoric acid onto the surface of the crystal[94,95] followed by diffusing/exchanging the sample using the conditions reported was unsuccessful and severely cracked the crystal. However, it is unlikely that the waveguide produced by this technique would possess a step-like refractive index profile especially in the reaction time and temperature ranges reported (150-280^{o}C for 5 min - 6 hours) in the literature,[94] since the source of diffused ion is finite and it is analogous to the situation for Ti-diffusion from a Ti film deposited on the surface of the crystal. In addition, the 'buffering' effect, observed in this study when small quantities of acid was used for the exchange reaction, influences the extent of reaction. This is analogous to the case of benzoic acid when buffered with large mole ratio of lithium benzoate in which the fabricated waveguides possess a graded refractive index/depth profile.

The relationships between the waveguide depths and the square root of the exchange time were linear, figure 4.6 and 4.7, confirming that the hydrogen-exchange reaction is governed by a diffusion process.[118] The slope of the plot of the band area versus the square root of the reaction time ($t^{\frac{1}{2}}$) for ortho phosphoric acid samples was larger than the counterpart obtained for benzoic acid previously.[57] The

same trend was observed for the plots of the waveguide depths versus $t^{\frac{1}{2}}$. This trend indicates that the extent of the reaction for samples fabricated in phosphoric acid is higher than that for the samples fabricated in benzoic acid exchanged under identical temperature.

To test the correlation between the infrared measurements and the waveguide depth measurements, from the plots of band area versus $t^{\frac{1}{2}}$, the ratio:

$$\frac{\text{slope of phosphoric acid samples}}{\text{slope of benzoic acid samples}}$$

was 1.139, compared to the ratio obtained from the plots of the waveguide depth versus $t^{\frac{1}{2}}$ which was 1.127. The test show a good correlation between the infrared and optical measurements.

The difference in the maximum change in the refractive indices between OF7 and PF3 ([^{1}H] hydrogen-exchanged in ortho and pyrophosphoric acid respectively at 215^{o}C for 4.4 hours and 6 hours). is 4 x 10^{-3} which may be considered to be small if one takes into account the significant changes in the refractive index produced in general, by the hydrogen-exchange ($\Delta n_e \geqslant 0.12$) or the Ti-indiffusion techniques ($\Delta n_e \leqslant 0.04$). Therefore, the changes in refractive index resulting from hydrogen-exchange in pyro or orthophosphoric acid are approximately identical.

To examine the significance of the difference observed in the diffusion coefficients between ortho and pyrophosphoric acid, the depths of waveguides were calculated

using equation 1.10. The depth of waveguides were calculated using the diffusion coefficients above, and reaction times of 25 min and 6 hours which produce a relatively shallow monomode waveguide and a deep, highly multimode waveguide respectively. The results are presented in table below:

Fabrication time (h,min)	depth of waveguide prepared in orthophosphoric acid (μm) ($D(T) = 0.2182\mu m^2h^{-1}$)	depth of waveguide prepared in pyrophosphoric acid (μm) ($D(T) = 0.2313\mu m^2h^{-1}$)
0,25	0.6030	0.6209
6,0	2.2884	2.3561

The results demonstrated that it is possible to estimate the depth of a monomode waveguide fabricated by either ortho or pyrophosphoric acids to within ± 0.018μm and that of a multimode waveguide to within ± 0.067 μm. These values are not large enough to affect considerably the optical properties of the waveguides.

Therefore, both ortho and pyrophosphoric acids produced waveguides possess essentially identical optical properties. Further work may be needed to investigate the optical losses of waveguides fabricated by ortho and pyrophosphoric acid.

5.5 ANNEALING OF THE [^{1}H] AND [^{2}H] HYDROGEN-EXCHANGED WAVEGUIDES.

Annealing the hydrogen-exchanged waveguides has been shown by Rutherford back scattering (RBS)[51] and infrared spectroscopy[131] to re-distribute the hydrogen in the waveguides.

This re-distribution reduces the strain built up by the exchange process, thereby reducing the optical attenuation, which in turn, improves the quality of the waveguides. Annealing causes the depth of the waveguides to increase, indicating the diffusion of hydrogen to deeper levels and it also reduces the surface refractive index.

It has been shown that annealing [^{1}H] hydrogen-exchanged waveguides in wet oxygen [$^1H_2O/O_2$] produces waveguides which are more stable with regard to interaction with the atmosphere.[57] In the present work, this was confirmed in the annealing experiments performed on [^{1}H] hydrogen-exchanged waveguides. Annealing of [^{1}H] hydrogen-exchanged waveguides in [^{2}H]-hydrogen labelled wet oxygen [$^2H_2O/O_2$] substantially reduced the [^{1}H] hydrogen content and introduced [^{2}H] hydrogen into the crystal from the high temperature atmosphere (365^{o}C), see figure 3.7C. This also confirmed preliminary experiments carried out previously at Glasgow University.[131]

Gonzalez et al[77] has concluded that the minimum temperature at which [^{2}H] hydrogen diffuses in annealed bulk z-cut $LiNbO_3$ was 427^{o}C. In contrast, annealing of the [^{1}H] and [^{2}H] hydrogen-exchanged waveguides in [^{2}H]-hydrogen labelled wet oxygen [$^2H_2O/O_2$] at 365^{o}C showed a remarkable increase in the [^{2}H] hydrogen content of the waveguides, accompanied by a substantial decrease in the [^{1}H] hydrogen content, figure 3.7a, b and c.

Annealing of [^{2}H] hydrogen-exchanged waveguides at the same temperature in wet oxygen [$^1H_2O/O_2$] caused the [^{2}H] hydrogen content to vanish completely from the waveguiding

layer, while the [^{1}H] hydrogen content increased, as can be seen in figure 3.8.

It is necessary to point out that the flow rate of the carrier gas can critically effect the yield of the annealing process. The conventional flow rates used for annealing the hydrogen-exchanged waveguides and during the Ti-diffusion process are from 1.3 to 1.75 l min^{-1}. For crystal dimensions of (15 x 5 x 1mm^3), these flow rates corresponded to space velocities of (1.73 - 2.33) x $10^4 min^{-1}$ and contact times of (5.78-4.28) x 10^{-5} min, (3.47, 2.57 milliseconds). The infrared spectrum of a [^{2}H] hydrogen-exchanged waveguide annealed at a rate of 1.5lmin^{-1} in [^{2}H]-hydrogen labelled wet oxygen [$^2H_2O/O_2$] showed a decrease in the [^{2}H] hydrogen content of the waveguide, indicating out diffusion of the [^{2}H] hydrogen content from the waveguide.

These results also suggested that annealing involves a chemisorption process where the hydrogen carried by the gas adsorb on the surface of the crystal and are then, absorbed into the bulk, figure 5.6 Meanwhile, the hydrogen in the guiding layer migrate towards the surface, are desorbed and then carried away by the gas.

It is known that the adsorption rate of the hydrogen onto the surface of the crystal is inversely related to the flow rate of the carrier gas and the desorption rate is directly related to the annealing temperature. The purpose of the annealing process is to re-distribute and introduce the hydrogen into the crystal. Therefore, it is preferable to decrease the gas flow rate when the annealing temperature is increased, assuming that the gas has sufficiently high water content.

Figure 5.6 Schematic illustrates the possible mechanism of the adsorption, absorption and desorption occurring on the surface of the crystal or waveguide during the annealing process.

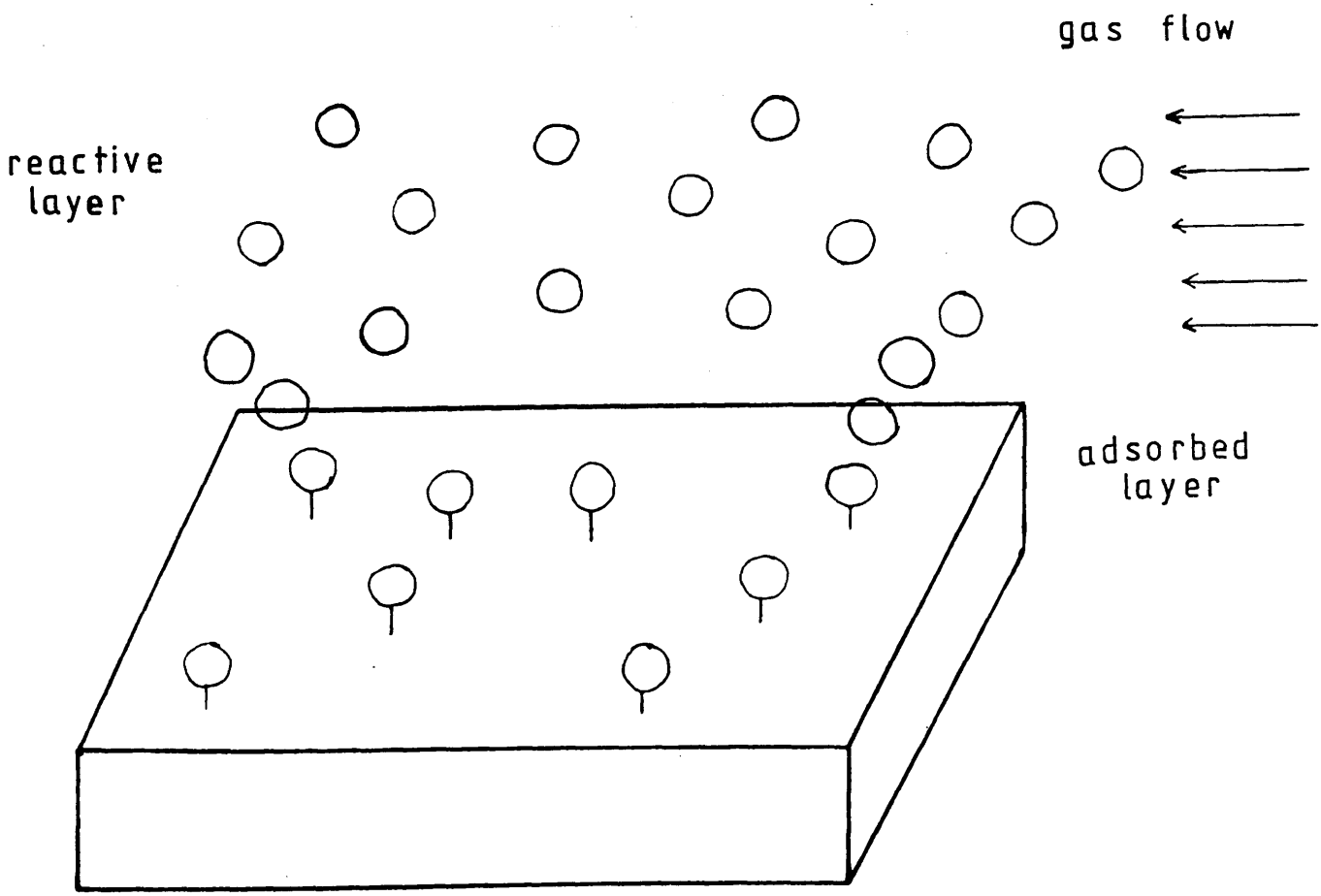

In the literature, there is a lack of appreciation of the significance of the chemistry of the annealing process and the effects the annealing parameters have on the optical properties and quality of the waveguide. It is worth pointing out that the annealing process is as important as the initial fabrication process, since annealing is an essential stage in realizing high optical quality hydrogen-exchanged waveguides.

It is interesting to compare the isotopic exchange at room temperature with that at elevated temperatures (annealing). At room temperature, the isotopic exchange is a continuous reaction between the hydrogen content of the waveguide and the atmospheric hydrogen. Whereas the annealing process ceases this reaction and creates more stable waveguides.

Annealing also can change the optical properties of the waveguides, like the depth, the number of modes supported and the refractive index profile. It increases the depth by diffusing the hydrogen to deeper levels into the bulk of the crystal to occupy sites which were occupied by Li ions. Thus, it re-distributes the lithium in or below the waveguiding layer which eventually reduces the strain created by the exchange reaction.

In contrast, the isotopic exchange at room temperature neither involves any re-distribution of the lithium nor apparently effects the optical properties of the waveguide.

5.6 THE LITHIUM ANALYSIS OF THE ACID RETAINED BY ATOMIC ABSORPTION SPECTROSCOPY.

Atomic absorption analysis was used to determine quantitatively the extent of the exchange reactions performed in this study. All the Li concentrations calculated from the analysis were close to the lower sensitivity limit of this technique where great attention is required in the preparation of the standard and aliquot solutions and in the other stages of the analysis in order to realize reproducible and precise results.

Atomic absorption analysis of the acid retained after the reaction indicates a greater lithium mass in the benzoic and phosphoric acids used to fabricate x-cut samples than that in z-cut samples. This result is consistent with the optical measurements which indicate higher exchange extent for the x-cut samples and confirms the results given in the literature.[55,56,57]

It has been shown by the lithium analysis that 10% - 33% of the lithium in the exchanged volume was exchanged with hydrogen and detected.[145] The ratios determined in this study were 35% and 5% - 8.5% for [^{1}H] and [^{2}H] hydrogen-exchanged acid samples respectively. These ratios are lower than the values from 65% to 75% estimated by a resonant nuclear reaction to determine the concentration of hydrogen in single crystal $LiNbO_3$.[52]

The paths for lithium loss were; (i) the distribution of Li^+ in the melt could be non-uniform, (ii) Li could be lost at some point during the hydrogen-exchange either by evaporation

to the atmosphere (presumably as Li_2O) or absorption into the fused silica beakers and PTFE holders and (iii) there could be some re-distribution of Li^+ ions within (i.e. into) the sample substrate. Atomic absorption analyses carried out to test the non-unifromity of the Li^+ ions distribution in the acid melt suggested a uniform distribution. Tests for loss of Li^+ ions by studying the changes in the Li^+ content of benzoic acid into which lithium benzoate was added, suggest that no loss of Li has occurred (a more conclusive test would be to analyse the PTFE and silica glass for Li^+ ions). The obvious possibilities left are that, some of the lithium re-distributes into the sample substrate[145] or it has been lost to the atmosphere.

The effect that the amount of acid has on the extent of reaction was tested separately for benzoic acid and phosphoric acids by fabricating two waveguides in two acid weights chosen to be at either extreme of the range of weights of acid used.

A direct relationship was observed between the amount of acid used and the amount of lithium detected by atomic absorption spectroscopy. This relationship was more obvious for the benzoic acid samples which may indicate that the extent of reaction had been slowed down by some form of buffering effect.

Infrared areas of the exchanged crystals showed larger area for the samples exchanged in larger volumes of acid which support the above possibility.

Finally the lithium weights detected in the concentrated orthophosphoric acid samples were 202 ± 65 μg.

The large error in this estimate can be explained by the fact that different amounts of acis was used in each experiment, hence the acid weight dependency of the lithium amounts detected may occur. In addition, these acids were analysed separately in which new standard solutions were prepared for each experiment.

Conclusions.

Optical waveguides have been successfully fabricated on x-cut $LiNbO_3$ using pyrophosphoric acid for the first time by [^{1}H] hydrogen-exchange at 200°C for times ranging from 4 to 30 min. No significant differences, neither optical nor spectroscopic, are observed between waveguides fabricated in pyro or orthophosphoric acids. Waveguides fabricated in phosphorus containing acid possess a surface refractive index higher than the corresponding waveguides fabricated in benzoic acid. The refractive index values calculated by the inverse WKB program are comparable with the value reported in the literature,[83] but higher than the values calculated using the step-index program.

Lithium determination by atomic absorption spectroscopy in the [^{2}H]-hydrogen labelled benzoic and phosphoric acids after waveguide fabrication is less than that in the [^{1}H]-labelled acids used for samples processed identically. The values of "X" in the formula $Li_{1-x}H_xNbO_3$, determined from atomic absorption measurements were less than values produced by the analysis of hydrogen in the crystal be resonant nuclear reaction.[53] Possible paths for lithium loss have been tested and more studies should be conclusive. Atomic absorption results are consistent with the infrared measurement and proved to be useful for determining relative values of "X" based on data obtained from the analyses of the acid, but they do not provide precise estimates of the concentration of hydrogen in the crystal. The behaviour of z-cut [^{2}H] hydrogen-exchanged waveguides is reversible with respect to

the hydrogen isotopic-exchange reactions, unlike the x-cut [^{2}H] hydrogen-exchanged waveguides which exhibit non-reversible behaviour. A combination of both the anisotropy of the crystal structure of $LiNbO_3$ and the isotopic mass effect may contribute to the surprising behaviour of the [^{2}H] hydrogen-exchanged $LiNbO_3$ waveguides.

From detailed comparison of the infrared spectra obtained in this work, it is tentatively proposed that the microstructure of the [^{2}H] hydrogen-exchanged $LiNbO_3$ differs from that of the [^{1}H] hydrogen-exchanged $LiNbO_3$. An asymmetric bifurcated hydrogen bond model is suggested for hydrogen-exchanged $LiNbO_3$ waveguides.

Annealing in [^{2}H]-H_2O water vapour at relatively slow flow rates increases the [^{2}H] hydrogen concentration in the [^{1}H] and [^{2}H] hydrogen-exchanged waveguides whereas, at faster flow rates, reduction in the [^{2}H] hydrogen content is observed.

REFERENCES

REFERENCES

1. Kao K.C. and Hockham G.A., Proc.I.E.E.E., (1966), 113, 1151.

2. Miya T., Terunuma Y., Hosaka T. and Miyasita T., Electron Lett., (1979), 15, 106.

3. Tien P.K., Rev. Modern Phys., (1977), 49, 361.

4. Zachariasen W.H., Skr. Norske Vid. Ada., Oslo. Mat. Naturv, (1928), 4.

5. Ballman A.A., J.Am. Ceram. Soc., (1965), 48, 112.

6. Raüber A., Chemistry and Physics of Lithium Niobate in E. Kaldis "Current topics in Material Science", North Holland, (1978), 48.

7. Ohmachi Y., J. Appl. Phys., (1973), 44, 3928.

8. Kaminow I.P., in Introduction to Electronic Devices (A.P. New York, 1974) also, Kaminow I.P., I.E.E.E. Trans on Microwave Theory and Tech., (1975), MTT23, 57.

9. Yeougi N. and Kimura T., Appl. Phys. Lett., (1976), 29, 22.

10. Reisman A. and Holtzberg F., J. Am. Chem. Soc., (1956), 80, 6503.

11. Lerner P., Legras C. and Dumas J.P., J. Crystal Growth (1968), 3/4, 231.

12. Svaasand L.O., Erikonid M., Grande A.P. and Mo F., J. Crystal Growth, (1973), 18, 179.

13. Svaasand L.O., Eriks M., Nakken G. and Grande A.P., J. Crystal Growth, (1974), 22, 239.

14. O'Bryan H.M., Gallagher P.K. and Brandle C.D., J. Am. Ceram. Soc., (1985), 68, 493.

15. Abrahams S.C. and Marsh P., Acta Cryst., (1986) B42, 61.

16. McLachlan A.D., Ph.D. Thesis, University of Glasgow (1981).

17. Bergman J.G., Ashkin A., Ballman A.A., Dziedzic J.M., Levinstein H.J. and Smith R.G., Appl. Phys. Lett., (1968), 12, 92.

18. Kondo S., Miyazawa S., Fushimi S. and Sugii K., Appl. Phys. Lett., (1975), 26, 489.

19. Korb E.D. and Landise R.A., J. Crystal Growth (1976), 33, 145.

20. Fushimi S. and Sugii K., Japan, J. Appl. Phys. (1974) 13, 1895.

21. Lithium Niobate Crystal Information sheet, Barr and Stroud Ltd, Pilkington Electrooptic Materials.

22. Nassau K., Levinstein H.J. and Loiacono M., J. Phys. Chem. Solids, (1966), 27, 989.

23. Personal Communication with officials from Barr and Stroud Ltd., 4th European Conference for integrated optics Glasgow, (1987).

24. Haycock P.W. and Townsend P.D., Appl. Phys. Lett., (1986), 48, 698.

25. Abrahams S.C., Reddy J.D. and Bernstein J.L., J. Phys. Chem. Solids., (1966), 27, 997.

26. Abrahams S.C., Hamelton W.C. and Reddy J.M., J. Phys. Chem. Solids., (1966), 27, 1013.

27. Kovacs L. and Polgar K., Cryst. Res. Technol., (1986) 21, K101.

28. Gotz G., Rad. eff. (1986), 98, 189.

29. Kaminow I.P. and Carruthers J.R., Appl. Phys. Lett., (1973), 22, 326.

30. Van Wood E., Hartman N.F. and Austin A.E., J. Appl. Phys., (1981) 52, 1118.

31. Schmidt R.V. and Kaminow I.P., Appl. Phys. Lett., (1974), 25, 458.

32. Armenise M.N., DeSourio M., Canali C., Franzasi P., Singh J., Hutchins R.H. and De La Rue R.M., Appl. Phys. Lett., (1984), 45, 326.

33. Singh J. and De La Rue R.M., J. Lightwave Tech., (1985), LT3, 67.

34. Sugii K., Fukuma M. and Iwasaki H., J. Mat. Sci., (1978), 13, 523.

35. Burns W.K., Klein P.H., West E.J and Plew L.E., J. Appl. Phys., (1979), 50, 6175.

36. Armenise M.N., Canali C., De Sario M., Carnera A., Mazzoldi P. and Celott G., I.E.E.E. Trans. On C.H.M.T., (1982), C.H.M.T.5, 212.

37. Read P.M., Speakman S.P., Hudson M.D., and Consildine L. Nucl. Inst. and Methods in Phys. Res., (1986), B15, 398.

38. Buretskii H.S. and Cherrykh V.A. Sov. J. Quntum. Electron., (1986), 16, 1424.

39. Jackel J.L., Ramaswamy V., and Lyman S.P., Appl. Phys. Lett., (1981), 38, 509.

40. Jackel J.L., Glass A.M., Peterson G.E., Rice C.E., Olson D.H. and Veselka J.J., Appl. Phys., (1984), 55, 269.

41. Barfoot K.M., Al-Chlabi S.A., Webb R.P. and Weiss B.L., Rad. Eff. (1986), 98, 249.

42. Barfoot K.M. and Weiss B.L., J. Phys.D. Appl. Phys., (1984), 17, 147.

43. Destefauis G.L., Gailliard J.P., Ligeon E.L., Veillette S., Farrnery B.W., Townsend P.D and Rerey A., J. Appl. Phys., (1979), 50, 7818.

44. Naden J.M. and Weiss B.L., J. Lightwave Tech., (1985) LT.3 , 855.

45. Jackel J.L. and Rice C.E., Ferroelectrics, (1981), 38, 801.

46. Rice C.E. and Jackel J.L., J. Solid State Chem., (1982), 41, 308.

47. Jackel J.L., Rice C.E. and Vaselka J.J., Appl. Phys. Lett., (1982), 41, 607.

48. Rice C.E. and Jackel J.L. Mater. Res. Bull., (1984), 19, 591.

49. Jackel J.L. and Rice C.E., Appl. Phys. Lett., (1982), 41, 508.

50. Li M.J., DeMicheli M.P., Ostrowsky D.B. and Papuchon M.P., Optics Commun., (1987), 62, 17.

51. Al-Shukri S.M., Dawar A., De La Rue R.M., Nutt A.C.G., Taylor M.R.S., Tobin J.R., Mazzi G., Carnera A. and Summonte C., 7th Topical Meeting on Integrated and Guided Wave Optics. Florida (1984).

52. Canali C., Carnera A., Dellamea G., Mazzoldi P., Al-Shukri S.M., Nutt A.C.G. and De La Rue R.M., J. Appl. Phys., (1986), 52, 2643.

53. Canali C., Carnera A., Della Mea G., De La Rue R.M., Nutt A.C.G. and Tobin J.R., Proc. S.P.I.E., 460, L.A. Symposium Calif., 22nd-26th Jan. 1984.

54. Sanford N.A. and Lee W.E., S.P.I.E., (1985), 587, 7.

55. Wong K.K., Nutt A.C.G., Clark D.F., Winfield J.M., Laybourn P.R.J. and De La Rue R.M., I.E.E.E. Proc., (1986), J-133, 113.

56. Clark D.F., Nutt A.C.G., Wong K.K., Laybourn P.J.R. and De La Rue R.M., J. Appl. Phys., (1983), 54, 6218.

57. Loni A., Ph.D. Thesis, University of Glasgow, (1988).

58. Al-Shukri S.M., Duffy J., De La Rue R.M. Armenise M.N., Canali C and Carnera A., S.P.I.E., (1985), 578, 2.

59. Suhara T., Fujiwara S. and Nishihara H., Appl. Opt., (1986), 25, 3379.

60. Yu.Z.D., Opt. Commun. (1983), 47, 248.

61. Wong K.K., De La Rue R.M. and Wright S., Opt. Lett. (1982), 7, 546.

62. Minakata M., Kumogai K. and Kawakam S., Appl. Phys. Lett. (1986), 49, 992.

63. Duffy J.F., Ph.D. Thesis, University of Glasgow (1986).

64. Mahapatra A. and Robinson W.E., Appl. Opt., (1985), 24, 2285.

65. Neveu S., Barety J.P., De Micheli M., Sibrillot P. and Ostrowsky D.B., 7th Topical Meeting on Integrated and Guided Wave Optics 24th April Florida (1984), PD6.

66. Veselka J.J. and Bogert G.A., Electron Lett., (1987), 23,29.

67. Yi-Yan A., Appl. Phys. Lett., (1983), 42, 633.

68. Jackel J.L., Veselka J.J. and Rice C.E., Ferroelectrics, (1983), 50, 165.

69. Campari A., Ferrari G., Mazzi G., Summonte C., Al-Shukri S.M., Dawar A., De La Rue R.M and Nutt A.C.G., J. Appl. Phys., (1985), 58, 4521.

70. Backer R.A., Appl. Phys. Lett., (1983), 43, 131.

71. Armenise M.N., Al-Shukri S.M., Dawar A., De La Rue R.M., and Nutt A.C.G., I.E.E.E. International Workshop on Integrated Optics and Related Technologies for Signal Processing. Technical Digest 21st Sept, Italy (1984).

72. Jackel J.L., Rice C.E. and Veselta J.J., Electro. Lett., (1983), 19, 387.

73. Wong K.K., G.E.C. J. Res., (1985), 3, 243.

74. Canali C., Carnera A., Mazzi G., Mazzoldi P. and De La Rue R.M., I.E.E.E. International Workshop on Integrated Optics and Related Technologies for Signal Processing Technical Digest, MF-2.1, 21st Sept, Italy (1984).

75. Loni A., De La Rue R.M. and Winfield J.M., Topical Meeting on Integrated and Guided Wave Optics, 28th - 30th March, Santa Fe, New Mexico, (1988).

76. Rice C.E., Jackel J.L. and Brown W.L., J. Appl. Phys., (1985), 57, 4437.

77. Gonzalez R., Chen Y., Tsang K.L. and Summers G.P., Appl. Phys. Lett., (1982), 41, 739.

78. Loni A., De La Rue R.M. and Winfield J.M., J. Appl. Phys., (1987), 61, 64.

79. De Micheli M., Boteneau J., Sibillot P., Ostrawsky D.B., and Papuchon M., Opt. Commun., (1982), 42, 101.

80. De Micheli M., J. Opt. Commun., (1983), 4, 25.

81. Dawar A.L., Al-Shukri S.M., De La Rue R.M., Nutt A.C.G. and Stewart G., Optics Commun., (1987), 61, 100.

82. Jackel J.L. and Holmes R.H., Proc. I.E.E.E., Conference (1983), 38.

83. Yamamoto K., Tanuichi T., Opt. Fibre. Communication, Integrated Optics and Optical Communication Joint Conference (OFC/IOOC) (1987), P65.

84. Rice C.E., J. Solid State Chem., (1986), 64, 188.

85. Fourquet J.L., Reuon M.F., De Pope P., Theveneau H., Man P.P., Lucas O. and Pannetier J, Solid State Ionics (1983), 9 & 10, 1011.

86. Nassau K., Levinstein H.J. and Lovacono G.H., J. Phys. Chem. Solids, (1966), 27, 983.

87. Feld R., Lehmann M.S., Muir K.W. and Speakman J.C., Z. Kristallogr. (1981), 157, 215.

88. Bruno G. and Randaccio L., Acta. Crystallogr. B, (1980), B36, 1711, 2857.

89. Furic K., Croat. Chem. Acta., (1983), 56, 1.

90. Weast R·C·in Handbook of Chemistry and Physics, 68th Ed., CRC Press, 1988, C-126.

91. Bollmann W., Phys. State Sol. (a), (1987), 104, 643.

92. Yamamoto K. and Tanuichi T., First Optoelectronic Conference (OEC 86) Post deadline paper Technical Digest Tokyo, July 1986, B11-4.

93. Tanuichi T. and Yamamoto K., Proc of European Conference of Optical Communication, (1986), 171.

94. Tanuichi T. and Yamamoto K., Conference on Lasers and Electro Optics (CLEO), San Francisco (1987), 198, WP6.

95. Tanuichi T. and Yamamoto K., Optoelectronics - Devices and Tech., (1987), 2, 53.

96. Sanford N.A. and Conners J.M., Conference on Lasers and Electro Optics (CLEO), San Francesco (1988) WM-47.

97. Corbridge D.E.C in Phosphorus, An outline on its Chemistry, Biochemistry and Technology, 3rd Ed., Elsevier, (1985), 70, 121, 652.

98. Greenwood N.N. and Earnshaw A., in Chemistry of the Elements, Pergamon Press (1984), 588, 603.

99. Munsen R., J. Phys. Chem., (1964), 68, 3343.

100. Van Wazer J.R., in Phosphorus and its Compounds, Interscience Pub. (1958) 619, 747.

101. Nichollas G.H., Proc. 2nd Inter. Conger. Phos. Compounds (1980), Boston, U.S.A.

102. Personal communication from Professor Y. Fugii.

103. Vinogradov S.N. and Linnell R.H. in Hydrogen Bonding, Van Nostrand Reinhold Co. (1971), 23.

104. Colthup N.B., Daly L.H. and Wiberley S.E. in Introduction to Infrared and Raman Spectroscopy, Academic Press, 2nd Ed. (1975), 1, 75, 257.

105. Smith R.G., Fraser D.B., Denton R.T. and Rich T.C., J. Appl. Phys., (1968), 39, 4600.

106. Herrington J.R., Dischler B., Raüber A. and Schneider J., Solid State Commun., (1973), 12, 351.

107. Kovacs L., Szalay V. and Capelletti R., Solid State Commun., (1984), 152, 1029.

108. Hadzi D. and Thompson H.W. in Hydrogen Bonding: Papers presented at the Symposium on hydrogen bonding held at Ljubljana, 29th July - 3rd August, 1957, Pergamon Press (1959), 85-339.

109. Lippincott E.R. and Schroeder R., J. Chem. Phys., (1955), 23, 1099.

110. Price W.J. in Analytical Atomic Absorption Spectroscopy., Heydon & Son Press. (1972), 1.

111. Kirkbright G.F. and Sargent M. in Atomic Absorption and Flaurescente Spectroscopy.A.P., (1974), 620.

112. Perkin Elmer 306 Manual.

113. Tien P.K. and Ulrich R. J. Opt. Soc. Am., (1970), 60,1325.

114. Kogelnik H. and Ramaswany V., (1974), 13, 1857.

115. Wilkinson C.D.W. and Walker R.G., Electron Lett., (1979) 14, 599.

116. Finak J. Jerominek H., Opilski Z. and Wetjala K., Opt. Acta., (1982), X11, 11.

117. White J.M. and Heidrich P.F., Appl. Opt (1976), 15, 151.

118. Crank J. in The Mathematics of Diffusion, Claredon Press, Oxford, (1975), 45.

119. Bratoz S., Hadzi D. and Shappard N., Spectro. Chim. Acta., (1956), 8, 249.

120. Pinchas S. and Laulicht I. in Infrared Spectra of Labelled Compounds, Academic Press, (1971), 130.

121. Buswell A.M., Rodebush W.H. and Rony M.F., J. Am. Chem. Soc., (1938), 60, 2239.

122. Dudley D., Williams B. and Plyler E.K. J Am. Chem. Soc., (1937), 59, 319.

123. Von Simon A., Z. Electrochem., (1943), 49, 413.

124. Chapman A.C. and Thirlwell L.E., Spectro. Chimica Acta, (1964), 20, 937.

125. De Micheli M., Botineau J., Neveus., Sibillet P and Ostrowsky D.B., Opt. Lett. (1983), 8, 114.

126. Eckschlager K. in Error Measurement and Results in Chemical Analysis, Van Nastrand Rainhold Co, London (1969), 99.

127. Dudley R.J., Mason S.F. and Peacock R.D., J. Chem. Soc. Faraday II., (1975), 71, 997.

128. Tamir T. in Topics in Applied Physics Integrated Optics 2nd Ed. Springer Verlay (1985), 61.

129. Nutt A.C.G, Ph.D. Thesis University of Glasgow, (1985).

130. De Micheli M. and Russell P.S.J., Appl. Opt., (1986), 25, 3896.

131. Loni A., Hay G., De La Rue R.M and Winfield J.M. Paper Submitted to J. Light Wave Tech.

132. De La Rue, R.M., Loni A., Lambert A., Duffy J.F., Al-Shukri S.M, Kopylov Y.L. and Winfield J.M., Proc. of 4th European Conference on Integrated Optics, Glasgow 11th-13th May (1987), 48.

133. Carruthers J.R., Peterson G.E. and Grasso M, J. Appl. Phys., (1971), 42, 1846.

134. Peterson G.E. and Bardenbough P.M., J. Chem. Phys., (1968), 48, 3402.

135. Canali C., De Bernardi C., De Sanio M., Laffredo A., Mazzi G.and Morasca S., J. Lightwave Tech. (1986), LT4 951.

136. Armenise M.N., Canali C., De Sanio M., Carnerd A., Mazzoldi P. and Celotti G., J. Appl. Phys., (1983), 54, 6223.

137. De Sanio M., Armenise M.N., Canali C., Canera A., Mazzoldi P. and Celotti G., J. Appl. Phys., (1985), 57, 1482.

138. Suchocki P.G., Abou el Leil M.M., Findakly T.K. and Leonberger F.J. Proc. of 4th European Conference on Integrated Optics 11th-13th May 1987.

139. De La Rue R.M., Foad M.A., Loni A., McMeekin S., and Winfield J.M., Invited paper for the optoelectronic conference (OEC'88) held in Japan 2-4th Oct. 1988.

140. Craven P. and Tamei R., Acta Cryst., (1969), B25, 546.

141 Redek J.,Jr., Ashew B., Ballester P., Buhr C., Costero A, Jones S.and Williams K.,J. Am. Chem. Soc., (1987), 109, 6866.

142. Lutz H.D., Buchmeuer W. and Engelen B., Acta Cryst., (1987), B43, 71.

143. Sikka S.K.and Chidambaram R., Acta Cryst, (1967), 23, 107.

144. Donohue "Selected Topics in Hydrogen Bonding" in Structural Chemistry and Molecular Biology., Rich and Davidson Freeman, San Francisco (1964), 443.

145. Loni A., De La Rue R.M.,Foad M.A. and Winfield J.M. Paper submitted to the topical meeting of Integrated and Guided Wave Optics to be held in Houston, Texas Feb 1989.

APPENDICES

APPENDIX A.

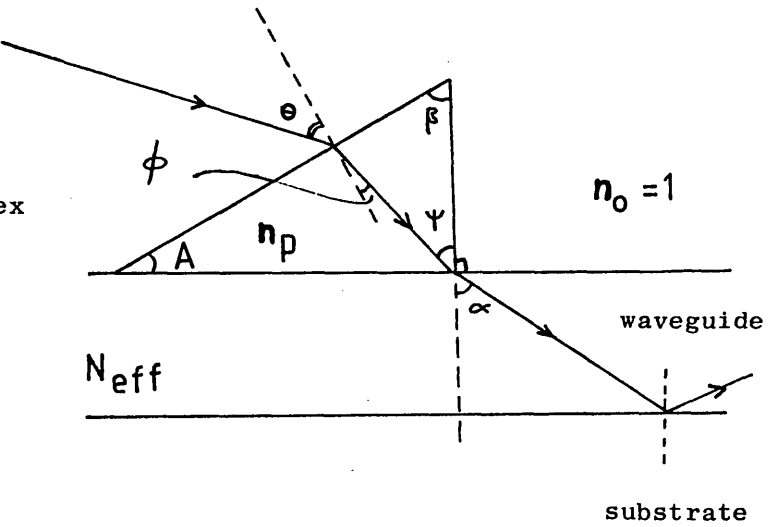

The effective refractive index equation can be derived by applying Snell's law:

$$n_o \text{Sin}\,\theta = n_p \text{Sin}\,\phi \qquad (A.1)$$

$$\phi = \text{Sin}^{-1}\left(\frac{\text{Sin}\theta}{n_p}\right) \qquad (A.2)$$

from simple geometry

$$90 + \Psi = A + \phi + 90 \qquad (A.3)$$

$$\therefore\ \Psi = A + \text{Sin}^{-1}\left(\frac{\text{Sin}\,\theta}{n_p}\right) \qquad (A.4)$$

$$N_{eff} = n_p \text{Sin}\,\Psi \qquad (A.5)$$

$$N_{eff} = n_p \text{Sin}\left(A + \text{Sin}^{-1}\left(\frac{\text{Sin}\,\theta}{n_p}\right)\right)$$

APPENDIX B.

Assume that the [^{2}H]hydrogen vibrates symmetrically along the z-axis over the centre of mass of the oxygen ions triangle.

By analysing the three O- H bonds to their components along the major axes of the crystal.

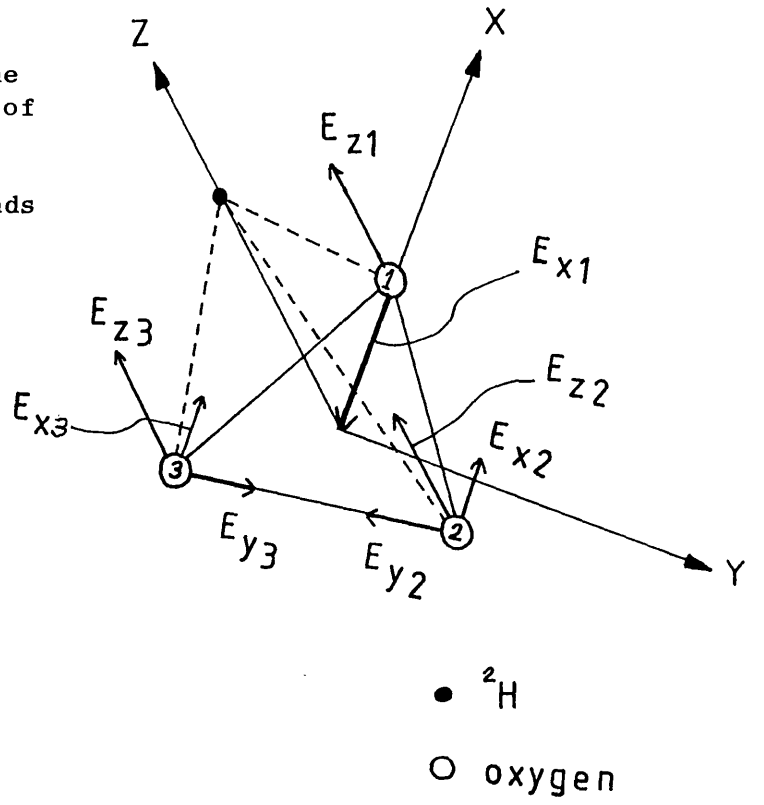

We obtain

$E_{y1} = 0$ (B.1)

$E_{y2} = -E_{y3}$ (B.2)

Since the oxygen triangle is equilateral, i.e. the centre of mass divides the height (h) by the ratio 2/3h:1/3h

$E_{x2} = E_{x3}$ (B.3)

$E_{x1} : E_{x2} = 1/3h : 2/3h$ (B.4)

$E_{x1} = E_{x2} + E_{x3}$ (B.5)

$\therefore E_{x1} - E_{x2} - E_{x3} = 0$ (B.6)

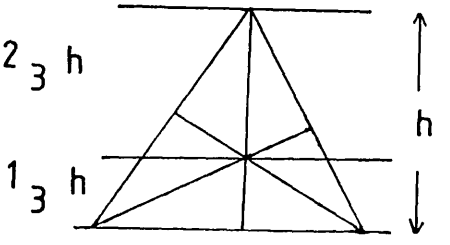

The x-components cancel each other since they are equal and opposite in direction therefore, the only components left are those along the z-axis.

$(E_{z1} + E_{z2} + E_{z3})$ (B.7)

This implies a pure vibration along the z-axis and there should not be any vibration component along the x- or y-axis in the infrared spectra recorded when the radiation is polarized along the x- or y-axis of the crystal. This is not the case for $LiNbO_3$ since weak bands are observed in the recorded spectra. Therefore, the [^{2}H] bifurcated bonds are asymmetrical and possess components along the x- and y-axes as can be seen in figure 5.4.